Subsidence Mechanisms of Sedimentary Basins Developed over Accretionary Crust

HOLT, PETER,JONATHAN

Department of Earth Sciences

Durham University

Subsidence Mechanisms of Sedimentary Basins Developed over Accretionary Crust

Peter Jonathan Holt

Thesis submitted for a Doctorate of Philosophy (PhD)

2012

Subsidence Mechanisms of Sedimentary Basins Developed over Accretionary Crust

Abstract

Peter Jonathan Holt

This thesis uses forward modelling to investigate the formation of intercratonic basins upon accretionary crust. It began from the hypothesis that accretionary crust forms with a near normal thickness crust, but a thin lithosphere inherited from the terranes that compose it. After the accretion process has ceased the lithosphere stabilises and begins to cool, causing it to grow thicker and this in turn drives subsidence of the accretionary crust. A 1-D finite difference computer code was developed to model conductive heat flow through a column of cooling lithosphere and asthenosphere. To test the hypothesis, the subsidence produced by the modelling of this process was compared to the observed subsidence from backstripping numerous basins situated on accretionary crust

The model produced a good fit to the subsidence in a detailed case study of two of the Palaeozoic basins in North Africa. The study was then extended to test the applicability of to accretionary crust globally. It found that while using measured values of the crust and lithospheric thickness for each region the model produced subsidence curves that matched the observed subsidence in each basin. It makes a more coherent argument for the formation of these basins that is able to explain a wider variety of features than other proposed subsidence mechanisms such as slow stretching or dynamic topography. These results suggest that such subsidence is an inherent property of accretionary crust which could influence the evolution of the continental crust over long time periods.

The model was used to investigate the subsidence of the West Siberian Basin and found the subsidence patterns to be consistent with the decay of a plume head which thinned the lithosphere. This subsidence patterns indicate the plume material thinned the lithosphere over an area of 2.5 million km^2 resulting in uplift before it cooled and subsided.

Department of Earth Sciences

Durham University

Subsidence Mechanisms of Sedimentary Basins Developed over Accretionary Crust

Peter Jonathan Holt

Thesis submitted for a Doctorate of Philosophy (PhD)

2012

Table of Contents

1. Introduction **1**

1.1 Basin forming mechanisms 1

1.2 The nature of accretionary crust 4

1.3 Forward modelling basin formation 10

1.4 Aims and outline of the Thesis 11

2. Methodology **14**

2.1 Introduction 14

2.2 Backstripping 14

2.2.1 Decompaction 15

2.2.2 Correcting for the weight of the sediments . . . 18

2.2.3 Correcting for changes in water depths and sea-level . . 19

2.2.4 Complete backstripping process 21

2.2.5 Implementing backstripping in a computer code . . . 22

2.3 Forward modelling 25

2.3.1 Conductive heat flow 26

2.3.2 Calculating the subsidence 28

2.3.3 Discretising the equations 31

2.3.4 Description of the key points in the computer code . . 35

3. Lithospheric cooling and thickening as a basin forming mechanism: A case study from the Palaeozoic basins of North Africa **39**

3.1 Introduction 39

3.2 Geological background and hypothesis 41

3.3 Tectonic subsidence history of the basckstripped North African basins . 43

3.3.1 Methodology 45

3.3.2 General Stratigraphy 46

3.3.3 Results 49

3.4 Forward modelling 51

3.4.1 Methodology of the forward modelling 51

3.4.2 Results: Effects of varying parameters and the best fit model for the backstripping 53

3.5 Discussion 57

3.5.1 Comparison of tectonic subsidence from backstripping and forward modelling 57

3.5.2 Discussion of other potential subsidence mechanisms . . 60

3.6 Conclusions 62

4. A global study of subsidence upon accretionary crust **63**

4.1 Introduction 63

4.2 Methodology 65

4.3 Regional analysis of the observed and modelled subsidence . . 67

4.3.1 South America – Geological background 67

4.3.2 South America – Results 69

4.3.3 South Africa – Geological background 70

4.3.4 South Africa – Results 72

4.3.5 Arabia – Geological background 74

4.3.6 Arabia – Results 76

4.3.7 Scythia and Turan – Geological background . . . 77

4.3.8 Scythia and Turan – Results 80

4.3.9 Eastern Australia – Geological background . . . 81

4.3.10 Eastern Australia – Results 83

4.4 Discussion 85

4.4.1 A comparison with other suggested basin forming mechanisms . 85

4.5 Conclusions 88

5. Subsidence of the West Siberian Basin: Effects of the impact of a mantle plume 89

5.1 Introduction 89

5.2 Geological background 91

5.2.1 Tectonic and geological evolution 91

5.2.2 Present day crust and lithosphere structure . . . 94

5.2.3 Temperature, thickness and depth of a potential plume head . 95

5.3 Methodology 96

5.3.1 Model construction 96

5.4 Results and discussion 98

5.4.1 Model sensitivity and the standard model . . . 98

5.4.1.1 Crustal thickness 98

5.4.1.2 Plume head conditions 99

5.4.2 Thermal subsidence curves 101

5.4.3 Discussion 104

5.5 Conclusions 106

6. Discussion: implications for lithosphere thickness and evolution, and potential future avenues for research 109

6.1 Introduction 109

6.2 The effect of lithospheric growth on subsequent volcanism . . . 109

6.3 Growth of the final lithosphere and the final thickness . . . 111

6.4 Evolution of the continental crust 115

6.5 Summary 117

7. Summary and conclusions **118**

Appendices **123**

Appendix A – Example of the backstripping computer code . . . 123

Appendix B – Example forward modelling code 127

Appendix C – Ghadames composite well cross section 132

Bibliography **133**

Acknowledgements

First and foremost, thanks and praise to the LORD God for making me with an inquiring mind and the ability to write a thesis of sorts. Equally thanks for the amazing world, which I am able to spend my time exploring and studying.

Thank you to my parents and family for putting up with my inquiring mind and many questions of 'Why' and 'How' as I grew up. I'm very grateful for your support even as the thesis may have been slightly longer in coming than expected. Thank you for your wise council whenever I needed it.

Many thanks to my supervisors, Hans Morten Björnseth, Jeroen van Hunen and Mark Allen for great ideas and input, tireless editing and asking the difficult questions which expose the weakness in a piece of work, but ultimately make it stronger. Thanks for your encouragement as well.

My appreciation also goes to Statoil for providing funding, abundant data, hosting meetings and encouraging discussion with other researchers. Without the funding ultimately this work would not have been possible. Also to GRL for allowing me to work part time while I finished writing up.

Thank you to Paul Ryan for his early input to modelling and allowing me to use his Grabiso model even if ultimately I ended up making my own.

I must express my gratitude to the coffee room crew for lightening the mood, constant chat about radiators and the like. Thank you Jen, Alex, Joël, Amelie, J.C., David, Alan, Jon, Jo, Mark and many more.

Thank you to the bay too, for providing instant feedback and alternate wording when my mind drew a blank. Steve, Aaron, Chris and Peter.

Finally how could I forget, Thanks to Dom for cutting me down to size and making sure I did not get ideas above my humble station as a Sherpa.

“Where were you when I laid the foundation of the earth?

Tell me, if you have understanding.

Who determined its measurements—surely you know!

Or who stretched the line upon it?

On what were its bases sunk,

or who laid its cornerstone,

“Have you entered into the springs of the sea,

or walked in the recesses of the deep?

Have the gates of death been revealed to you,

or have you seen the gates of deep darkness?

Have you comprehended the expanse of the earth?

Declare, if you know all this.

(Job 38:4-6, 16-18 ESV)

Chapter 1 – Introduction

Cratonic basins hold 61 % of the world's oil reserves (Condie, 1997), they contain important fresh water aquifers (Gossel et al., 2004) and they are hugely important sediment sinks preserving and recording changes in climatic and tectonic processes occurring on the earth's surface (Allen and Allen, 2005). Yet the process (or processes) that form these basins is still a matter of debate within the literature (Allen and Armitage, 2011; Klein, 1995). Cratonic basins (also referred to as intracontinental basins, intracratonic basins, and interior continental sag basins) are situated in the interior of a continent, far from any active margins upon stable continental lithosphere. They are generally circular to oval shaped in plan and saucer shaped in cross section. They have a sedimentary fill recording subsidence spanning several hundred million years (>200 Myrs normally) (Klein, 1995). The aim of this thesis is to determine what forms a particular group of these cratonic basins which are formed upon accretionary crust. Strictly speaking these should be referred to as intercratonic basins because they form on accretionary crust between the older cratons.

1.1 Basin forming mechanisms

Allen and Allen, (2005) suggest that there are two generic basin forming mechanisms, under which the majority of basin forming mechanisms fall: lithospheric stretching and flexure. When a classic example of a basin formed by stretching and a basin formed due to lithospheric flexure are compared to an intercratonic basin (Fig. 1.1) it is clear that neither of these look similar either in size or magnitude.

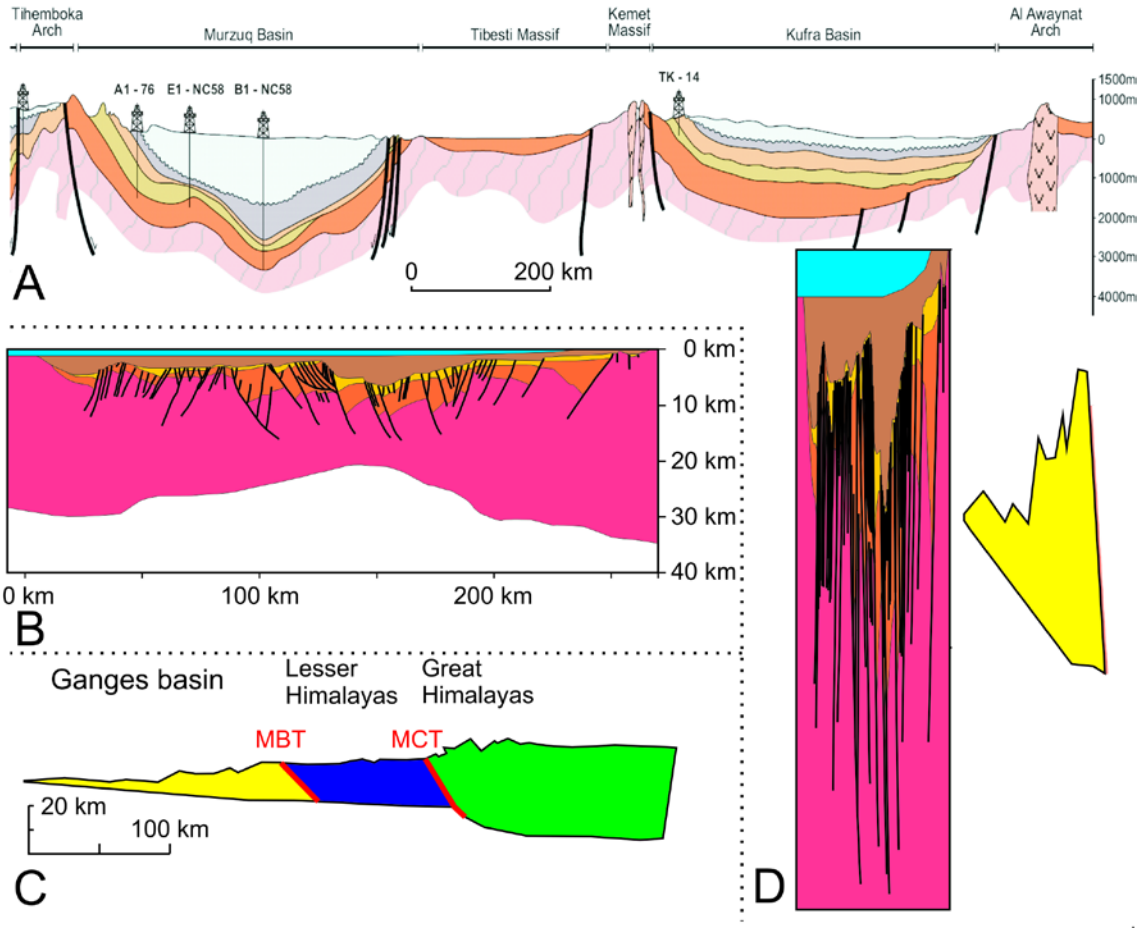

Figure 1.1: A cross section through two intercratonic basins compared to a classic example of a rift basin and a foreland basin. A) shows a cross section from two intercratonic basins in North Africa from Craig et al., (2008). B) is a cross section from the Viking Graben and East Shetland basin in the north sea modified from Christiansson et al., (2000). C) is a cross section across the Himalayas showing the Ganges foreland basin taken from the Encyclopaedia Britannica (1994). D) shows both the Viking Graben and the Ganges foreland basin on the same scale as the intercratonic basins in A.

Therefore a number of alternative subsidence mechanisms have been proposed to explain the formation of these basins. These include

- An excess mass within the lower crust which isn't isostatically compensated. This may be either due to a phase change to a dense mineral assemblage such as ecologite (Artyushkov, 1992) or emplacement of a magmatic underplate (De Rito et al., 1983; Stel et al., 1993).
- Thermal subsidence following heating by a plume (Kaminski and Jaupart, 2000), the emplacement of anorogenic granites (Klein and Hsui, 1987) or extension at depth which only thins the lithosphere (Xie and Heller, 2009).

- Reactivation of older structures which underlie the basin possibly due to a change of the stress field of the basin (Guiraud et al., 2005; Zalán et al., 1990).
- Foreland basins related to fold and thrust belts created in accretionary orogens (Catuneanu, 2004).
- Doming and rifting above a plume accompanied by erosion followed by subsidence due to sediment loading (Sahagian, 1993).
- Subsidence over a region of downwelling in the convecting mantle beneath (dynamic topography) (Heine et al., 2008).
- Extension at the surface caused by magmatic upwelling (Lüning et al., 1999; Neumann et al., 1992).
- Extremely slow rifting at low strain rates (10^{-16} s^{-1}) caused by a change in the stress field to extension associated with supercontinent break up (Allen and Armitage, 2011).

Other authors have suggested some combination of the above, such as emplacement of anorogenic granites which focuses later extension and lithospheric thinning, followed by thermal subsidence and subsidence caused by the excess mass emplaced during the initial period of volcanism (Klein, 1995). These are discussed in greater detail in later chapters and compared to the hypothesis put forward in this thesis. This hypothesis is a variant on thermally driven subsidence, but where the initially thin lithosphere is an inherent property of accretionary crust.

Any theory which attempts to explain the formation of these basins must be able to act over a long period of time, it should match the shape and magnitude of the subsidence curves observed from the sedimentary succession within the basins and it should fit with other observations, such as the scarcity of imaged rifts within the basins. This is one aspect of the problem, but as well as considering purely academic questions related to the formation of the basins, Statoil who funded the project, were interested in economic questions. In basins which are targets for exploration it is important to understand how the timing of subsidence affects the fill within these basins and burial of key stratigraphic layers (the source rocks and reservoirs). Statoil also wanted to understand the basement heat flow into the basins as this is important for determining the timing of source rock maturation and hydrocarbon production. This is applicable in the exploration phase, but also when carrying out detailed basin modelling in basins already producing oil or gas.

1.2 The nature of accretionary crust

Accretionary crust is defined as continental crust which forms at an accretionary orogen. It may also be referred to as juvenile crust (in relation to older cratonic crust) or mobile belts. Unlike a collisional orogeny an accretionary orogeny maintains an active subduction zone throughout its history. Therefore it occurs on the margin of the continental mass and is a potential area for crustal growth (Jahn, 2004). In contrast collisional orogens occur between two larger plates and therefore are located within the interior of the continent. They are sites of crustal reworking rather than growth (Dewey, 2007).

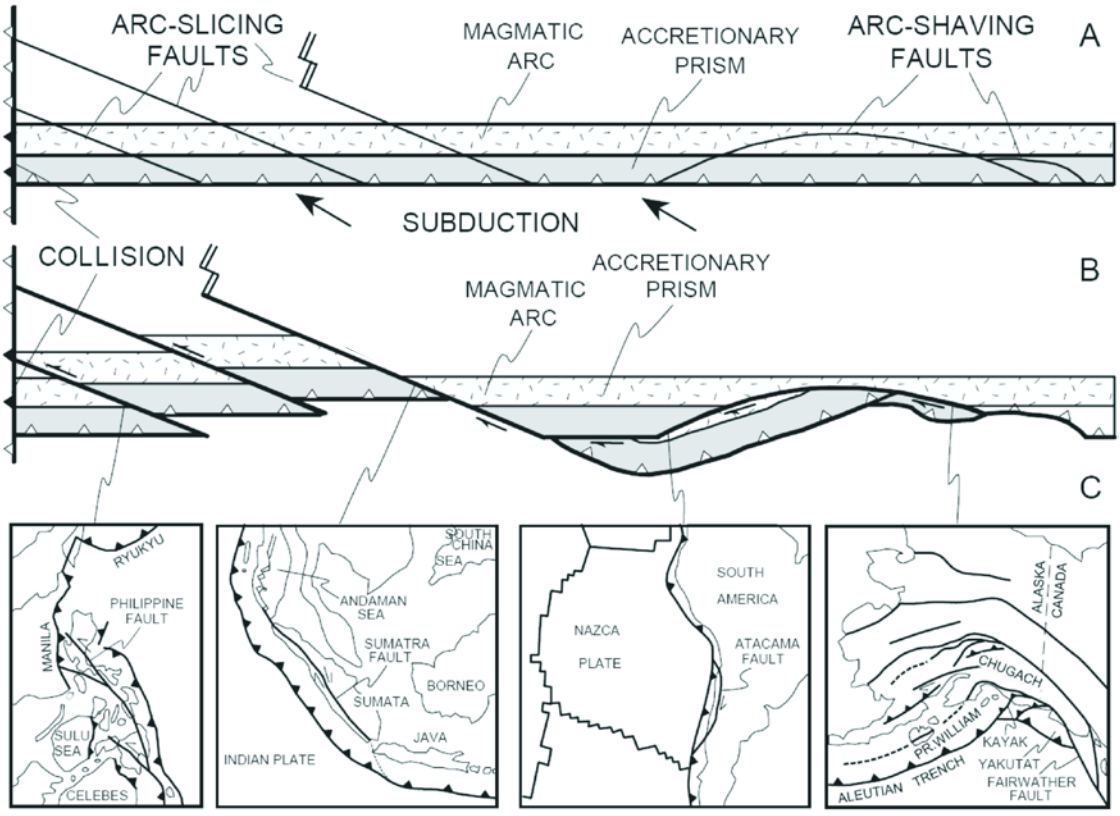

Figure 1.2: Arc slicing and arc shaving faults reproduced from Natal'in and Şengör, (2005). A and B show the evolution of these faults and how they can stack up an island arc in an accretionary orogen. C shows a number of localities in the world where these processes are occurring at the present day.

The first stage in an accretionary orogen is the onset of subduction, which is poorly understood (Stern, 2002). The early stage of an accretionary orogen involves the accretion of Island arcs to each other (Maruyama, 1997) and to the continental margin. Accretion can continue for hundreds of millions of years (Glen, 2005; Metcalfe, 2006; Stern, 1994). The process can be as simple as the subducting plate carrying terranes towards the continental margin followed by collision, or can be more complex involving stacking of a single arc through

strike slip arc shaving or arc slicing faults where the subduction has a significant oblique component as shown in Figure 1.2 (Natal'in and Şengör, 2005). Once terranes have accreted there is then a process of cratonisation where accretion ceases and the terranes behave as a coherent block of continental crust. However, there are a number of different theories as to how this happens (Cawood et al., 2009). It has been suggested that it is due to the collision of buoyant blocks, such as a microcontinental block or thickened oceanic crust (Moores and Twiss, 1995) or due to flat subduction (Collins, 2002). Both these mechanisms are generally confined in time and space so only affect part of the collision zone. Large scale plate reorganisation, such as the breakup of a supercontinent has also been suggested as a method for causing widespread cratonisation (Cawood and Buchan, 2007). This could have a wider affect and cause the accretion to cease. Another method for ending accretionary orogenesis is a collisional orogen occurring along the continental margin halting subduction. This is what appears to have taken place in the Appalachian-Caledonide orogeny (van Staal et al., 1998)

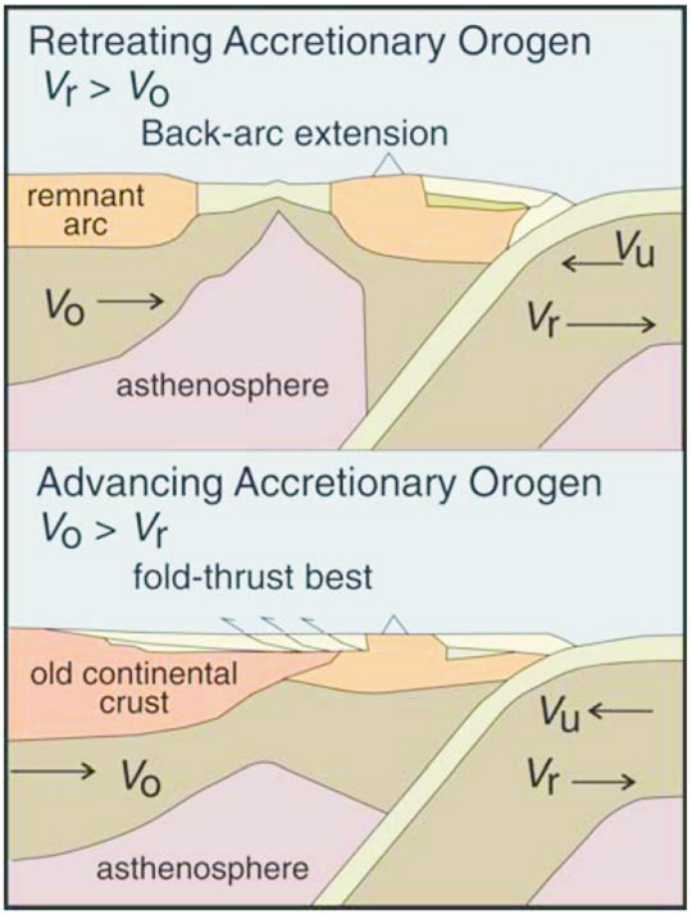

Figure 1.3: The retreating and advancing end members of accretionary orogens. V_O is the velocity of the overriding plate, V_r is the velocity of rollback of the subduction zone hinge and V_U is the velocity of the subducting plate.

Accretionary orogens can be divided into two end members: retreating and advancing accretionary orogens (Fig. 1.3). They are said to be retreating when the rollback of the subduction zone is migrating backwards faster than the overriding plate is advancing. This results in extension of the overriding plate, normally leading to back arc spreading. The western pacific coast of Asia is a present day example of this type of orogen. In an advancing accretionary orogen the overriding plate is moving towards the subduction zone faster than the rate of rollback of the subduction zone hinge. Crustal thickening and uplift are characteristic of an advancing accretionary orogen. This is occurring at present in the Central Andes continental arc. Over the course of its history an accretionary orogen can switch between both modes and may go through a number of cycles (Glen, 2005).

Accretionary crust can vary in thickness from <30 km to >50 km. It is made up of a variety of differing terranes including island arcs, slivers of back arc crust, accretionary wedges from the forearc, thickened oceanic crust and older microcontinental blocks. Many of these building blocks have thin lithosphere, but crustal thicknesses which are near normal for continental crust. Island arcs have been shown to have thin lithosphere from geochemical studies, numerical modelling and seismic tomography. Macpherson (2008) studied volcanoes along the East Philippine Arc where subduction has been propagating southward since the Mid Miocene. The correlation of the Dy/Yb ratio with SiO_2 is used as an indication of fractionation of the melt in the presence of garnet. A positive correlation represents the influence of garnet while a negative correlation indicates that garnet was not present while the melt fractionated. The presence of garnet is depth dependant and therefore provides information about the depth of fractionation. Fractionation occurs when rising magma is arrested by the base of the lithosphere. The results showed that the as a volcanic centre from the propagating subduction zone ages, the depth of fractionation decreases suggesting that subduction thins the lithosphere of the overriding plate. Similar results are shown for the volcanoes from the cascades (Elkins Tanton et al., 2009). This is supported by numerical models which show that the lithosphere beneath the overriding plate is weakened by fluid migrating from the subducting slab and then eroded by corner flow in the mantle wedge driven by the down going slab (Arcay et al., 2006; Stern, 2002; van Keken, 2003). Flow parallel to the trench has a similar effect. These results also fit with slow velocities seen from seismic tomography (Isse et al., 2009) or from refraction studies carried out across active island arcs (Takanami et al., 2000).

Accretionary wedges may also have very thin lithosphere. They are floored by the down going slab during subduction, but when subduction ceases the slab may break off and juxtapose the

accretionary wedge directly against the asthenosphere as has been suggested for the East Anatolian accretionary complex (Zor et al., 2003). Another method which could potentially thin the lithosphere in the overriding plate is extension within the back arc. All these mechanisms combine to support the initial conditions proposed of accretionary crust with a thinned lithosphere. An exception to this may be the older microcontinental blocks. However, these will still spend time as part of the overriding plate during accretion and so may be thinned by subduction along its margin as described above.

Present day examples of accretionary orogens, such as the Eastern margin of the Americas show that they can be 1000's of km long, however other regions of accretionary crust show that they can also assemble areas of crust which are 1000's of km wide (Craig et al., 2008). The back arc region of an accretionary orogen is an area of increased heat flow even where the crust is uplifted and thickened (Currie and Hyndman, 2006). In the North American Cordillera the uplift is consistent with a thinned lithosphere, which also causes the high heat flow (Hyndman and Currie, 2011). This allows compressional features from the accretionary orogen to affect the crust up to 1000 km in land of the subduction zone. A thin lithosphere and active delamination has also been suggested for the central Andes based on seismic tomography (Schurr et al., 2006). A joint seismic refraction and gravity modelling study supported this suggesting that anomalously low velocities in the lower crust and accompanying negative Bouguer anomalies are best explained by partial melting in the lower crust caused by high geothermal gradients (Schmitz et al., 1997). This is consistent with the convecting asthenosphere being closer to the surface in this region. There is conflicting evidence from further south in the central Andes, where S wave receiver analysis suggests that the lithosphere asthenosphere boundary is at 80 km depth below the active arc and thickens away from the arc to 120 km (Heit et al., 2008). Studies of surface waves are inconclusive, they show an increase in velocities at the base of the crust (50-60 km depth), but then increase little below this and actually decrease over the down going slab (Baumont et al., 2002).

The majority of these studies suggest that the accretionary crust keeps the thinned lithosphere inherited from its building blocks until accretion ceases. This is the preferred method for producing accretionary crust with a normal thickness crust and an initially thin lithosphere. In North Africa lithospheric delamination at the end of the Pan-African orogeny has been suggested as an alternative mechanism for thinning the lithosphere (Ashwal and Burke, 1989). The argument for this relies on the Pan-African orogeny producing a mountain range similar to

the Himalayas. However, there is little evidence for this so this is not my preferred mechanism. Both mechanisms are shown schematically in figure 1.4.

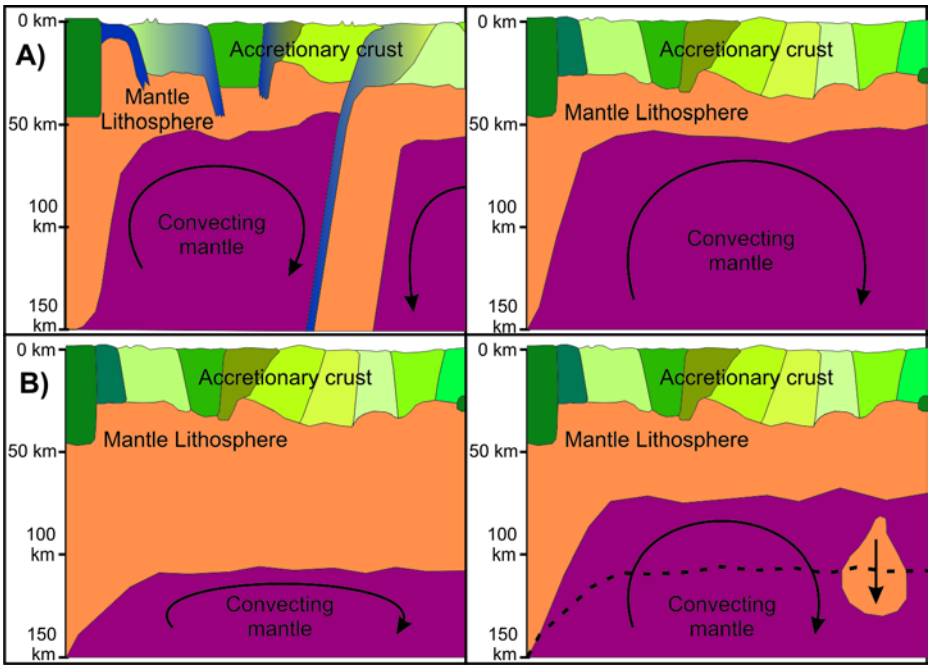

Figure 1.4: A schematic representation of how accretion can produce a near normal thickness continental crust with at thin lithosphere. **A)** Many of the different blocks involved in the accretionary orogen have thin lithosphere due to forming or sitting in the overriding plate of a subduction zone and this is maintained during the accretionary process. **B)** Alternatively the accretionary crust forms with a near normal thickness lithosphere, which is then thinned through a wide scale delamination event at the end of the accretion process.

How far back in the Earth's history accretionary orogens have been operating is not clear, but there is evidence in Fennoscanadia that they may have been occurring as far back as the Mid Archean (~3 Ga) (Windley and Garde, 2009). The Hoggar uplift in North Africa forms a good case study of accretionary crust which is exposed on the southwester margin of the Ghadames basin mentioned in Chapter 3. It is a region of domal uplift where the basement rocks have been exposed by erosion. As Figure 1.5 shows it is made up of 23 north south trending terranes. These are composed of shelf sediments metamorphosed between 870-730 Ma, island arc terranes with calc alkaline volcanism dating from 730-550 Ma as well as two older terranes with 1.8 Ga rhyolites and 2.1 Ga granulites.

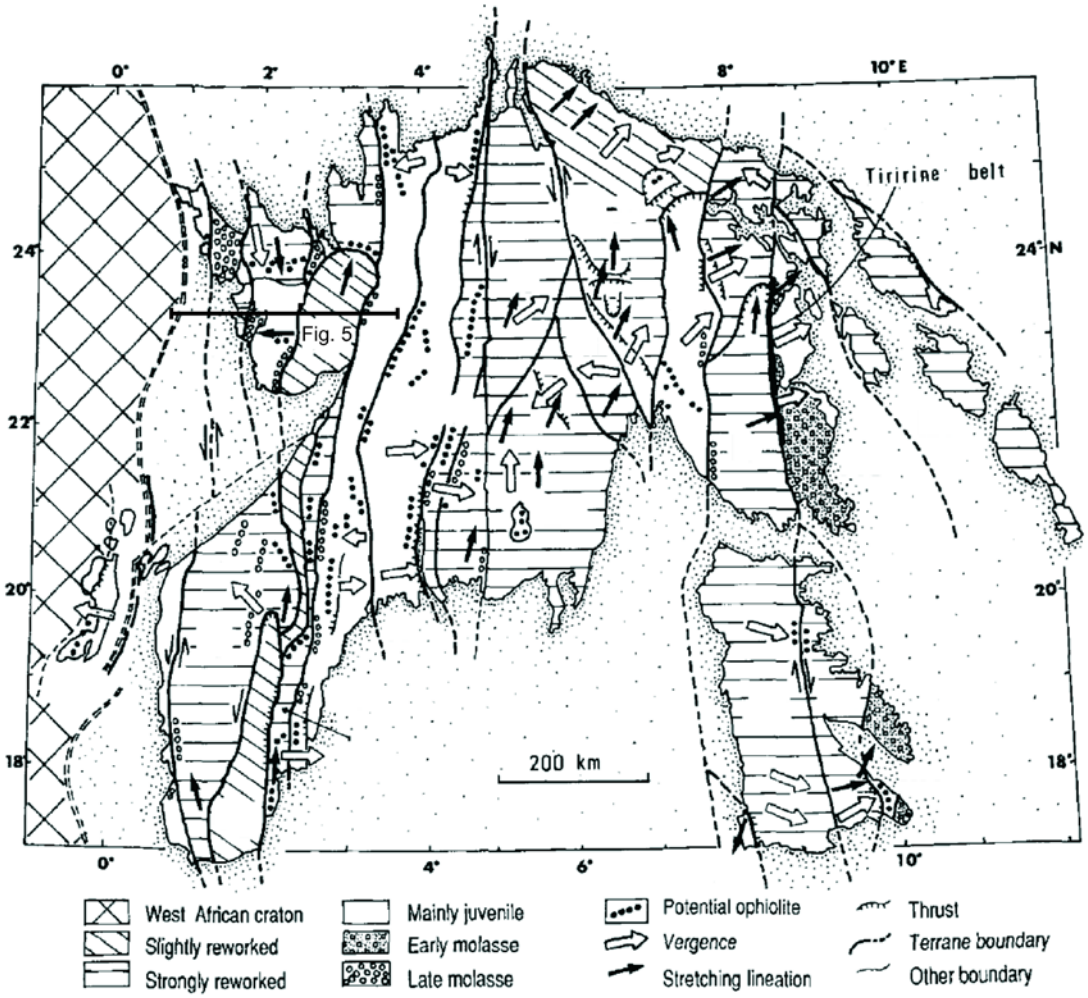

Figure 1.5: The terranes of the Tibesti-Hoggar massif in North Africa modified from Black et al., (1993). The location of the map is shown on Figure 1.6. The map shows 23 different terranes are composed of oceanic sediments, island arcs, palaeoproterozoic microcontinents and accretionary wedges. The approximate location of the cross section from Figure 1.5 is marked on the map.

When the sutures between the terranes are examined in detail many of them show exhumed low temperature high pressure metamorphic rocks characteristic of subduction zones (Caby and Monié, 2003). Figure 1.6 shows a cross section through part of the Hoggar massif illustrating the structure of the sutures between terranes. Greater detail of accretionary crust and orogens can be found in the review by Cawood et al., (2009). However, the important elements to consider when looking at the subsidence of the basins formed upon it have been described here. Crustal composition and structure like this is indicative of accretionary crust and can be used to identify areas where the proposed subsidence mechanism should be considered. In areas covered by sediments gravity, magnetic and well logs can be used to recognise areas of accretionary crust (Natal'in and Şengör, 2005).

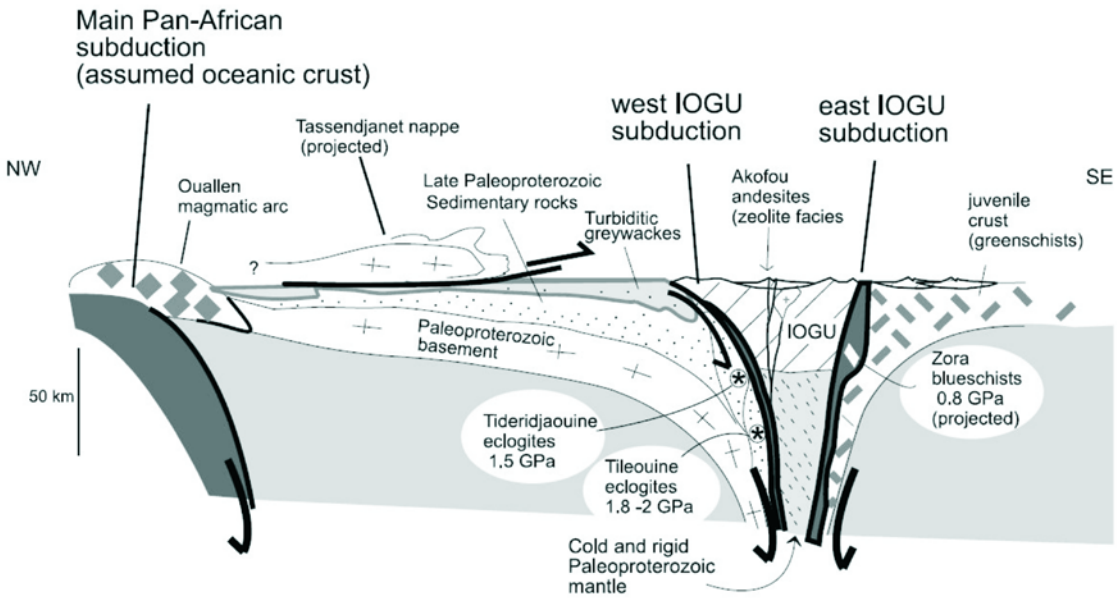

Figure 1.6: Cross section through the northwestern corner of the Hoggar massif illustrating the vertical relationship between terranes. This shows the preserved subduction zones terminated by collision of terranes and associated cratonisation. This figure is reproduced from Caby and Monié, (2003). IOGU = In Ouzzal granulite unit.

1.3 Forward modelling basin formation

Testing a process which is happening at depth in the earth, such as growth of the lithosphere, is difficult because it cannot be observed directly. This is especially true when the process was occurring in the past. Modelling is a good tool to test the effects of a physical process like cooling and growth of the lithosphere against observable data such as the subsidence data from the basins. There two approaches to modelling a problem like this. Inverse modelling is where the observed data are used as an input for the model and are then inverted to find the model which has the best fit to the data. Alternatively forward modelling may be used. This technique involves running the model and then comparing the results to the observed data. The parameters are then changed to produce a better fit to the observed data. This is done iteratively until the best fit is found. This method allows for exploration of the parameter space to see how variations in different parameters affect the results from the model. For this reason forward modelling was used in this thesis.

Computer modelling is useful for exploring physical processes operating within the earth, but can never capture the full complexity of the real world. Therefore it forms a useful tool, which can show whether a certain process is able to account for observed features, but by itself does

not prove that this is what is happening. The results must be interpreted with this in mind to avoid drawing conclusions which cannot be supported by the model.

1.4 Aims and an outline of the Thesis

The main aim of the thesis is to determine what process forms intercratonic basins upon accretionary crust and study the properties of accretionary crust related to this process. Particularly to look at whether thermal subsidence following creation of a normal thickness crust with a thin lithosphere at an accretionary orogen is the primary cause of these basins. A secondary aim leading from this is to use the model developed to look at thermal subsidence in other cases with differing starting parameters, such as those following a plume head impinging on the base of the lithosphere. From an economic point of view, another of the aims of this work is to produce a predictive model for the subsidence of basins on accretionary crust which can be used by Statoil when exploring in a new basin. Alongside this the model needs to output heat flow so that this can be used in basin models looking at source rock maturation. Finally this study aims to consider what the formation of intercratonic basins tells us about the controls on lithospheric thickness and its evolution. Similarly what influence the evolution of accretionary crust has on the wider evolution of continental crust.

The thesis begins by explaining the methodology used and developed to meet these aims. The next chapter contains an in depth case study of a series of basins that Statoil were exploring at the start of this PhD. These basins are located in North Africa and are shown on Figure 1.7. This was of immediate importance for Statoil, but also provided a good case study with a lot of high quality data provided by Statoil and collected by numerous oil companies on a regional scale. The thesis then moves on to test the applicability of the subsidence mechanism proposed for North Africa to other basins situated on accretionary crust. This was done to test if it is an inherent subsidence mechanism for accretionary crust. Numerous basins were studied from around the world as shown on Figure 1.7. The last major data chapter looks at another potential example of thermal subsidence from the West Siberian basin, but where it has been suggested that the formation of the basin is influenced by a plume head. This is followed by a discussion of the broader implications of this work and suggestions of future work there was not time to carry out within this PhD. Finally the conclusions are presented.

Some of the chapters have been published or are in the process of publication. Chapter 3 was published as a paper in Tectonophysics (Holt et al., 2010) . It was aided by editing and

discussion of the ideas, methods and results with my supervisors. Therefore they are included as authors on the published paper. Philip Allen and an anonymous reviewer also suggested expanding the discussion to look at a wider variety of subsidence mechanisms which could produce these basins and also consider the evolution of the Sirte basin to the north and to outline any trade off between parameters in greater detail. Chapter 5 has been accepted by Geology and is awaiting publication. Again my supervisors are included as authors because they provided feedback on the manuscript and helped to edit it down to the short paper format used by Geology. The writing and the underlying work were all carried out entirely by me. Some of the subsidence data from Chapter 4 was included in a publication in Sedimentary Geology (Turner et al., 2011). Detailed information about these papers is provided at the end of the relevant chapters.

Figure 1.7: A map of the different localities studied throughout the thesis (The figure is located on the next page). The location of the Tibesti-Hoggar massif from Figure 1.5 is also shown.

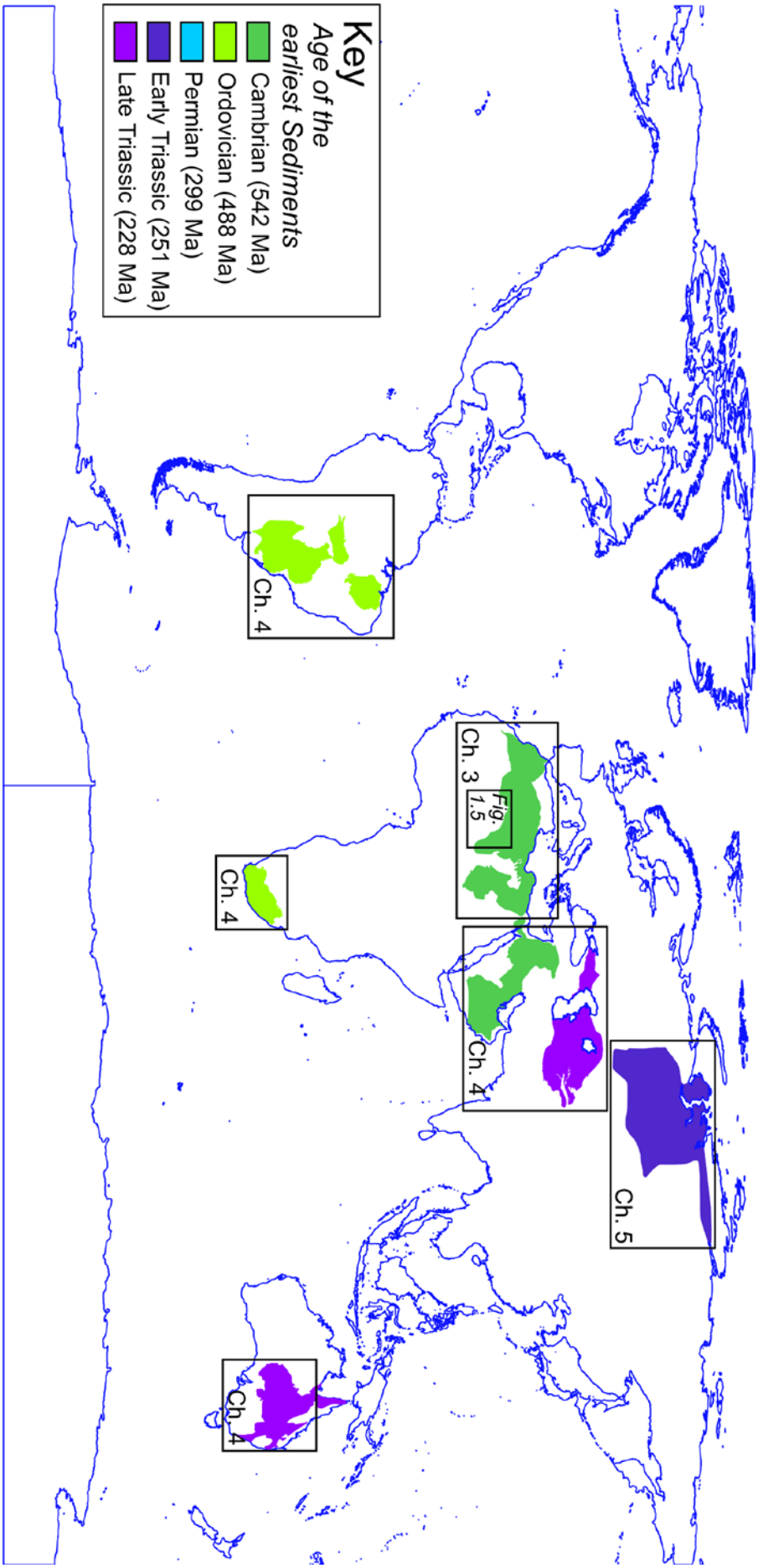
Key
Age of the earliest Sediments
Cambrian (542 Ma)
Ordovician (488 Ma)
Permian (299 Ma)
Early Triassic (251 Ma)
Late Triassic (228 Ma)
Ch. 4
Ch. 3
Fig. 1.5
Ch. 4
Ch. 4
Ch. 5
Ch. 4

Chapter 2 – Methodology

2.1 Introduction

In order to study the subsidence of accretionary crust a one dimensional backstripping code and a numerical forward model were developed. The aim of this chapter is look at the theory behind these techniques and then how they were implemented within the computer model.

2.2 Backstripping

The sediments within a basin contain a record of the evolution of the basin through time. This is a combination of a number of signals including the effects of changing water levels, climate, sediment supply and subsidence or uplift rates. The subsidence rates will be a mixture of the tectonic subsidence caused by the driving forces creating the basin and the isostatic response to the weight of the sediments being deposited. Backstripping is the process of analysing a sedimentary section to calculate the tectonic subsidence of a horizon within a basin through time. This can be the basement or another sedimentary horizon. To isolate the tectonic subsidence, the effects of changing water depth, sea level and sediment loading must be removed.

Backstripping was first used to study the subsidence of the Atlantic margins by Watts and Ryan (1976). It has since been applied to numerous situations and developed for two and three dimensions. The methodology herein follows a set of simple steps. First the sediments in the column are decompacted by removing the weight of the sediments above them, then the height of the column is corrected for the weight of the sediments and finally corrections are made for the water depth at the time of deposition and the change in sea-level through time. This adheres to the method used by Sclater and Christie (1980) and explained in detail in Allen and Allen (2005).

2.2.1 Decompaction

As sediments are deposited and subsequently buried they are compacted by the weight of the sediments above them. Before the tectonic element of the subsidence can be calculated each layer of sediments in the succession must be decompacted to their depositional thickness and then progressively compacted as each layer is added above it until they reach their present day thickness. Figure 2.1 demonstrates this process as the deepest layer from the present day sedimentary column (1) is decompacted to give column (2) and then each layer is added in turn. In column (3) the lowest layer will be partially compacted and the middle layer is uncompacted. By column (4) each layer matches the present day thickness. This ensures that the true thickness of the sediments at the time is used when calculating the tectonic subsidence.

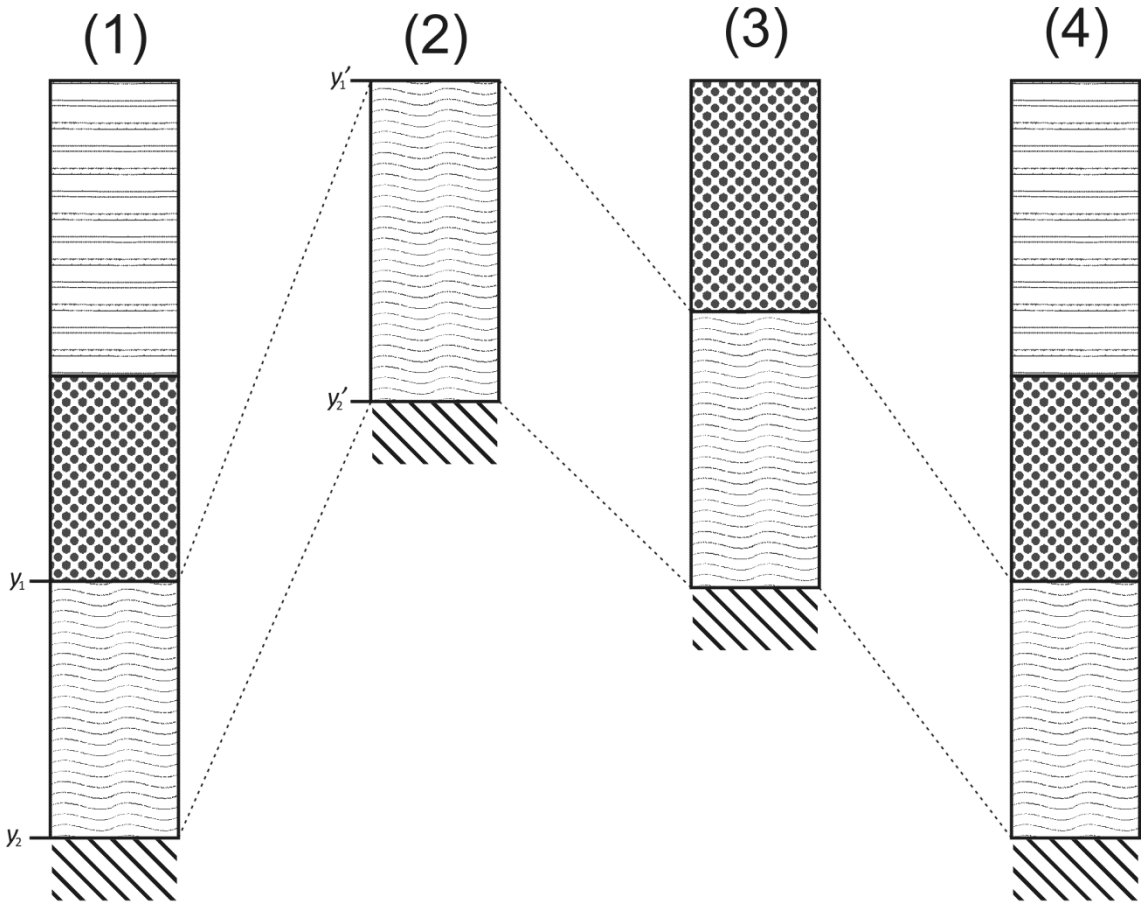

Figure 2.1: The decompaction process. Column (1) represents the present day sedimentary section being decompacted. The bottom layer, with a present day thickness of y_2-y_1, is first decompacted to its depositional thickness y_2'-y_1' shown in column (2). In column (3) the middle layer is decompacted to its depositional thickness while the bottom layer is partially compacted due to the weight middle layer above it. In the final column (4), the layers are all compacted to their present day thickness again. The subsidence of the basement through time can be seen through columns 2-4.

When sediments are originally deposited there is a large amount of pore space between the grains. This will be filled with water, another fluid or gas. As new sediments are deposited above the first sediment layer the pore space will begin to decrease. This can be due to the weight of the sediments above pressing the grains into each other, deforming the grains and closing up the pore space forcing the water out. This is known as mechanical compaction and is dependent on pressure and the composition of the grains. For instance, lithic grains will deform much more easily than silica grains. Pore space can also be lost due to deposition of cements or dissolution and reprecipitation of the grains. This is known as chemical compaction and is highly dependent on temperature and the chemistry of the pore fluid. It is not considered in the backstripping within this study because the chemical reactions involved are often poorly understood and estimates of changes in temperature and pore fluid composition are not accurate enough to attempt model its effect.

There have been a number of different empirical porosity-depth relationships proposed. They can be calculated from rock deformation tests in the laboratory (Karner et al., 2005) or from measurements of porosity from well logs (Halley and Schmoker, 1983; Sclater and Christie, 1980). The simplest porosity depth relationship is a linear decrease in the porosity. This can provide a good fit to well data e.g. from the North Sea (Allen and Allen, 2005), but leads to problems as it suggests that at some point porosity becomes negative, which is physically impossible. However, a linear relationship can be used down to a specified cut off depth to avoid this problem. This suggests the porosity is lost at a constant rate with depth, but also indicates that compaction stops below a certain depth, possibly because there is no pore space left to consume. Alternatively a logarithmic relationship for porosity with depth can be used, but this is actually another way of expressing an exponential relationship (Baldwin and Butler, 1985). Both indicate that the rate of porosity loss decreases with depth. This suggests that reducing the porosity becomes progressively harder. More complex porosity depth relationships have also been proposed where one mathematical equation is used until a critical porosity is reached after which a different relationship is used (Revil et al., 2002). The data often has a large amount of spread so it is not always easy to distinguish clearly which relationship is most appropriate. All the relationships mentioned above are not based on a physical understanding of process, but are empirical and are based on the best fit of the data.

A negative exponential decay is the most widely used, especially where there is not enough data to test which relationship works best for the sediments being decompacted (Allen and Allen, 2005). It does not result in negative porosity and a decreasing rate of porosity loss fits

nicely with the logic that compaction originally occurs due to grains realigning and then has to be accommodated by grains braking and warping. Therefore a negative exponential relationship is used in this thesis. This takes the form

$$\varphi = \varphi_0 \exp(-cy) \quad (2.1)$$

Where φ is the porosity at depth y. φ_0 is the porosity of the sedimentary unit at the surface and c is the compaction coefficient for the sediments. Both of these parameters are dependent on the lithology. If a layer of sediment is currently buried between the depths of y_1 and y_2 the aim of decompaction is to calculate what its thickness would be at a shallower depth of y_1' and y_2' (Fig. 2.1). For a one dimensional column the total volume of a rock layer is given by its thickness.

$$V_t = y_1 - y_2 \quad (2.2)$$

The volume of water held within the pore space of the section at its present day thickness can be given by integrating equation (2.1).

$$V_w = \int_{y_1}^{y_2} \varphi_0 \exp(-cy) dy \quad (2.3)$$

$$V_w = \frac{\varphi_0}{c}[\exp(-cy_1) - \exp(-cy_2)] \quad (2.4)$$

The volume of the sediments in a layer V_s is the total volume of the layer V_t minus the pore volume V_w.

$$V_s = Vt - Vw = y_2 - y_1 - \frac{\varphi_0}{c}[\exp(-cy_1) - \exp(-cy_2)] \quad (2.5)$$

When the layer is moved up to a new depth and decompacted it expands. The volume of sediments does not change in mechanical compaction so the only thing that changes is the volume of the pore space. Therefore

$$V_t' = V_s + V_w' \quad (2.6)$$

$$y_2' - y_1' = y_2 - y_1 - \frac{\varphi_0}{c}[\exp(-cy_1) - \exp(-cy_2)] + \frac{\varphi_0}{c}[\exp(-cy_1') - \exp(-cy_2')] \quad (2.7)$$

This process is shown schematically in Figure 2.1 where the bottom layer of sediments has all the sediments above it removed and is decompacted. Then each of the overlying layers are added in turn and decompacted while the layers beneath them are partially compacted until to reach the present day thicknesses. Due to the fact that y_1' and y_2' are on both sides of equation 2.7 it cannot be solved directly, but can be by iteration which makes decompaction

ideal for solving using a computer program. The depth to the top of the sedimentary layer y'_1 is known for the first layer because it is the surface, but the depth to its base y'_2 depends on the result of decompaction. The depth to the top of lower layers is calculated when decompacting the layer above because it is the base of the layer above.

2.2.2 Correcting for the weight of the sediments

Once the correct thickness of the sediments has been ascertained through decompaction the next stage is to calculate the weight of the sediments. The first step in this process is to calculate the porosity of the decompacted sedimentary layers. This is done by integrating equation 2.1 and dividing it by the thickness of the sediment layer.

$$\varphi = \frac{\varphi_0}{c}\frac{\exp(-cy'_1) - \exp(-cy'_2)}{y'_2 - y'_1} \quad (2.8)$$

This gives the average porosity for each sedimentary layer. The bulk density of each layer is a combination of the density of the water in the pore spaces and the density of the grains in between as expressed in equation 2.9.

$$\rho_b = \varphi\rho_w + (1-\varphi)\rho_{sg} \quad (2.9)$$

Once the bulk porosity for each layer is calculated the average density of the column can be calculated for the full sedimentary column *S* by summing all the layers together.

$$\bar{\rho}_b = \sum_i \left[\frac{\bar{\varphi}_i\rho_w + (1-\bar{\varphi}_i)\rho_{sgi}}{S}\right] y_i \quad (2.10)$$

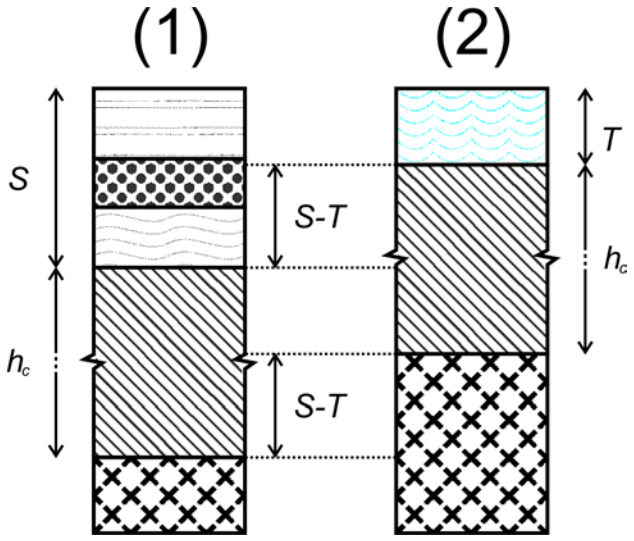

Figure 2.2: Removing the effect of sediment loading. Column (1) shows the column of sediments *S*, the crystalline crust h_c and mantle lithosphere with the hatched texture. In column (2) the loading due to the sediments have been replaced by water to give the tectonic subsidence *T*. The difference between the thickness of the sediments and the tectonic subsidence shows how much column (2) has risen when the sediment load is removed and therefore how much mantle lithosphere is required at the base of the

column to compensate for it.

In backstripping the subsidence calculated is that of a basin filled with water instead of sediments. This is known as the water loaded tectonic subsidence. Removing the isostatic effect of the sediments and replacing it with water is illustrated in Figure 2.2. The tectonic subsidence *T* is found using Airy isostacy, which effectively states that the weights of the two columns are balanced at the compensation depth (the base of the column). It then becomes apparent that if the loading from the sediment is removed it is compensated for in part by water and by a portion of mantle material at the beneath the crust. This is illustrated in Figure 2.2. The crystalline crust is treated as being incompressible therefore it does not change thickness during this process. This can be seen by equating the weight of the columns (1) and (2) from Figure 2.2:

$$column(1) = column(2)$$
$$\bar{\rho}_b S = \rho_w T + \rho_m (S - T)$$
$$(\rho_m - \rho_w) T = (\rho_m - \bar{\rho}_b) S$$
$$T = \frac{(\rho_m - \bar{\rho}_b)}{(\rho_m - \rho_w)} S \quad (2.11)$$

2.2.3 Correcting for changes in water depths and sea-level

Once the sediments have been decompacted and corrections have been made for the sedimentary load at each time interval, the next step is to correct for the weight effects of the water column. To plot the subsidence through time the top of the sediment column must be corrected to the same datum at each time step, in this case the present day sea level. Basinal sediments are usually deposited in water. The water depth can be notoriously difficult to interpret (Allen and Allen, 2005). The best method to calculate it is to carry out a detailed biostratigraphic study. This involves looking using the fossil assemblage in the sediments to work out what water depth they were deposited in. Water depths can also be estimated from the depositional environment of the sediments, but this is generally less accurate than using biostratigraphy. For shallow water depths, up to 200 m, estimating the water depth is easier and the errors associated are smaller. Even if the water depth used is wrong, a correction of a few 100 m will affect the shape of the subsidence curve much less than one of several 100 m. Deeper water depths are very difficult to estimate correctly even with biostratigraphic data because the fossil assemblages vary slowly at such depths. All the estimates for water depth used were taken from studies found in the literature. These are a specific to each study area so references are given where relevant. Therefore they are a mixture of biostratigraphy and

sedimentological studies depending on what was available. Once the water depth is known it simply needs to be subtracted from the subsidence to remove the effect.

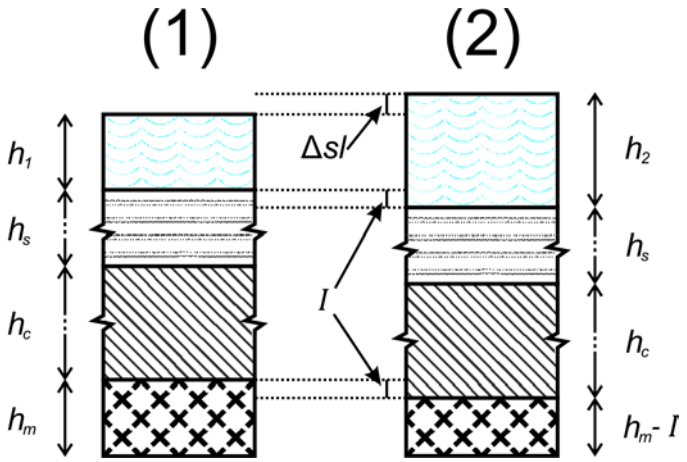

Figure 2.3: Correcting for changes in sea level with time. Column (2) shows the effect of an increase in sea level *Δsl* compared to column (1). The increase in water depth between h_1 and h_2 raises the sea level, but the increase loading also depresses the column by I. The thickness of the sediment h_s and crust h_c remain the same, but the thickness of the mantle lithosphere h_m will decrease by I.

However, correcting for changes in sea-level is more complicated as they a have two-fold effect. An increase in sea-level increases the water depth, but the weight of the water also depresses the crust. To correct for the change in water depth the difference between the palaeosea-level and present day sea-level is subtracted if the sea-level was higher in the past or added if it was lower. To correct for the isostatic effect of the water Airy isostacy is used. Flexure does not need to be considered because the sea-level rise will affect the whole of the basin equally. The effect of a sea-level rise is illustrated in Figure 2.3. The initial water depth h_1 is shown in column (1). In column (2) the sea-level rises by Δsl to give a new water depth h_2 causing an isostatic adjustment of I. The difference in the water depth in (1) and (2) is

$$h_2 - h_1 = \Delta sl + I \quad (2.12)$$

The thickness of the sediments h_s and crust h_c are the same for both columns so can be ignored. Using isostacy

$$column(1) = column(2)$$

$$\rho_w h_1 + \rho_m h_m = \rho_w h_2 + \rho_m (h_m - I)$$

$$\rho_m I = \rho_w (h_2 - h_1)$$

$$\rho_m I = \rho_w (\Delta sl + I)$$

$$I = \frac{\rho_w}{(\rho_m - \rho_w)} \Delta sl \quad (2.13)$$

The values of the palaeosea-level are taken from the long term curves of Haq and Schutter (2008) for the Palaeozoic and from Haq et al., (1988) for the Mesozoic and Cenozoic, which are then substituted into equation 2.13.

2.2.4 Complete backstripping process

All the sections from the different basins were backstripped using the basement as the tracked horizon. In summary all the sediment layers were removed so that only the oldest sediment layer remained ready to be decompacted first. The oldest layer was then decompacted to get its depositional thickness. The decompacted thickness was then backstripped to remove the loading due to the sediments, the loading due to difference in sea-level from the present day and the water depth to calculate the tectonic subsidence. This is shown mathematically by combining equation 2.11 and 2.13 to give the complete equation for the tectonic subsidence.

$$T = \frac{(\rho_m - \bar{\rho}_b)}{(\rho_m - \rho_w)} S - \frac{\rho_w}{(\rho_m - \rho_w)} \Delta sl + Wd - \Delta sl \quad (2.14)$$

There are limitations to the method. It only solves for a 1D case using Airy isostacy. This ignores the flexure of the crust under the weight of accumulating sediments. This is not a serious limitation as the basins investigated are such large uniform features with widths of > 500 km and breadths of up to 1000 km. This is large enough to overcome any effects of flexure from the crust. The amount of detail in the subsidence curve is dependent on the information that can be gained from the sedimentary column because the number of layers that the column can be split into controls the number points on the subsidence curve. This is a problem in North Africa for example, where often the first layer of the sedimentary column, such as in well A1-NC198, is Cambro-Ordovician undifferentiated. This layer covers a time span of 100 Myrs and is 1534 m thick, which means a lot of detail from the subsidence curve over this time period may be lost. The final limitation of the backstripping is that it does not take into account periods of uplift and erosion of the sedimentary column. This is because it is not possible to measure how much is missing, though in some wells there has clearly been erosion. Apatite fission tracking can be used to give an indication of the amount of uplift, but even this cannot easily be transformed into the amount of missing section. To avoid this problem, wells close to the centre of the basins were chosen where erosion should be at a minimum. In basins with good well coverage a composite well was made representing the entire stratigraphy of the basin and therefore the maximum subsidence in the basin.

Errors within the interpretation of the sedimentary column, such as errors in the ages assigned to the tops and bottoms of layers or the water depth will be carried through into the

backstripped subsidence curve. However, errors are rarely included in details of the well logs or sedimentary sections. Equally there is no indication of the error on the sea-level curve of Haq and Schutter (2008). In absence of other measurements of the error the backstripping was carried out assuming the column was entirely composed of shale and then entirely composed of sandstone to provide an upper and lower bound for the subsidence as in Corfield et al., (2005).

2.2.5 Implementing backstripping in a computer code

The backstripping program was created specifically for the PhD. While there are a number of commercial computer packages none were available within the department at the beginning of the PhD. The opportunity to create a program to perform the backstripping provided a much better understanding of the process avoiding the 'black box' mentality which can easily be the result of using a prebuilt program. MATLAB, a high level computer language, was used to write the computer code. It is designed specifically for solving computationally intensive problems. While backstripping is not particularly complicated MATLAB is easier to use than programming languages such as C++ or FORTRAN as it has a very complete help file and shows exactly which line mistakes in the code are situated on. It is also able to produce professional quality plots.

The starting point for the code was a backstripping code written by Sonia Scarselli which was available in the online supplementary material from Allen and Allen (2005). It has subsequently been altered significantly and new features have been added. An example of the backstripping code is shown in Appendix A. It is for well A1-NC198 in the Kufrah basin. The code can be split into 3 sections, the inputs, the processes and the outputs.

The input section is where all the necessary data are entered. In the Scarselli code this was done using names specific to each layer. This has been changed to arrays for each of the inputs. The advantage of this is that the variable names within the process section of the program do not have to be changed for each different well that is backstripped; only the inputs are changed. Some of the inputs required are taken from well or outcrop data such as the present day thickness of the layer (z) and the present day depth to the top of the layer (y). Other inputs such as the surface porosity (ϕ_0/fi), the compaction coefficient (c) and the sediment grain densities (ρ_{sg}/rho) depend on the composition of the layer. These come from well reports or from published regional studies. The values for the porosity depth relationships used are shown in Table 2.1. The palaeosea-level (sl) is taken from long term global sea-level curves (Haq et al., 1988; Haq and Schutter, 2008) and the palaeowater-depth (Wd) is taken

from relevant studies in the literature as described in 2.2.3. Each input is entered starting from the youngest layer and working down through the well or outcrop to the oldest.

	Surface porosity (ϕ_0)	Porosity depth coefficient (c) m^{-1}	Grain density (ρ_{sg}) kg/m^3
Sandstone	0.49	0.00027	2650
Shale	0.63	0.00051	2720
Sandy Shale	0.56	0.00039	2680
Carbonates	0.43	0.000575	2710

Table 2.1: Values of material properties used in backstripping. Sandstone, Shale and Sandy shale are taken from Sclater and Christie, (1980) while values for carbonates are from Halley and Schmoker, (1983).

The first step in the process section is to carry out the decompaction. This is done using two *for* loops, the first of which steps forward in time and the second moves up the sedimentary column and grows over time to add each new layer progressively through time. The decompaction is solved iteratively. This done using a *while* loop which means that the program will keep calculating the decompacted thickness until it converges on the correct answer. It will stop and save this answer once the difference between the current answer and the answer for the previous iteration drops below an error value, 10 cm in this case. Once the program has converged on the right answer for the first layer it will move on to calculate the next layer and so on. The second step is then to calculate the porosity of each layer and from this the bulk density of the sedimentary column and lastly the tectonic subsidence. The Scarselli model calculates the tectonic subsidence, but does not include any correction for sea-level or water depth. This was added to the new code making the results more accurate. All of these changes make the code neater and easier to use while carrying out extra calculations. This can be seen by the fact that the Scarselli code is 259 lines long and backstrips a column with 5 layers while the new code will backstrip a column with 10 layers using only 163 lines of code.

The final section of the code takes the results and plots them or outputs them into a format that can be used in other programs such as excel. Any of the variables can be outputted, such as the decompacted thickness of the sedimentary column or each individual layer through

time. This forms a useful way to check the backstripping process.

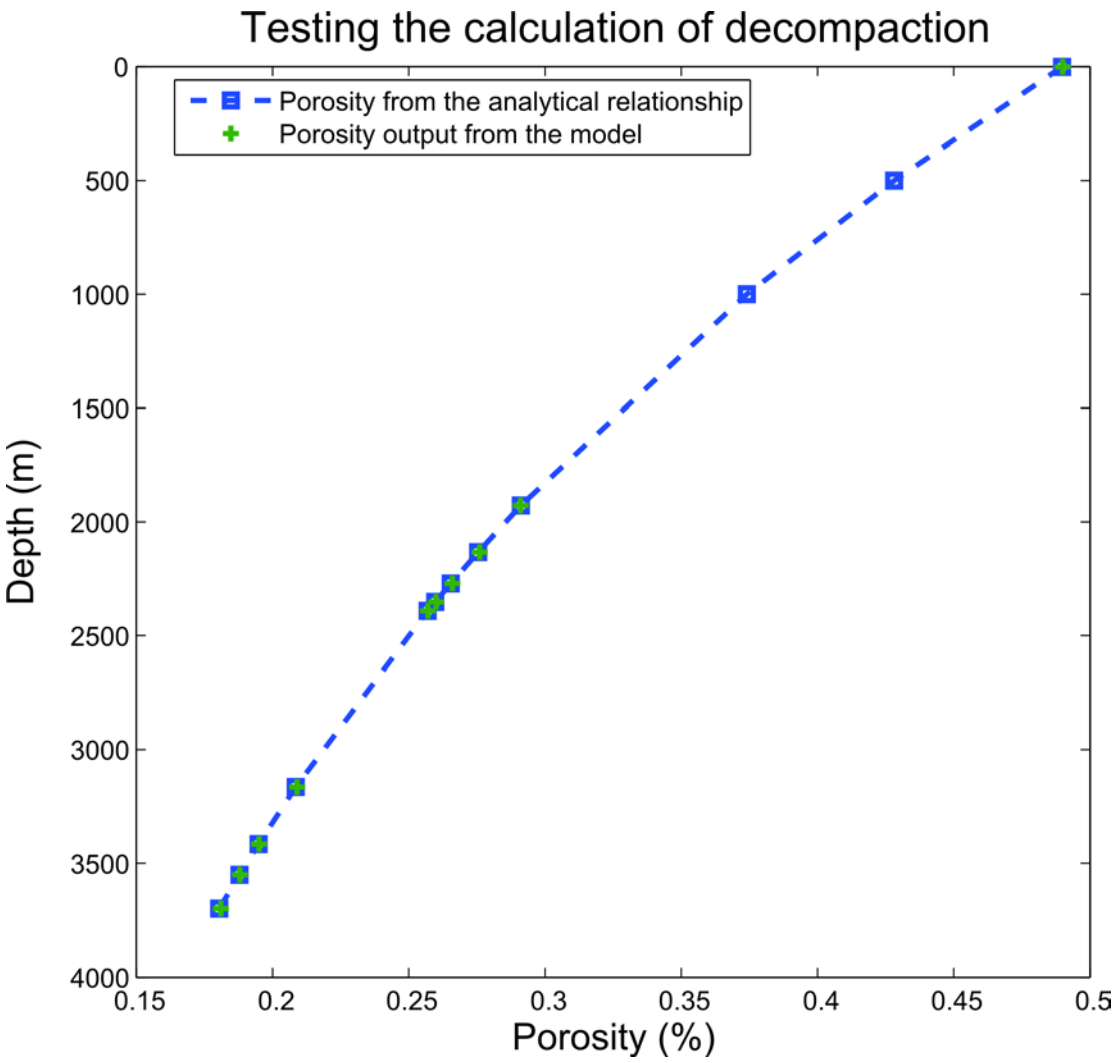

Figure 2.4: The analytical relationship for porosity in sandstone with depth from equation 1 plotted against the porosity taken from each decompacted layer when backstripping a column of pure sandstone. This demonstrates that the iterative approach to determining the decompacted thickness is converging on the correct answer because it is producing porosities which fit the expected relationship.

The evolution of decompacted thickness and porosity through time showed that in the first draft of the code the porosity depth coefficients were in the wrong units. Using this method it is possible to thoroughly test the decompaction by plotting the porosity of the lowermost layer against its depth through time and comparing it to an analytical solution. As Figure 2.4 shows, the results of the decompaction process returns the same results as the analytical porosity depth relationship used as the inputs. This shows the iterative calculations have reached the right answer.

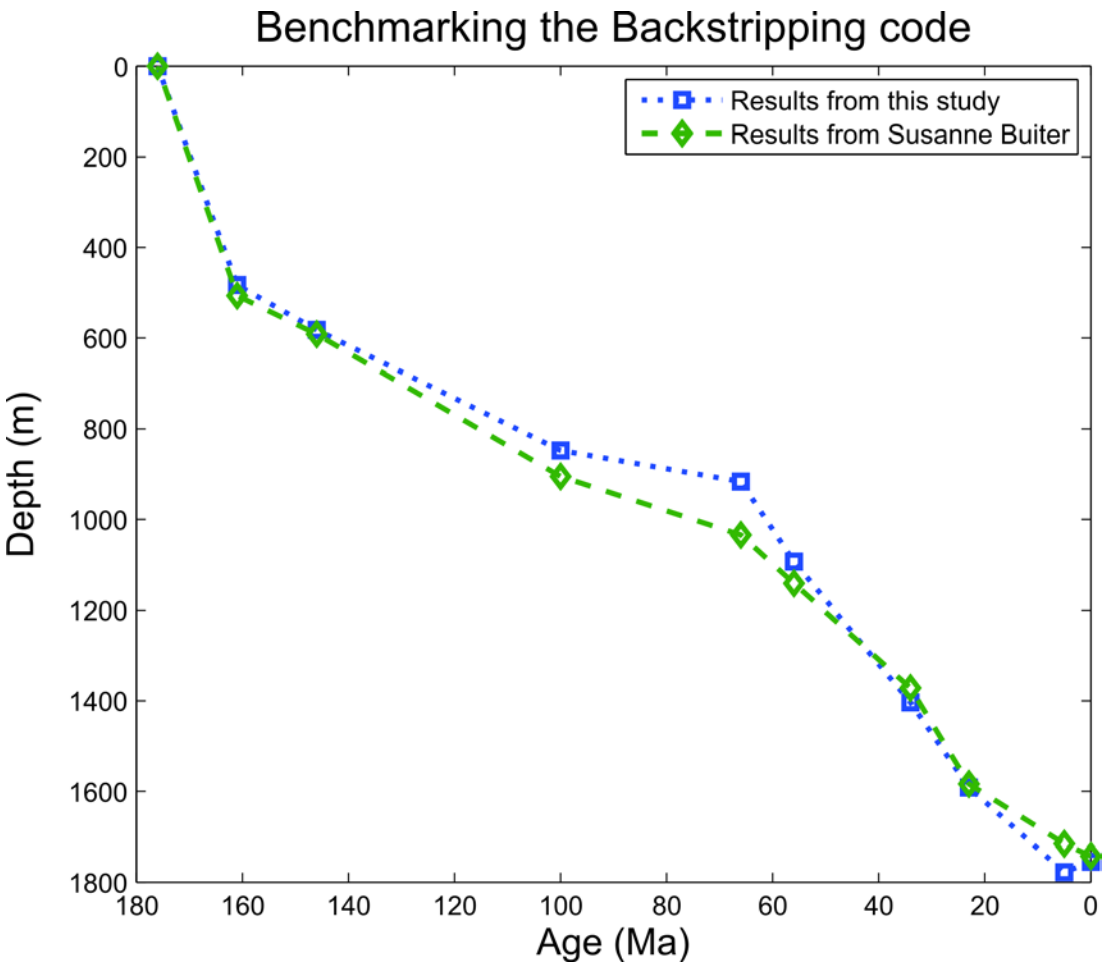

Figure 2.5: A comparison of the backstripping results from the code used in this study and that of Susanne Buiter's masters student. The maximum variation between the two is ~ 10%, but on average they agree to within 4% total water loaded subsidence. The reason for the variation is described in the text.

The code was also benchmarked against the Scarselli program and returned the same results. However, as it does not include the effects of the water depth or changes in sea-level it is not a complete test of the code. It was also tested against another backstripping code developed by a master's student of Susanne Buiter's of the Norwegian Geological Survey (NGU), which showed some differences, however these were less than 100 m. A comparison of the results from the two codes is shown in Figure 2.5. The differences are minor and when compared to the subsidence from the forward model described below make no difference to the best fitting model.

2.3 Forward modelling

In order to test what causes the subsidence observed from the backstripping a numerical

forward model was constructed. A 1D conductive heat flow model was used to calculate the cooling of a column of mantle lithosphere and crustal material and the subsidence resulting from this. To make it equivalent to the backstripping the subsidence calculated was for a water loaded basin. In this section the aim is to look at the underlying physics and assumptions that go into the model and then how this has been incorporated into a finite difference numerical model.

2.3.1 Conductive heat flow

Thermal energy can be transferred via a number of mechanisms such as convection and advection of hot material which involves the flow of hot material to a colder region or by conduction which involves the transfer of energy between neighbouring atoms. In the crust and lithosphere conduction predominates whereas in the mantle convection dominates. This is controlled in part by the change in viscosity which in turn is dependent on the temperature. Numerous studies of the growth of oceanic lithospheric as it moves away from a mid ocean ridge have shown that conduction alone provides a good fit to the surface heat flow and bathymetry data although hydrothermal convection also plays an important role, especially close to the ridge (McKenzie et al., 2005; Stein and Stein, 1992; Turcotte and Schubert, 2002). The thickening of an initially thin continental lithosphere is an extension of the oceanic case. However, in a continental environment the effects of hydrothermal convection will be negligible and therefore the forward model only solves for conductive heat flow. This is governed by the Fourier equation

$$q = -k\frac{dT}{dz} \quad (2.15)$$

and is depicted in Figure 2.6. The conductive heat flow *q* through material with a coefficient of conductivity *k* is proportional to the difference in temperature *dT* over the distance *dz*. The minus sign is introduced because heat flows against the temperature gradient i.e. from areas of high temperature to areas of low temperature.

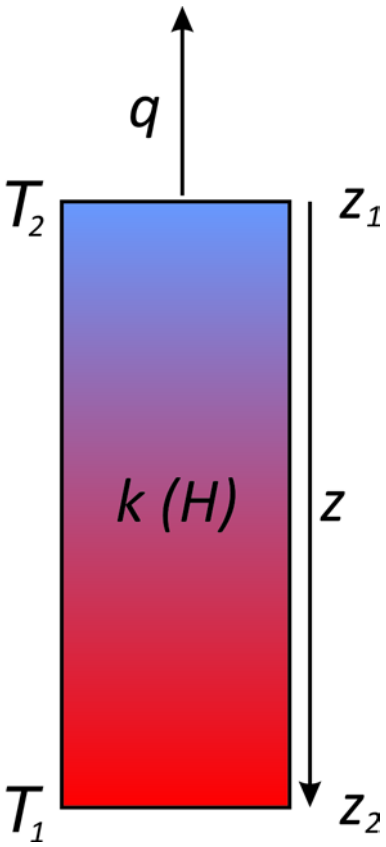

Figure 2.6: Conductive heat flow. A column of material which is hot at its base and cold at the surface, like a column of continental crust, will experience heat flow from the hot area to the cold area. The heat flow out of the surface *q* will depend on the difference in temperature *T* between the top and bottom, the distance *z* between them and the coefficient of conduction of the material. If the material contains radioactive elements the heat produced by radioactive decay *H* will also need to be taken into account.

The necessity of this can be seen when equation 2.15 is expanded with the notation from Figure 2.6.

$$q = -k\frac{T_2 - T_1}{z_2 - z_1} \quad (2.16)$$

The top line of the equation $(T_2\text{-}T_1)$ will be negative even though the heat is flowing in the same direction as increasing z. One of the major differences between oceanic crust and continental crust is the abundance of radioactive elements

The next step needed for the modelling is to look at how the heat flow into and out of a block of material changes through time. Conservation of energy applies even though equation 2.16 is a 1D representation of a 3D situation because the basins are so large that lateral temperature gradients are minor. Therefore conservation of energy can be used to formulate this problem. Figure 2.7 shows that the difference between the heat flow into and out of the material over a

given time must equal the amount of heat energy taken in or given out by the material to change its temperature over that time.

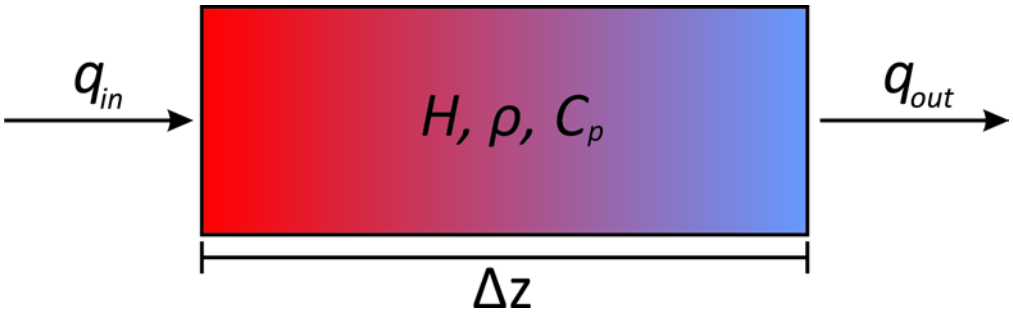

Figure 2.7: Heat flow with time. The heat flow out q_{out} of a material with a length of Δz over a certain time must be equal to the heat flow into q_{in} the material minus the heat energy lost heating the material plus the heat energy given out by radioactive decay *H*. The heat energy taken into the material is controlled by the specific heat of the material C_p and its density *ρ*.

Equation 2.17 expresses this.

$$\rho C_p \frac{dT}{dt} = \frac{q_{in} - q_{out}}{\Delta z} \quad (2.17)$$

C_p is the specific heat, which is a measure of the energy needed to increase 1 kg of the material by 1 ˚C and *dt* is the time that has passed. Fourier's equation (2.15) can then be substituted in for q_{in} and q_{out}.

$$\rho C_p \frac{dT}{dt} = \frac{-k\frac{dT_{in}}{dz} - (-k\frac{dT_{out}}{dz})}{\Delta z}$$

$$\rho C_p \frac{dT}{dt} = \frac{k(dT_{out} - dT_{in})}{\delta z^2}$$

$$\rho C_p \frac{dT}{dt} = \frac{\delta}{\delta z}\left(k\frac{\delta T}{\delta z}\right)$$

A term for the radioactive heat production *ρH* should also be introduced when dealing with continental crust, where H is the radioactive heat production rate per kg of material and ρ is the density of the material. When the equation is rearranged to give the change in temperature over time equation 2.18 is produced.

$$\frac{dT}{dt} = \frac{1}{\rho C_p}\frac{\delta}{\delta z}\left(k\frac{\delta T}{\delta z}\right) + \frac{H}{\rho C_p} \quad (2.18)$$

2.3.2 Calculating the subsidence

Once the temperature of the column has been calculated it is possible to calculate the density of the material in the column using the relationship in equation 2.19.

$$\rho = \rho_0\big(1 - \alpha(T - T_0)\big) \quad (2.19)$$

Where ρ_0 is the reference density of the material at a reference temperature T_0, and α is the coefficient of thermal expansivity. The density profile of the column is needed to calculate the height of the column relative to sea-level. The elevation of the column is then calculated using isostacy. However, to do this the column in the model must be compared to a column of material where the composition is well understood and is believed to be in isostatic equilibrium.

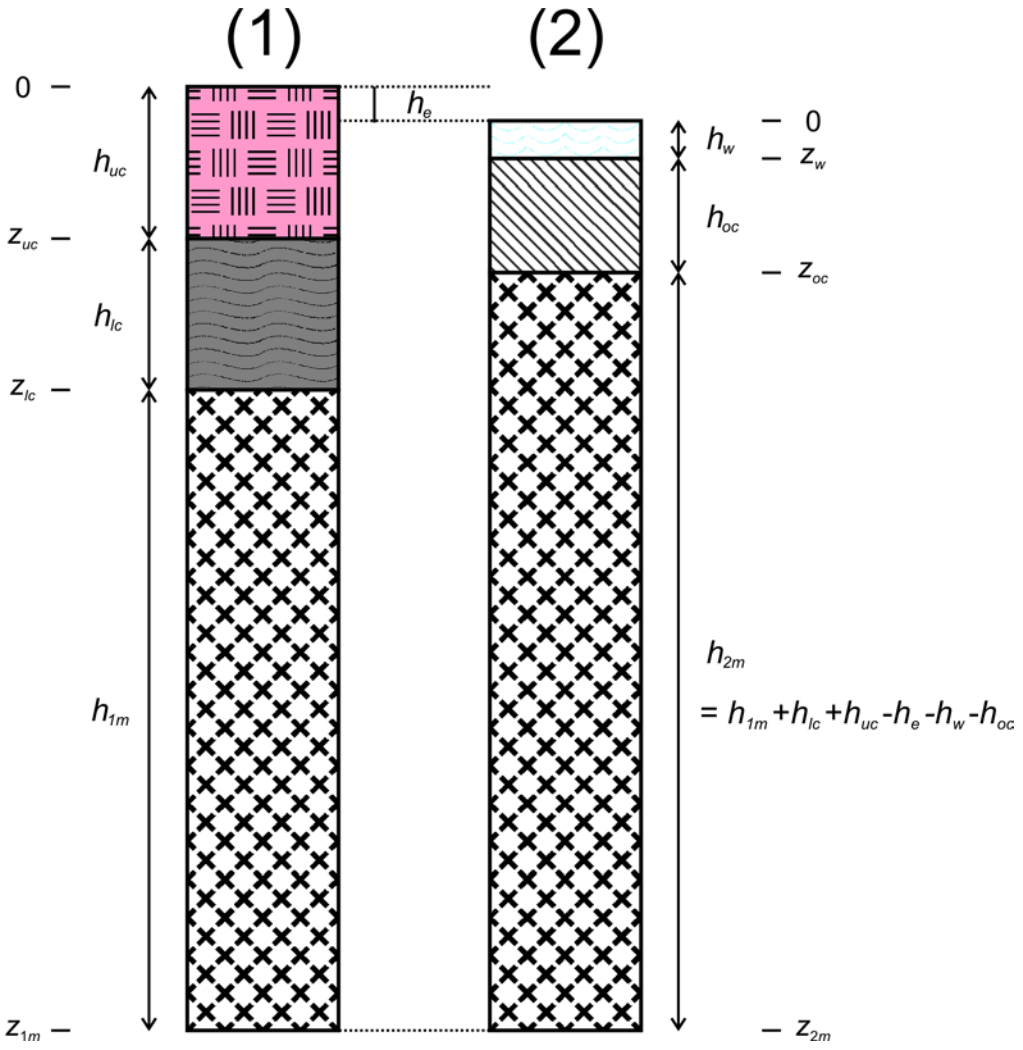

Figure 2.8: Elevation of the model. Column (1) represents the model. It is composed of upper crust h_{uc}, lower crust h_{lc} and mantle lithosphere/upper mantle h_{1m}. To calculate the elevation of the column it is assumed to be in hydrostatic equilibrium with column (2) which is a slice through a mid ocean ridge. It is composed of sea water h_w, oceanic crust h_{oc} and upper mantle h_{2m}. An alternative way of expressing the thickness of the mantle in column 2 is also shown, which is important for calculating h_e as shown in the text.

The mid-ocean ridge was chosen for this purpose as it has a well understood structure which is consistent around the globe. On average there is a water depth of 2.7 km overlying a 7 km thick crust composed of basalt, gabbro and mafic cumulates and is directly underlain by depleted upper mantle. The temperature profile through it can be simplified to a temperature of ~ 5 ˚C in the water column, which then increases linearly to upper mantle temperatures (~1300˚C) at the base of the crust and then increases along the adiabatic gradient. The two columns being compared are shown in Figure 2.8. The column of mid ocean ridge material is compared to the column of material from the model. This has an upper and lower crust composed of different rock types which overlie depleted peridotite. This can be part of the lithosphere or the upper mantle depending on its temperature because its rheology is temperature dependant. Using Airy isostasy the elevation of the modelled column can be calculated by using equation 2.20. This process of using isostacy is similar to that used to calculate the bathymetry away from a mid ocean ridge in the half space cooling model (Turcotte and Schubert, 2002) or plate model (Stein and Stein, 1992). The working required to reach equation 2.20 from the information displayed in Figure 2.8 and described above is shown below. Starting with the statement that the weight of both columns are balanced it is then rearranged to get an expression for the elevation h_e.

$$column\ (1) = column\ (2)$$

$$h_{uc}\rho_{uc} + h_{lc}\rho_{lc} + h_{1m}\rho_{1m} = h_w\rho_w + h_{oc}\rho_{oc} + h_{2m}\rho_{2m}$$

$$h_{uc}\rho_{uc} + h_{lc}\rho_{lc} + h_{1m}\rho_{1m} = h_w\rho_w + h_{oc}\rho_{oc} + (h_{uc} + h_{lc} + h_{1m} - h_e - h_w - h_{oc})\rho_{2m}$$

$$h_{uc}\rho_{uc} + h_{lc}\rho_{lc} + h_{1m}\rho_{1m} = h_w\rho_w + h_{oc}\rho_{oc} + h_{uc}\rho_{2m} + h_{lc}\rho_{2m} + h_{1m}\rho_{2m} - h_e\rho_{2m} - h_w\rho_{2m} - h_{oc}\rho_{2m}$$

$$h_e = \frac{h_w(\rho_w - \rho_{2m}) + h_{oc}(\rho_{oc} - \rho_{2m}) + h_{uc}(\rho_{2m} - \rho_{uc}) + h_{lc}(\rho_{2m} - \rho_{lc}) + h_{1m}(\rho_{2m} - \rho_{1m})}{\rho_{2m}}$$

However, the density of the column does not only vary with the rock type, but also with the temperature of the rock. The temperature varies with depth; therefore it is necessary to integrate the equation over the depth ranges to account for variation of density with depth in the two columns.

$$h_e = \frac{\int_0^{z_w}(\rho_w - \rho_{2m})dz + \int_{z_w}^{z_{oc}}(\rho_{oc} - \rho_{2m})dz + \int_0^{z_{uc}}(\rho_{2m} - \rho_{uc})dz + \int_{z_{uc}}^{z_{lc}}(\rho_{2m} - \rho_{lc})dz}{\rho_{2m}} + \frac{\int_{z_{lc}}^{z_{1m}}(\rho_{2m} - \rho_{1m})dz}{\rho_{2m}}$$

Both ρ_w and ρ_{oc} form part of the mid ocean ridge (column 2, from Fig. 2.8) and can therefore be substituted by ρ_{MOR}. ρ_{MOR} is the density of the mid ocean ridge column at a specified depth and depends on the rock type and temperature. Likewise ρ_{uc} , ρ_{lc} and ρ_{1m} make up column (1), from Fig. 2.8, so can be substituted with ρ_1 (the density profile with depth for column 1). This simplifies the notation in the equation above significantly.

$$h_e = \frac{\int_0^{z_{oc}} (\rho_{MOR} - \rho_{2m}) dz + \int_0^{z_{1m}} (\rho_{2m} - \rho_1) dz}{\rho_{2m}} \quad (2.20)$$

2.3.3 Discretising the equations

In reality the modelled column is a continuous body of material with an initial temperature profile through it as shown in Figure 2.9 a).

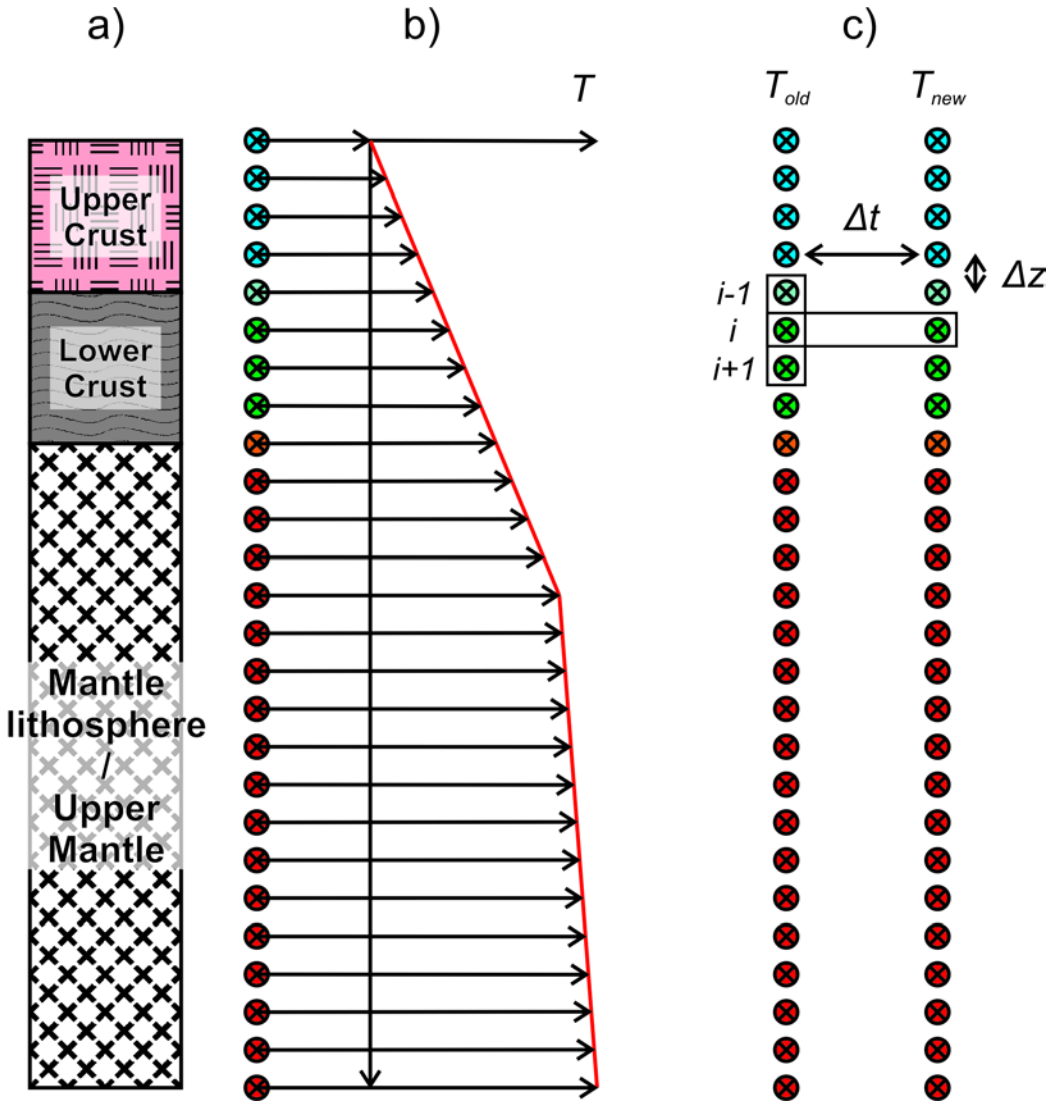

Figure 2.9: Schematic outline of the forward modelling code. a) is the column through the crust and mantle the model aims to describe. b) shows the set up of the model as a set of discrete points

representing the different materials and how the initial temperature conditions are mapped onto these points. c) visually shows the process of calculating the evolution of the temperature through time.

However, for the purpose of computer modelling it needs to be treated as a finite number of discrete points. The spacing between the points needs to be fine enough to adequately describe the changes in composition and temperature within the column. However, there is a trade off because using more points makes the code more computationally intensive. In the forward model the distance between each point Δz is 1000 m. This value was chosen for Δz because it gives sufficient coverage over the column of material being investigated and is a round number and therefore is easy to work with. The initial temperature conditions are then mapped onto the points as shown in Figure 2.9 b). Each point is then assigned the correct constants for the rock type it represents. The values used and the corresponding references are shown in Table 2.2. The top and bottom point are the boundary points and these have a prescribed temperatures which are kept constant throughout the modelling process. This is because both of these points are on the edge of the model so do not have a point either side, which makes it impossible to calculate the temperature through time using equation 2.18. In the case of the top point this is the surface temperature and therefore it is kept constant at 5 ˚C. The bottom point equates to a point just within the upper mantle and therefore its temperature depends on its depth (or the thickness of the model). How this is calculated is described in more detail in the following chapter.

	Reference density (ρ_0) kgm^{-3}	Radioactive heat production (H) Wkg^{-1}	Coefficient of thermal expansion (α) K^{-1}	Specific heat (C_p) $J\ kg^{-1}K^{-1}$	Coefficient of conductivity (k) $Wm^{-1}K^{-1}$
Sediments (ρ_s)	2200				
Basalt (ρ_{oc})	2900	0.6×10^{-6}	2.4×10^{-5}	790	3.1
Upper crust (ρ_{uc})	2700	1.31×10^{-6}	2.4×10^{-5}	790	3.1
Lower crust (ρ_{lc})	2900	0.6×10^{-6}	1.6×10^{-5}	790	2.1
Upper mantle peridotite (ρ_m)	3300	0.006×10^{-6}	3.3×10^{-5}	790	3.3

Table 2.2: Material parameters for various rocks used in the forward models. Values for density are taken from Allen and Allen, (2005), the values for heat production, α and C_p and k are from Shaw et al., (1986) and Turcotte and Schubert, (2002).

The next step is to calculate the evolution of the temperature after a time step Δt for each point from the temperature of the previous points using equation 2.18 (Fig. 2.9 c).

The left hand side of equation 2.18 is simple enough to discretise as *dT* becomes the difference between the new and old temperature of a point and *dt* becomes the time step. Discretising the right hand side of the equation is not so straight forward because there are 3 choices for the δT. The old temperature at the point T_{old} could be used, which is known as the forward Euler method or the new temperature T_{new}, which is known as the backwards Euler method or an average of the two which is known as the Crank-Nicholson method. The forward Euler method under predicts the result whereas the backwards Euler tends to over predict the result. The Crank-Nicholson lies between the two. This is exaggerated at large time steps, but the three methods approach each other as the time step is reduced. Using T_{new} for δT as in the backward Euler or Crank-Nicholson is complex because T_{new+1} and T_{new-1} have not been calculated when trying to calculate T_{new}. The temperature for every point in the column must be calculated simultaneously using matrices and vectors. Therefore the forward Euler method was used with a small time step of 10 000 yrs to minimise the systematic errors described above. This leads to equation 2.18 being modified as shown to give equation 2.21.

$$\frac{T_{(i)}^{new} - T_{(i)}^{old}}{\Delta t} = \frac{1}{\rho_{(i)} C_{p(i)}} \left[\frac{k_{(i+1/2)} \left(T_{(i+1)}^{old} - T_{(i)}^{old} \right) - k_{(i-1/2)} \left(T_{(i)}^{old} - T_{(i-1)}^{old} \right)}{\Delta z^2} \right] + \frac{H_{(i)}}{C_{p(i)}}$$

$$T_{(i)}^{new} = T_{(i)}^{old} + \frac{\Delta t}{\rho_{(i)} C_{p(i)}} \left[\frac{k_{(i+1/2)} \left(T_{(i+1)}^{old} - T_{(i)}^{old} \right) - k_{(i-1/2)} \left(T_{(i)}^{old} - T_{(i-1)}^{old} \right)}{\Delta z^2} \right] + \frac{\Delta t H_{(i)}}{C_{p(i)}} \quad (2.21)$$

This shows the temperature at the i^{th} point depends on the temperature of the point at the last time step and the temperature of the point on either side of it (see fig 2.9 c). The values for the constants are taken from Table 2.2 and vary according to the rock type.

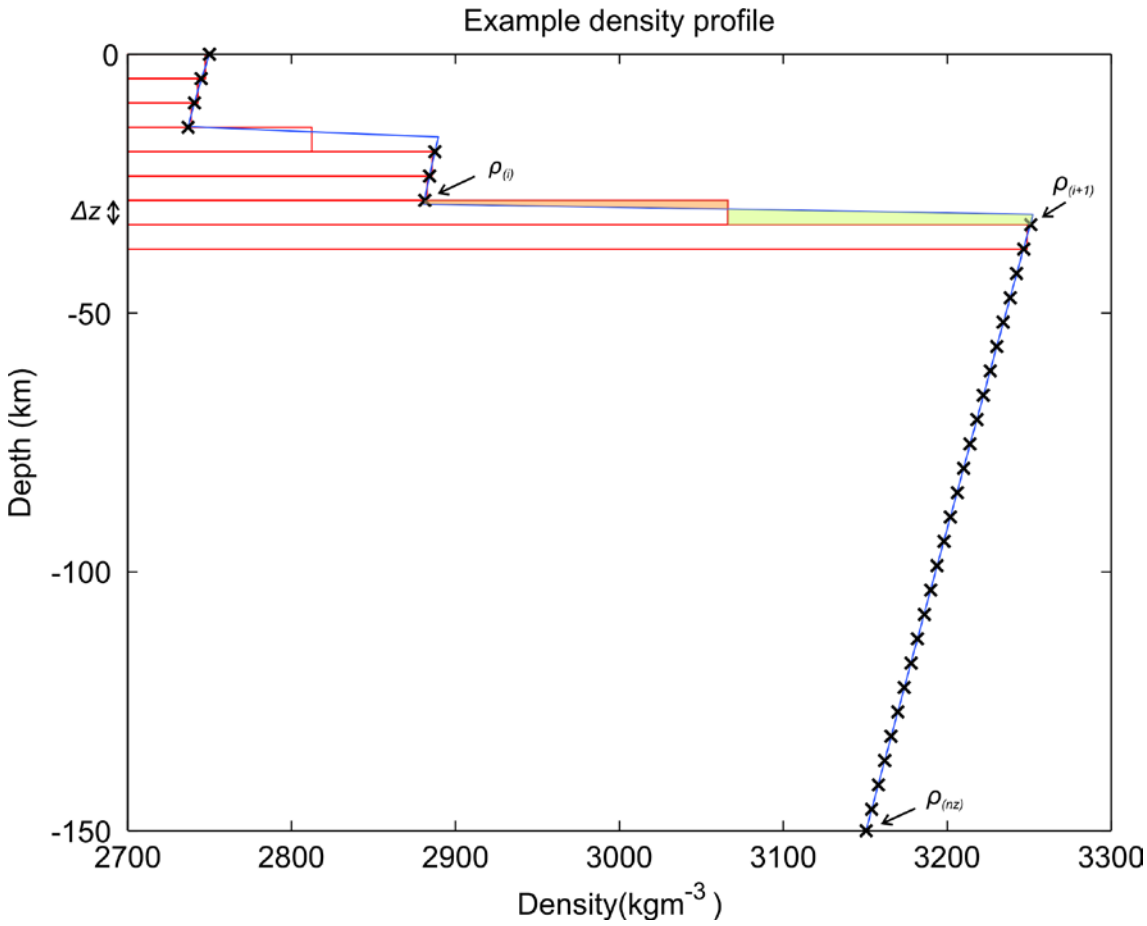

Figure 2.10: The trapezium method. This shows the process of going from an analogue density profile to calculating the area beneath the density profile from a set discrete points like that used in the modelling. The area is split into a set of rectangles which approximate the area under the curve because while part of each rectangle will lie above the curve (orange shaded area) an almost equal sized part of it will also lie beneath the curve (green shaded area). The discrete points shown are actually further apart than those shown in the model and each jump in the density would have a point directly on either side.

Once the temperature for each point has been calculated the density for each point is given using equation 2.19 and produces a profile like that in Figure 2.10. To calculate the elevation the area under the curve needs to be integrated as in equation 2.20. To do this for a set of discrete points the trapezium method was used, which replaces the area under the curve with a series of rectangles which lie between the points on either side (Fig. 2.10). These have a length that is an average of the two points on either side and a width of *dz*. When the areas of the rectangles are summed up it approximates the area under the curve reached by integration because although part of each rectangle lies above the curve an approximately equal area lies underneath the curve as demonstrated in Figure 2.10. This can be expressed as

$$\int_{0}^{150} \rho \, dz \approx \sum_{i=1}^{nz-1} \frac{(\rho_{(i)} + \rho_{(i+1)})}{2} \Delta z$$

This can then substituted into equation 20 to give

$$h_e = \frac{\sum_{i=1}^{oc-1} \frac{(\rho_{MOR(i)} - \rho_{2m(i)}) + (\rho_{MOR(i+1)} - \rho_{2m(i+1)})}{2} \Delta z}{\rho_m}$$

$$\frac{+ \sum_{i=1}^{m-1} \frac{(\rho_{2m(i)} - \rho_{1(i)}) + (\rho_{2m(i+1)} - \rho_{1(i+1)})}{2} \Delta z}{\rho_m} \quad (2.22)$$

which numerically calculates the elevation of the model column. When the elevation of the column becomes negative i.e. the column drops below sea level, another term needs to be added to equation 2.22 to calculate the effect of this depression being filled with either sediment or water. This is very similar to the process of calculating the tectonic subsidence in backstripping except that instead of replacing sediment with water, air is replaced with water or sediment.

2.3.4 Description of the key points in the computer code

An example of the code used to investigate the subsidence in the West Siberian Basin is shown in Appendix B and follows a similar pattern to the backstripping code. The first section of the code inputs the values for the necessary parameters and sets up the initial conditions of the model. The first step in the program is to set up the dimensions of the model and the length of time that the model is to run over. The initial conditions of the model are then input. Firstly the thickness of each of the rock layers is specified; in this case a layer of flood basalts, then a two layer crust and mantle lithosphere that has been thinned by a plume head. The inputs are entered initially as values in metres to make it easier for the user before being converted into the corresponding coordinates within the array. The initial temperature profile is then calculated from the chosen potential temperature and plume temperature and saved in the T^{old} array. Arrays are then set up for each parameter *k,* C_p*, H,* and ρ_0*.*The values used for the different rock types are taken from Table 2.2. These are taken from a variety of laboratory measurements or from global studies of the continental crust and can be easily updated with new data when new studies are carried out. Figure 2.11 shows an example of the initial set up for a model run in the West Siberian Basin. The code is written so that an individual point in any array e.g. the 50th number in the depth array will correspond to the 50th point in the *k* array and the T_{old} array e.t.c. The conditions of the mid ocean ridge reference column used in the isostacy calculations are also input in this part of the code. Arrays are also prepared for the

output data to be entered into. The reason for doing this is so that the computer sets aside this amount of memory.

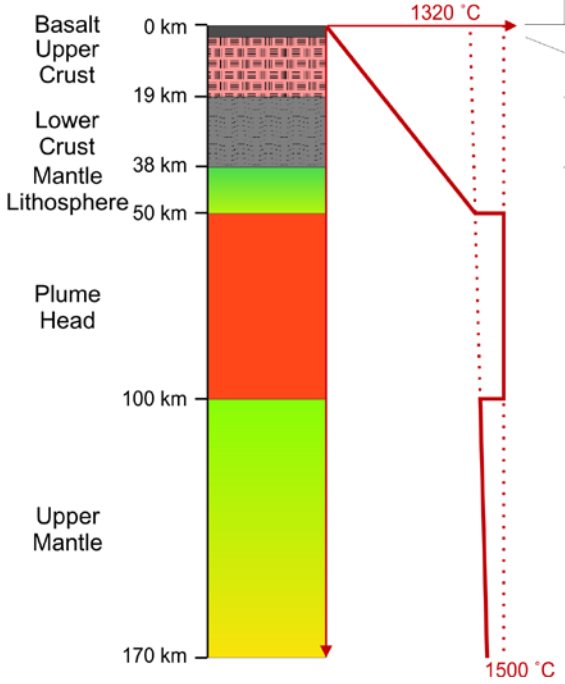

ρ_0 (kgm^{-3})	H (Wkg^{-1})	α (K^{-1})	k (Wm^{-1}K^{-1})	Cp (Jkg^{-1}K^{-1})
2900	0.6 x 10^{-6}	2.4 x 10^{-5}	3.1	790
2700	1.31 x 10^{-6}	2.4 x 10^{-5}	3.1	790
2900	0.6 x 10^{-6}	1.6 x 10^{-5}	2.1	790
3300	0.006 x 10^{-6}	3.3 x 10^{-5}	3.3	790

Figure 2.11: The initial set up of the model showing the structure, temperature profile and the material properties of the different layers in the model from Appendix B. In the West Siberian Basin the subsidence of a basin due to the cooling of a plume head is being investigated. This figure demonstrates that though the plume head and the base of the lithosphere are not compositionally different, they are defined by temperature instead.

The calculations are carried out largely as described in section 2.3.3. except that equation 2.21 and 2.22 are broken down into a number of sections. This was done so that each section could be evaluated to ensure it was giving the correct answer and to identify any mistakes in the syntax. When the subsidence was calculated new points are not added to the column for the sediment or water layer. This means the temperature is not calculated within the water or sediment. Instead they are treated as a layer with a uniform temperature and a single density value that is used in calculations of the subsidence. While the code could add new points to the array, conductive heat flow is not applicable to either a sedimentary column or water column because convection dominates in water even at low temperatures. In both cases the heat energy is transferred by flow of water, however, in the case of sediments this is through the pore space. When the sediment loaded subsidence is calculated the sedimentation is assumed to keep pace with the subsidence. The validity of this assumption depends largely on the sediment supply to the basin. In the majority of cases looked at in chapters 3-5, the

shallow water depth the sediments are deposited in shows that the influx of sediments to the basin kept pace with the subsidence of the basin floor and therefore this is a perfectly valid assumption.

The outputs are not limited to the end of the code. This is because they are used to check that the different sections of the code are operating properly. Therefore the initial conditions are plotted and the temperature profile is calculated every 10 time steps (100 000 yrs) to make sure it is evolving as expected. This creates an animation showing the cooling of the thermal anomaly. The primary output of the code is the water loaded and sediment loaded subsidence curves, but the heat flow and lithospheric thickness are also output. The heat flow is that from the basement rocks of the basin not the surface heat flow. This is a useful input for detailed basin modelling such as that carried out in the oil industry. Consequently the heat flow from the best fitting model of the Kufrah basin in chapter 3 was used internally by Statoil Hydro to assess the petroleum potential of the basin. This is an improvement on the heat flow data often used in these models which is generally hypothetical. It may be based on knowledge of the tectonic history, but is essentially an informed guess e.g. (Makhous and Galushkin, 2003). Alternatively the basin is assumed to form by rifting and heat flow from a rift model is used (Van Wees et al., 2009). Using this model means it is possible to determine which formation mechanism fits the subsidence patterns of the basin best and therefore use the most appropriate heat flow. To output the base of the lithosphere the 1200˚C isotherm was used as a proxy, (Turcotte and Schubert, 2002). 1200˚C represents the approximate temperature above which upper mantle material will transfer heat through convection rather than conduction. This allows the model results to be tested against other observations such as measurements of lithospheric thickness from measurements of shear wave velocities (Priestley and McKenzie, 2006), modelling of long-period surface wave dispersion (Pasyanos, 2010) or from deep seismic refraction profiles e.g. (Morozova et al., 1999). This helps to constrain the different parameters used as inputs for the model and therefore makes the results more robust. The primary output, the water loaded subsidence curve, is used for comparison to the backstripped subsidence curves to see what initial conditions and parameters provide the best fit. To facilitate this, the backstripped subsidence curves can be loaded into the program and plotted alongside the model curves.

Chapter 3 - Lithospheric cooling and thickening as a basin forming mechanism: A case study from the Palaeozoic basins of North Africa

3.1 Introduction

Conventional basin formation mechanisms can be divided into two categories, lithospheric stretching followed by thermal subsidence proportional to the extension (rift basins) and flexure caused by tectonic loading (foreland basins) (Allen and Allen, 2005). However, there is scant evidence for either of these mechanisms forming a group of basins normally classified as "intracontinental sags" – a term that describes their geometry rather than the process of formation. Examples include the Williston and Michigan basins of North America (Klein, 1995), the Palaeozoic basins of North African and Arabia (Boote et al., 1998; Konert et al., 2001); and the Mesozoic Scythian and Turan platforms (Natal'in and Şengör, 2005). The basins are large features, commonly over 1000 km in length, with remarkably uniform, prolonged, gentle subsidence across them, lasting over 200 Myrs. They generally have a polyphase history with a main subsidence phase either preceded or followed by other periods of subsidence and uplift which modify the basin. Armitage and Allen, (2010) recently proposed that these basins are formed by stretching under low strain rates. They argued this based upon the modelling of rifting under low strain rates and the observation that the initiation of subsidence in many intracontinental basins coincides with supercontinent breakup and therefore a broad extensional regime. However, in many basins the evidence for rifting is poor; the imaged rifts are too small to account for the subsidence across the basin or no rifts have been discovered. Therefore a number of other mechanisms have been proposed. Subsidence due to cooling of thermal anomalies in the

lithosphere has been proposed for the North American intracontinental basins (Kaminski and Jaupart, 2000). The main evidence for this is matching modelling results with the shape and thickness of the present day sedimentary cover. A density change in the crust due to phase changes such as a basalt underplate changing to eclogite has also been suggested based on high velocities in the lower crust interpreted from seismic refraction data (Artyushukov, 2005). However, beneath the Barents/Kara sea region a high density area in the lower crust, suggested by modelling gravity data, has been deemed too local to cause subsidence across the basin. Instead Ritzmann and Faleide, (2009) have suggested that a deeper high velocity zone visible in seismic tomography is evidence of a thick cratonic lithosphere, which causes the subsidence. Heine et al. (2008) noted that many intracratonic basins overlie areas of mantle which have been down welling over the last 100-150 Myrs in their coupled plate and mantle flow model. They proposed that dynamic topography could form these basins. Other subsidence mechanisms and variations on those above have been suggested and are debated in more detail by Armitage and Allen (2010) and Klein (1995) and in the chapter 1 of this thesis. It is likely that one mechanism does not explain the formation of every intercontinental basin and in some cases the basin may be formed by a combination of mechanisms.

This chapter demonstrates that cooling and thickening of initially thin mantle lithosphere, beneath crust of normal thickness (~30 km) is a viable mechanism for producing basin-scale subsidence. Such initial conditions are typical of accretionary crust, a term used to summarise the vast orogenic collages of largely juvenile crust and mantle lithosphere, formed by the collision of non-cratonic terranes: island arcs, accretionary prisms, ophiolites and isolated microcontinents (Murphy and Nance, 1991; Şengör et al., 1993). This would neatly explain the formation of many of the intracratonic basins on juvenile continental crust such as the Pan African mobile belt or the Scythian and Turan platform. However, this chapter also shows that where the lithosphere is thinned by a thermal anomaly it is also possible to form broad, slowly subsiding basins.

The proposed subsidence mechanism is discussed in greater detail in section 3.2 below, followed by a case study of two of the North African Palaeozoic basins. Thermal subsidence has been suggested as the cause of intracratonic basins before (Guiraud et al., 2005; Kaminski and Jaupart, 2000; Kominz, 1995). The contribution of this study is to model the subsidence, compare it to subsidence from two case studies and to discuss why the lithosphere is plausibly thin in the first place. The subsidence histories of the basins are analysed using backstripping. This analysis is compared to results from a

numerical forward model of thermal subsidence acting on accretionary crust, designed to test if it is a mechanism capable of producing the observed subsidence.

3.2 Geological background and hypothesis

Seismic refraction studies show that present day island arcs can have a crustal thickness of 25-35 km, similar to normal continental crust (Holbrook et al., 1999; Takahashi et al., 2007). However, seismic tomography shows slow velocities in the mantle wedge below island arcs which are interpreted as evidence for the presence of melts and thin (~20 km) mantle lithosphere because it is weakened by the addition of fluids from the subducting slab and then eroded by the corner flow in the mantle wedge (Gorbatov et al., 1999; Zhao et al., 1994). This is supported by numerical models of subduction (Arcay et al., 2006; Stern, 2002; van Keken, 2003), by geochemical evidence from the southward initiation of the Philippine subduction zone (Macpherson, 2008) and from the Cascades (Elkins Tanton et al., 2009). These studies suggest an average overall lithospheric thickness of about 50 km beneath island arcs and continental arcs (Fig. 3.1a).

Accretionary prisms may be 30 km thick, largely composed of off-scraped and imbricated fragments of oceanic crust and its sedimentary cover. Whilst subduction is active such prisms are underlain by the oceanic plate. When subduction has recycled the oceanic plate in to the mantle, the base of the prism may be in contact with the asthenosphere, particularly if ocean closure resulted in the collision of two such prisms, initially on opposite sides of the ocean, rather than collision of the prism with a continental margin. The Cenozoic East Anatolian Accretionary Complex may be an example of such a lithospheric structure, where tomographic studies suggest a thin or even absent mantle lithosphere (Zor et al., 2003).

A notable feature of accretionary orogenic belts is that they often lack evidence for substantial crustal thickening (and presumably lithosphere thickening): there is rarely evidence for pre-collision passive continental margins indicating the collision of two large continental blocks, Alpine-type nappes, or overfilled foreland basins (“molasse”) (Şengör and Okurogullari, 1991). This means that putative lithospheric delamination following an orogeny of this type, as hypothesised by Ashwal and Burke, (1989), is not our preferred mechanism for thinning the lithosphere. However, it would produce similar starting conditions to those in the model proposed by this study.

As accretionary crust is assembled through subduction and collision, the thin mantle lithosphere of the original terranes is inherited by the final collage (Fig. 3.1b). I hypothesise that once accretion is completed, and subduction has ceased beneath an area, the underlying asthenosphere will cool, thickening the mantle lithosphere. This cooling will cause prolonged subsidence, forming basins (Fig. 3.1c).

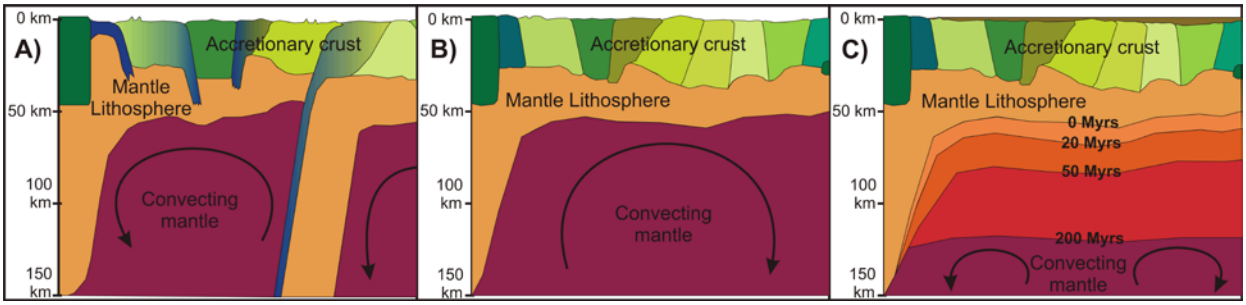

Figure 3.1: Formation of accretionary crust and subsequent lithospheric thickening and subsidence. a) Assembly of accretionary crust from island arcs and other crustal fragments through subduction. b) Newly formed accretionary crust with a thinned lithosphere. c) Lithospheric thickening due to cooling causing subsidence.

The proposed model is similar to the thermal subsidence phase of McKenzie style rifting (McKenzie, 1978) or the subsidence of the ocean floor away from a mid ocean ridge, except that the crust involved is continental, albeit juvenile, and has not been thinned in any way. This chapter will proceed to show how this mechanism could produce the basins in North Africa. However, there are many other intracratonic basins on accreted crust where this mechanism could apply. Table 3.1 provides a sample of some of the basins I am aware of, but is by no means an exhaustive list. Allen and Armitage, (2011) note a clustering in time of the initiation of intracratonic basins which they link to the breakup of supercontinents. Table 3.1 shows that the start of the subsidence within the basins closely follows the end of accretion and the clustering may be related to the end of periods of accretion of crust. The basins are long lived features and so many have later phases of subsidence which potentially have other causes.

Basin Name	End of basement accretion	Beginning of platformal subsidence
South America	~510 Ma (Cordani and Teixeira, 2007)	
Parnaíba Basin		Silurian (Oliveira and Mohriak, 2003) ≤ 444 Ma
Paraná Basin		Ordovician (Brito Neves, 2002; Zalán et al., 1990) ≤ 488 Ma
Choco-Paraná Basin		Ordovician (Brito Neves, 2002) ≤ 488 Ma
North Africa	~550 Ma (Caby, 2003)	
Mouydir Basin		Cambrian (Boote et al., 1998) ≤ 542 Ma
Ahnet Basin		Cambrian (Boote et al., 1998) ≤ 542 Ma
Reggane Basin		Cambrian (Boote et al., 1998) ≤ 542 Ma
Ghadames Basin		Cambrian (Boote et al., 1998) ≤ 542 Ma
Al Kufrah Basin		Cambrian (Boote et al., 1998) ≤ 542 Ma
South Africa	~550 Ma (Bumby and Guiraud, 2005)	
Cape Basin		Cambrian (Tankard et al., 2009) ≤ 542 Ma
Arabia	~550 Ma (Stern, 1994)	
Arabian Platform		Cambrian (Konert et al., 2001) ≤ 542 Ma
Central Asia	~210 Ma (Natal'in and Şengör, 2005)	
Scythian Platform		Jurrassic (Natal'in and Şengör, 2005) ≤ 200 Ma
Turan Platform		Jurrassic (Natal'in and Şengör, 2005) ≤ 200 Ma
Eastern Australia	~250 Ma (Glen, 2005)	
Eromanga Basin		Jurassic (Gallagher et al., 1994) ≤ 200 Ma
Surat Basin		Jurassic (Gallagher et al., 1994) ≤ 200 Ma

Table 3.1: Compilation of intracratonic basins situated on accretionary crust from around the world. The table shows their locations and the temporal link between the end of the accretion event forming the underlying crust and the beginning of subsidence across the basin as a whole.

3.3 Tectonic subsidence history of backstripped North African basins

In order to test whether the proposed mechanism of subsidence provides a good explanation for anomalous basins developed over accretionary crust, subsidence histories for the Ghadames and Al Kufrah basins were investigated using backstripping. These are Palaeozoic basins situated on the North African crust, which was accreted in the Pan African orogeny during Neoproterozoic times (Caby, 2003; Stern, 1994). Most of the basement to North Africa and Arabia is juvenile, generated and assembled during the Pan African orogeny. The western margin is the West African Craton. The southern limit is the Congo Craton. The eastern and northern limits are not so well defined because of later rifting and collision with Eurasia. For example, similar basement underlies much of the territory of Iran, but with a

more complicated Mesozoic and Cenozoic magmatic and tectonic history. The outcrop or sub-Mesozoic subcrop of the Palaeozoic strata of North Africa and Arabia is shown in Figure 3.2.

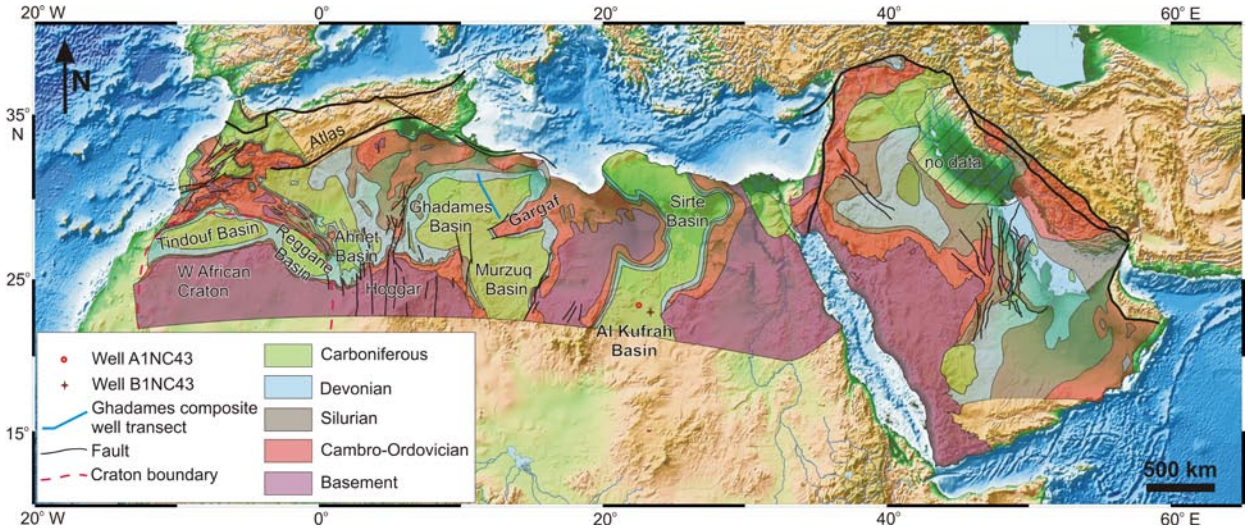

Figure 3.2: Present day outcrop and sub-Mesozoic subcrop of Palaeozoic sediments across North Africa and Arabia (Boote et al., 1998; Konert et al., 2001). Four wells used to construct the Ghadames composite well are located along the line of the transect shown.

The proportion of cratonic nuclei within this vast, 10,000,000 km^2 orogen is debated, but plausibly is small. There are indications of pre Late Proterozoic crust within North Africa, based on Meso- or Palaeo-Proterozoic isotopic model ages and detritial zircons in younger metamorphic terranes (Black et al., 1993; Sultan et al., 1990). However, the Late Proterozoic tectonic overprint is severe; suggesting that extensive magmatic and metamorphic re-working and additions took place during the Pan African orogeny, and no single, regionally extensive block survived the Late Proterozoic orogeny with its original structure and boundaries preserved. An older significantly re-worked region called the Saharan metacraton has been proposed (Abdelsalam et al., 2002), but this is not recognised by all workers e.g. (Bumby and Guiraud, 2005). Whatever the nature and origins of the Saharan metacraton, it appears to have had little impact on the overlying Phanerozoic basins (Fig. 3.2). These are continuous across the metacraton margins, without discernible change in sedimentary thickness or composition.

The end of the Pan African orogeny was diachronous. Local timings for the last deformation vary from Late Precambrian to the Early Cambrian e.g. (Paquette et al., 1998). Present-day lithosphere thickness across North Africa is on the order of ~100 km (Pasyanos and Nyblade, 2007; Priestley and McKenzie, 2006); except for the West African Craton where it reaches >200 km. Crustal thicknesses are not well-

constrained, but are variously estimated at 30 to 40 km thick from gravity and seismic interpretations (Seber et al., 2001), or 25 to 35 km from the inversion of surface waves (Pasyanos and Nyblade, 2007).

The Ghadames Basin is well studied because large hydrocarbon accumulations have been discovered within it (Echikh, 1998). Several wells have penetrated the crystalline basement and there are large amounts of seismic data from the basin. This means the geometry of the basin is well understood. This allows the most complete stratigraphic sections to be identified, which is helpful when backstripping. The Al Kufrah Basin is less well studied and has only two published wells which reached the crystalline basement (Grignani et al., 1991). To a first order, it has a similar Palaeozoic stratigraphy to the Ghadames Basin. Enough well data is available for Al Kufrah to make it viable for modelling.

3.3.1 Methodology

Backstripping is a well known technique for calculating the tectonic subsidence of a particular horizon in a basin over time. I used the basement/cover boundary, which reveals the overall subsidence (Allen and Allen, 2005; Sclater and Christie, 1980). The technique first decompacts each sedimentary layer through time. This gives the total subsidence curve for the basement which is assumed to be composed of the tectonic subsidence, the isostatic effect (weight) of the sediments and the changes in water depth compared to the present day sea level. The effects of the sediments and sea level changes are removed so that the remaining subsidence is due purely to the tectonic driving force. A global eustatic sea-level curve of (Haq and Schutter, 2008) is used to remove the effects of sea-level changes.

The backstripping method assumes that the compaction of the sediments is purely mechanical (due to the weight of the sediments above) and ignores chemical processes, such as cementation, which are very difficult to take into account because they depend on a complex series of factors such as fluid flow, composition, temperature and pressure. Backstripping assumes that the sediments are laid down in successive layers throughout time and does not take into account periods of uplift and erosion or non deposition. These are difficult to include in backstripping because generally the amount of eroded material is poorly constrained. If the present day burial depth of the basement is the deepest it has been, then any erosion will make no difference because the sediments are at their peak pressure. Otherwise the compaction of the sediments will be underestimated. There are no porosity depth relationships available for the sediments in North Africa and so a standard relationship from published work is used (Sclater and Christie, 1980). This assumes that the compaction curves, which are based on

sediments from the North Sea, are applicable to the sediments in North Africa. This is justifiable because the North African sediments are entirely siliciclastic which is similar to those in the North Sea. A more complete description of the backstripping technique can be found in the methodology chapter.

This method was applied to a composite well from the Ghadames Basin. A composite well was used because it gives the most complete section possible from the basin therefore showing the maximum subsidence and limiting the effect of erosion. The composite well was created using four unpublished wells from the transect shown on Figure 3.2, to identify the most complete sections and to ensure that the differences in the thickness of the layers were due to variations in erosion rather than deposition rates. This minimises the errors related to eroded sections of the stratigraphy. It also produces a subsidence curve which emphasises the subsidence phases rather than any uplift. This allows us to see clearly the main subsidence phase associated with basin formation, rather than later phases of uplift or subsidence. The cross section from the Ghadames basin is shown in Appendix C. This approach was not possible in the Al Kufrah Basin because of the scarcity of available well data, and instead the backstripping methodology was applied directly to the two available wells.

3.3.2 General Stratigraphy

Detailed descriptions of the stratigraphy in the Ghadames, Al Kufrah and other North African basins can be found in papers such as Bellini and Massa (1980), Echikh (1998), Fekirine and Abdallah (1998), Grignani et al. (1991) and Lüning et al. (1999). Therefore I only present a brief summary of the evolution of the Palaeozoic basins on the accretionary crust of North Africa collated from Boote et al. (1998), Bumby and Guiraud (2005), Craig et al. (2008), Guiraud and Bosworth (1999) and Guiraud et al. (2005) alongside more detailed observations from the basins themselves. The basins are filled with a largely siliciclastic succession with some evaporites and carbonates towards the end of the Palaeozoic. The whole of North Africa subsided as a large platform from roughly the start of the Palaeozoic, depositing a wedge of sediments that thinned to the south (Selley, 1997). Only localised Late Proterozoic/Early Palaeozoic rifting is known (see Fig. 6 of Guiraud et al. (2005)), and as several of the main basins are mature in terms of hydrocarbon exploration it is unlikely that major rifts have been missed. Seismic lines through the Kufrah Basin show Late Proterozoic/Cambrian rifts (Lüning et al., 1999), however these are only seen on seismic lines in the south of the basin (Ghanoush and Abubaker, 2007) and do not explain subsidence across the whole basin or in neighbouring basins. Nor do the dimensions of the

subsiding area (>>1000 km) fit a flexural, foreland basin mechanism. This point is illustrated by Figure 1.1 in the introduction to this thesis. In any case, there is no record of an appropriate orogeny lasting through the Palaeozoic along the Gondwanan continental margin (Stampfli and Borel, 2002). The initial sediments are largely fluvial sandstones and conglomerates in the Cambrian, changing to marine sandstones in the early Ordovician. The Cambrian age for the earlier sediments is inferred because there are very few trace fossils to date the sediments until the marine incursions (Grignani et al., 1991). In the mid to late Ordovician there was major glaciation creating a regional erosional surface (Le Heron et al., 2010). The amount of erosion varies greatly reflecting the geometry of the ice sheets. Locally in Al Kufrah the erosion cuts down to the Cambrian, but in other areas a complete section to the Mid Ordovician is preserved. In these areas the erosion is minimal and the glaciation reflects a period of non deposition. The erosion becomes less severe to the north into the Murzuq and Ghadames basins (Bellini and Massa, 1980; Fekirine and Abdallah, 1998).

Coarse to medium grained sandstones and tillites related to the retreat of the glaciers were deposited at the end of the Ordovician. This was followed by a major marine transgression leading to the deposition of shales throughout the Early Silurian, but water depths decreased with time and the shales grade up to shoreface sandstones. The shales at the base of the Silurian are one of the main source rocks and record the maximum water depth experienced by the basins during the Palaeozoic. Turner (1978) interpreted it as a shallow shelf environment with water depths of about 200 m. Separation of individual basins began during the Silurian caused by a period of compression most likely related to the Acadian collision (Guiraud and Bosworth, 1999). This resulted in a regional unconformity across the basins of North Africa, but within basins it is localised over arches, such as uplift of the arch between the Ghadames and Murzuq basins (Boote et al., 1998). During the Devonian the basins were filled with shallow marine sandstones and siltstones, and fluvial sandstones, corresponding to fluctuations in sea-level. The transgressions and regressions, as well as prograding systems, can be correlated between basins (Bellini and Massa, 1980). The southern basins (i.e. Al Kufrah) show a greater continental influence compared with the basins further to the north (i.e. Ghadames) (Boote et al., 1998).

Deposition at the start of the Carboniferous was similar to the Devonian, with variations in siliciclastic sediments controlled by sea-level changes, but with some carbonates deposited locally in the Ghadames Basin (Fekirine and Abdallah, 1998). The Palaeozoic sediments were terminated by the Late Carboniferous-Permian Hercynian orogeny, which was an important period of compression, causing uplift along the flanks of many of the basins and forming much of the Palaeozoic subcrop pattern seen

in Figure 3.2. In some areas, such as beneath the Sirte Basin, it eroded down to the Cambrian sediments (Abadi et al., 2008). Mesozoic and Cenozoic tectonics related to the opening and closing of Tethys to the north of North Africa, and the opening of the Atlantic Ocean, modified some of the basin geometries and subsidence patterns.

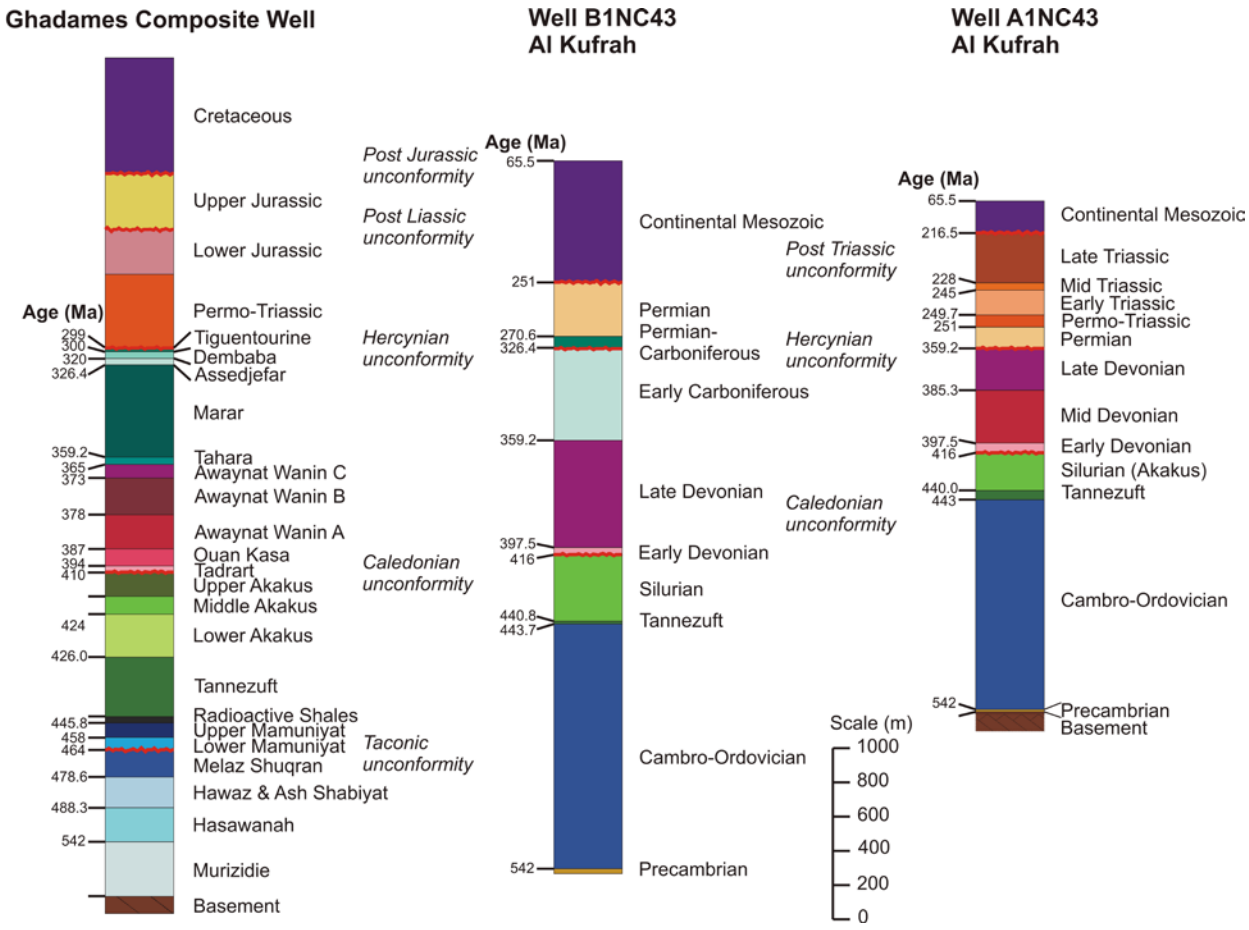

Figure 3.3: Stratigraphy of the Ghadames and Al Kufrah basins used for backstripping analysis. The lithologies of different layers are described in the accompanying text. The Ghadames composite well is constructed from four wells located along the transect shown in Fig. 3.2, to give the most complete sedimentary record. The cross section showing the wells used is found in Appendix C. The locations of the wells from Al Kufrah are also marked on fig 3.2.

The Sirte Basin began forming as a rift basin during the late Cretaceous (100-70 Myrs), and continued to the Early Eocene. Extension was due to far-field stresses related to changes in the spreading rate of the Central and South Atlantic (Guiraud et al., 2005; Janssen et al., 1995). However, this has recently been challenged by Capitanio et al. (2009) who suggest this does not fit the timing of extension, and that a better explanation is that the African plate was placed under tensile stress by avalanching of its

subducted northern edge through the 660 km discontinuity, beneath the Hellenic arc. This basin borders the Murzuq and Al Kufrah basins, but was formed later, and so is not analogous to the basins specifically considered in this study. There is little evidence of similar extension in the surrounding basins at this period as shown by the thickness of the Cretaceous deposits seen in the wells from Figure 3.3. Similar Palaeozoic successions are seen in the Reggane, Ahnet and Tindouf basins to the north of the West African Craton (Boote et al., 1998). The next major event affecting the Paleozoic basins is the Alpine unconformity caused by uplift related to collision of Africa and Europe at the end of the Eocene. See Brunet and Cloetingh (2003) and papers therein for descriptions of the Carboniferous-Recent evolution of basins within northern North Africa and Arabia. These events uplifted the basin margins, and in some areas obscured the earlier subsidence by removing significant thicknesses of sediments. Much of the erosion is focused on the flanks of the basins, although some does occur within the basins, as evidenced by missing Carboniferous section in the well A1 from Al Kufrah (Fig. 3.3). I have sought to minimise the effects of erosion as outlined in our methodology. Details of the stratigraphy for the three wells which were backstripped are shown in Figure 3.3.

3.3.3 Results

Figure 3.4 shows the tectonic subsidence profiles derived from the backstripping. The profiles start at the beginning of the Cambrian, but the precise time of the onset of subsidence is poorly constrained because the sediments are fluvial sandstones, with no fossils. The subsidence rates are fairly rapid to begin with and slow gradually through time with little or no tectonic subsidence during the Mesozoic and Cenozoic (fastest rates are 22.2 m/Myr in Ghadames and 10.1 m/Myr in Al Kufrah). The subsidence profiles are steadily decaying curves without clear separate rift and thermal subsidence phases, i.e. they resemble the thermal subsidence that typically follows rifting, without a rift phase being apparent. The subsidence curves show very little tectonic subsidence affected the basins after 250 Myrs, showing that later periods of subsidence, such as that in the Sirte basin, only slightly modified the Ghadames and Al Kufrah basins. The tectonic subsidence is not smooth; the curves show the periods of erosion and uplift evident in the sedimentary record, e.g. Late Palaeozoic, Hercynian, uplift.

Both basins show very similar tectonic subsidence patterns, both in the timing and the amount of the tectonic subsidence. This is evidence that one causal mechanism generated the Palaeozoic subsidence across North Africa. The total tectonic subsidence in the Ghadames composite well is ~2230 m. This is similar to the ~1740 m of subsidence calculated for the B1NC43 well in the Al Kufrah Basin. As Figure

3.4 shows, well A1NC43 appears to have had less subsidence (~1260 m). However much of the Carboniferous stratigraphy has been removed by the Hercynian deformation, so this lower total is plausibly an effect of erosion rather than differential subsidence.

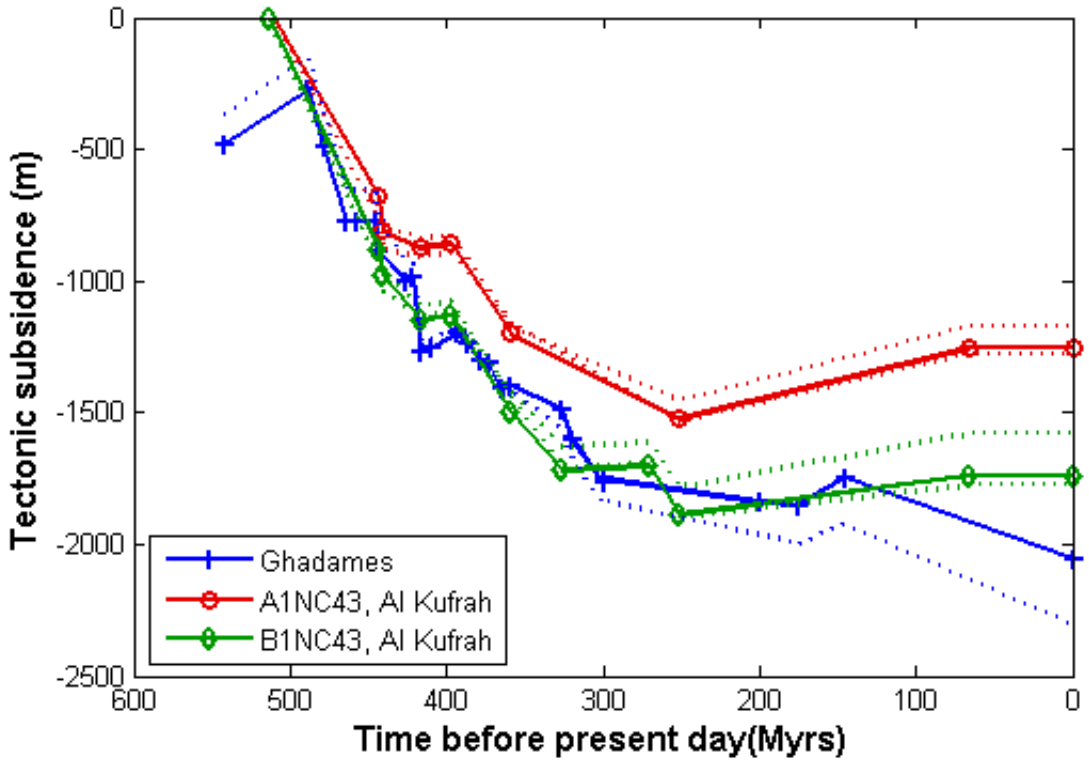

Figure 3.4: Tectonic subsidence curves for the Ghadames and Al Kufrah basins. The solid lines are the tectonic subsidence of the top of the basement and the dotted lines show the subsidence if the stratigraphy is entirely shale or sandstone. This envelope is the maximum possible range of variation in the subsidence possible from varying the proportions of the lithologies.

The uncertainties involved come from the assumptions made in the basckstripping and the input parameters. These include the thickness and depths of the sedimentary layers, which may have uncertainties from errors in picking horizons from well logs or due to erosion. Estimates of these are not provided by Grignani et al. (1991). Assuming that compaction is entirely mechanical also introduces uncertainties. The errors from using the general compaction curves were estimated by carrying out the backstripping with the entire sedimentary column being made of either shale or sandstones which form the two end members of the compaction curves (Sclater and Christie, 1980). Depositional water depth can contribute to large uncertainties because it is difficult to tell the depth of sediments deposited in deep water. As shown in section 3.3.2, in the basins in North Africa this is not such an issue because all

sediments were deposited in shallow waters less than 200 m (Grignani et al., 1991). The uncertainties in water depth estimates for shallow water sediments are much smaller (10s of meters). There are also errors related to corrections for the eustatic sea-level. The largest sea-level fluctuations do not exceed 200 m, so the uncertainties in water depths and eustatic sea-level will have little effect on the overall shape of the curves. The errors from the backstripping calculations are shown as the dashed lines in Figure 3.4. The errors make a negligible difference to both the shape of the curves and the overall amount of subsidence.

3.4 Forward Modelling

Numerical forward modelling of basement subsidence was used to test whether lithospheric cooling and growth is a realistic mechanism for the subsidence of accretionary crust. This is compared to the backstripped results from basins in North Africa to determine if it fits the observed subsidence. The modelling was carried out using Matlab and the code was tested against analytical solutions.

3.4.1 Methodology of the forward modelling

The numerical subsidence model is based on and tested against the plate models for sea floor spreading (Parsons and Sclater, 1977; Stein and Stein, 1992). It is modified to include layered continental crust with radioactive heat production. It solves the vertical conductive heat flow through a one-dimensional column of the lithosphere and upper mantle.

$$\rho C_p \frac{\partial T}{\partial t} = \frac{\partial}{\partial z}(k \frac{\partial T}{\partial z}) + A \qquad (3.1)$$

Equation 3.1 is solved using a finite difference technique with a grid resolution of 1 km. *T* is the temperature of the rock at a particular point in the grid at depth *z*. *A* is the contribution of radioactive heat production and *t* is the time over which the temperature is changing. Time-stepping is performed with an Euler forward time-integration scheme. The material properties of the rock are the thermal conductivity (*k)*, the specific heat capacity (C_p) and the density (ρ). The density of the rock is dependant on the temperature and is calculated using equation 3.2.

$$\rho = \rho_0(1 - \alpha(T - T_0)) \qquad (3.2)$$

In equation 3.2 the reference density (ρ_0) and the coefficient of thermal expansion (α) are dependant on the rock type (Turcotte and Schubert, 2002). The values used for all the parameters in equations 3.1 and 3.2 are shown in Figure 3.5.

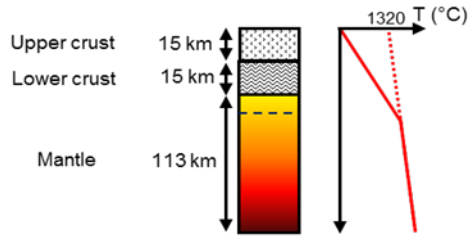

ρ_0 (kgm^{-3})	A (mWm^{-3})	α (K^{-1})	k (Wm^{-1}K^{-1})	Cp (Jkg^{-1}K^{-1})
2750	1.31	2.4 x 10^{-5}	3.1	790
2900	0.8	1.6 x 10^{-5}	2.1	790
3300	0.006	3.3 x 10^{-5}	3.3	790

Figure 3.5: The right-hand side shows structure and initial temperature conditions for the numerical forward model. The dashed black line indicates the base of the lithosphere (the position of the 1200 °C isotherm). The red solid line is the initial temperature profile while the dashed line indicates the potential temperature. The left hand side shows the best estimates for the material properties for the different layers of crust and mantle from the literature. (Allen and Allen, 2005; Shaw et al., 1986; Turcotte and Schubert, 2002)

The model is set up with a two layer crust composed of a felsic upper crust and granulitic lower crust which is underlain by mantle lithosphere. The base of the lithosphere is purely thermal rather than compositional and describes the temperature below which the mantle rock does not deform significantly over geological timescales. Ideally the lithosphere would be classified as the layer cooled by conduction. However, heat flow is calculated using conduction throughout the model therefore the 1200 °C isotherm is used (Turcotte and Schubert, 2002). The model starts with a 20 km thick mantle lithosphere, which matches the starting conditions described in section 3.2. The temperature at the surface of the model is set as 0°C. The temperature at the base of the model is calculated using a potential temperature at the surface using an adiabatic gradient of 0.3°C per km. Constant temperature boundary conditions are used at the top and bottom of the model. The initial temperature conditions follow the mantle adiabat to up to a transition point 20 km below the crust above which they follow a linear gradient to the surface. The depth and therefore temperature at this transition point is dependent on the thickness of the crust and the potential temperature for the surface. The initial conditions for the model are shown in Figure 3.5. The temperature profile is used to calculate the density at each grid point in the column from the reference density using equation 3.2. The elevation is calibrated from the density profile of the column using a column of hot mid ocean ridge material with a 7 km thick basaltic-gabbroic crust at 3 km below sea-level as reference. Standard Airy isostasy (Allen and Allen, 2005) is used. When the topography of the model drops below sea level the basin is filled with water. The thermal boundary condition is applied to the basement floor because water in the

basin would have an almost uniform temperature due to convection. However, the water is included in the isostasy calculation so the model effectively produces water loaded tectonic subsidence. The derivations for equations 3.1 and 3.2 and an in depth description of how the model works are included in Chapter 2.

One inherent weakness of the plate model is that it only calculates the heat transfer by conduction (Parsons and Sclater, 1977). At the base of the plate heat transfer changes from conduction to convection (Huang et al., 2003; Richter and Parsons, 1975; van Hunen et al., 2005). The plate model does not explicitly describe the physics of this transition, but provides a very good fit to the bathymetry and heatflow data ((Huang and Zhong, 2005) and included references). It does not help explain the physical process that cause the thermal boundary layer to become stable at this depth. The temperature dependence of k, C_p and α are not calculated. This assumption slightly overestimates temperatures in the top half of the model and underestimates temperatures in the bottom half of the model (McKenzie et al., 2005). This means the depth to the base of the lithosphere is an upper limit.

3.4.2 Results: Effects of varying parameters and the best fit model for the backstripping

The model is set up so that the each of the parameters from equation 3.1 can be changed and the structure of the model, shown in Figure 3.5**,** can be altered. Changing these will alter the subsidence produced. It is important to understand how these different parameters affect the subsidence before trying to find the best fitting model because there may be a trade off between different parameters.

The model is most sensitive to changes in the thickness of the crust and the plate thickness because they change the isostacy by varying the amount of low density crust and high density lithosphere. However, changing the plate thickness affects the duration of the subsidence whereas changing the crustal thickness only affects the total subsidence so their effects can be distinguished. There is not a direct trade-off between the two parameters (see Fig. 3.6 a and c). The model is less sensitive to variations in the potential temperature and radioactive heat production respectively (Fig. 3.6). In each case only the parameter under investigation is changed and the estimates for North African crust shown in Figure 3.5 are used as the default the parameters. The amount of variation in the input parameters is based on the uncertainties and variation across North Africa from the literature. The present day thickness of the crust of North Africa was calculated to be between 30 and 40 km thick from low resolution gravity and seismic interpretations and gravity modelling in the 3-D crustal model

of Seber et al. (2001) over the area of interest. This is thicker than the crustal thickness of 25-35 km estimated from the inversion of surface waves given by Pasyanos and Nyblade (2007). Due to the uncertainty in crustal thickness the model calculations were run for a range of crustal assemblages between 20 and 40 km thick. The results are shown in Figure 3.6a. With a crustal thickness of 40 km, ~ 1.2 km of tectonic subsidence takes place, however the crust is too buoyant to drop below sea-level, so no basin is formed. When the crust is reduced to 36 km thick the total subsidence increases to ~1.9 km and 1 km of water loaded tectonic subsidence is recorded. A 20 km thick crust starts at 1.4 km below sea-level and experiences ~2.7 km of tectonic subsidence as the lithosphere cools and thickens. There have been no deep crustal seismic lines of North Africa published so the proportion of upper crust and lower crust is unknown. Therefore the model was run with a 30 km thick crust where the thickness of the upper crust was varied between 10 and 20 km. This alters the total subsidence by about 500 m. A 1 km decrease in the total crustal thickness causes ~150 m of additional subsidence, whereas changing 1 km of upper crust to lower crust only increases the total subsidence by ~ 50 m. The main reason both these parameters affect the overall subsidence is that they change the isostacy by varying the amount of low density crust. In all these scenarios the duration of the subsidence does not change because it is controlled by the lithosphere thickness, most of the subsidence occurs in the first 100 Myrs and the subsidence after 200 Myrs is negligible.

The model was run for different amounts of radiogenic heat production. Estimations of heat production in the continental crust vary between 1.31 mWm^{-3} and 0.8 mWm^{-3} for the upper crust and 1.0 mWm^{-3} and 0.6 mWm^{-3} for the lower crust. The values reflect calculations of bulk crustal heat production from the literature (Christensen and Mooney, 1995; Gao et al., 1998; Shaw et al., 1986; Wedepohl, 1995). Changing the heat production for the upper and lower crust between these extremes causes a small variation of 100 m in the tectonic subsidence. The heat production of the bulk continental crust will be higher than that of accretionary crust and heat production would have been higher during the Palaeozoic, so the model was also run with a higher heat production of 2.0 mWm^{-3} (upper crust) and 1.2 mWm^{-3} (lower crust). This does reduce the overall amount of tectonic subsidence from ~ 1800 to 1550m, but does not alter the timing. Figure 3.6b shows that varying the heat production in the crust has a small effect compared to varying the crustal thickness.

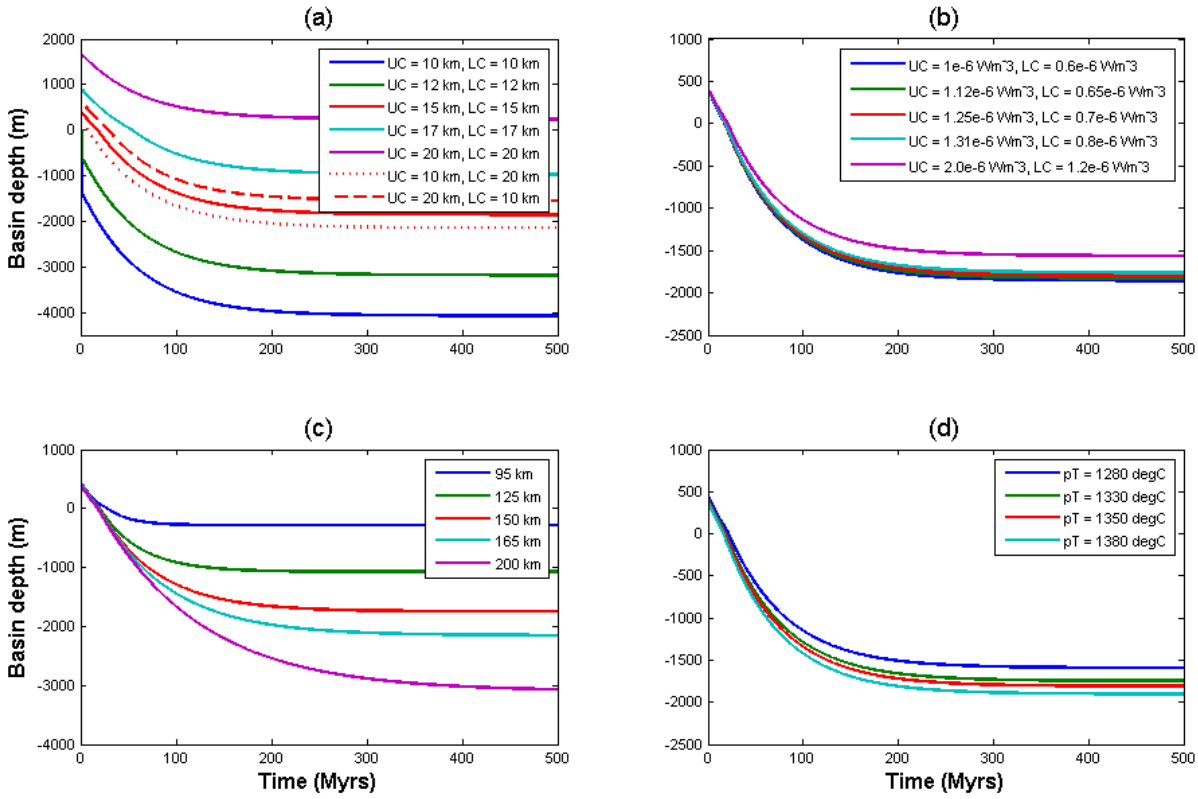

Figure 3.6: The sensitivity of the forward model to variations **(a)** in the crustal thickness and proportion of lower crust (LC) and upper crust (UC), **(b)** the heat production, **(c)** the model thickness and **(d)** the potential surface temperature of the mantle adiabat.

The other main parameter which has a big effect on the subsidence is the thickness of the model (Fig. 3.6c). A model thickness of 95 km, which is the preferred thickness for the oceanic lithospheric cooling model of Stein and Stein (1992) results in 200 m of subsidence, of which 80% has occurred within ~70 Myrs, with a final lithospheric thickness (i.e. depth to the 1200 °C isotherm) of 81.1 km. At the other extreme when a model thickness of 200 km is used, similar to an Archean craton (Priestley and McKenzie, 2006), ~3050 m of subsidence is produced, and it takes longer for the subsidence to tail off. 80% of the subsidence is completed within 200 Myrs. The lithosphere thickness after 500 Myrs is 166.5 km. As the model thickness is increased the final lithospheric thickness also increases. A thicker, dense lithosphere results in more subsidence, occurring over a longer time period.

The temperature at the base of the model is controlled by both the potential temperature at the surface (the temperature at which the mantle adiabat intersects the surface) and the thickness of the model (Fig. 3.5). Increasing the potential temperature by 1°C increases the temperature at the base of

the plate by 1°C whereas increasing the thickness of the model causes the temperature at the base of the model to increase along the mantle adiabat i.e. 3°C for every 10 km. The potential temperature was varied from 1280 °C, which was suggested by McKenzie et al. (2005) to 1410 °C suggested by Parsons and Sclater (1977). As Figure 3.6d shows this variation of over 100 °C in the potential temperature produces less than 500 m difference in the overall subsidence.

Van Wees et al. (2009) report a trade off between parameters, such as the final lithospheric thickness (plate thickness) and crustal thickness, when investigating the uncertainties in surface heat flow using modelling. This study found that varying the plate thickness to fit the time span of the subsidence and then varying the crustal thickness to fit the amount of subsidence allows a unique solution to be obtained for these parameters. However, there is a direct trade off between the crustal thickness, heat production and potential temperature because they all only affect the total subsidence. The model is not sensitive to reasonable variations in the heat production or potential temperature, but is sensitive to variations in crustal thickness suggested for North Africa. Therefore the trade off between these parameters is of low importance when trying to fit the modelled subsidence to the observed subsidence.

The effect of varying the initial lithospheric thickness is not shown in Figure 3.6 because it is difficult to predict exactly what the initial lithospheric thickness was post accretion. Therefore a standard initial thickness of 50 km was used (including the crust) which is thin when compared to normal continental lithosphere, but does not presume there is no mantle lithosphere beneath the crust. However, the effect of different initial lithospheric thicknesses was investigated. It does not affect the shape of the subsidence curve, but affects the starting point of the model along the subsidence curve. Starting with a thicker lithosphere will effectively move the left hand axis of the graphs in Figure 3.6 to the right. Conversely starting with a thinner lithosphere will increase the initial elevation of the model and prolong the time before the surface of the crust drops below sea level, effectively delaying the formation of a basin. This means it does not affect how well the modelled subsidence fits the observed subsidence, but could explain the gap in timing between the end of accretion and the onset of sedimentation in the basins seen in Table 3.1. The gap varies between 10 and 50 Myrs. A 50 km thick initial lithosphere, including a 30 km thick crust, results in the surface of the model dropping below sea level ~20 Myrs after cooling begins. This fits into the range from Table 3.1. Some of the variation in the length of the gap could be caused by changes in the initial lithospheric thickness, but as Figure 3.6a)

shows varying the crustal thickness also effects the initial elevation and length of time taken for the basement to drop below sea level. Therefore it is not possible to say for certain it is the cause.

The sensitivity of the model to *k*, C_p and α was also investigated, but because much less is known about the amount of variation that is found in the crust for these parameters they are not discussed here and the standard values from the literature (Fig. 3.5) are used. The forward model produces significant subsidence for a large variety of crustal assemblages and for wide variation in the parameters. It supports the hypothesis that lithospheric cooling and thickening caused the subsidence seen across North Africa.

3.5 Discussion

3.5.1 Comparison of tectonic subsidence from backstripping and forward modelling

The results of the forward modelling show a good fit to the backstripping from both basins as demonstrated by Figure 3.7.

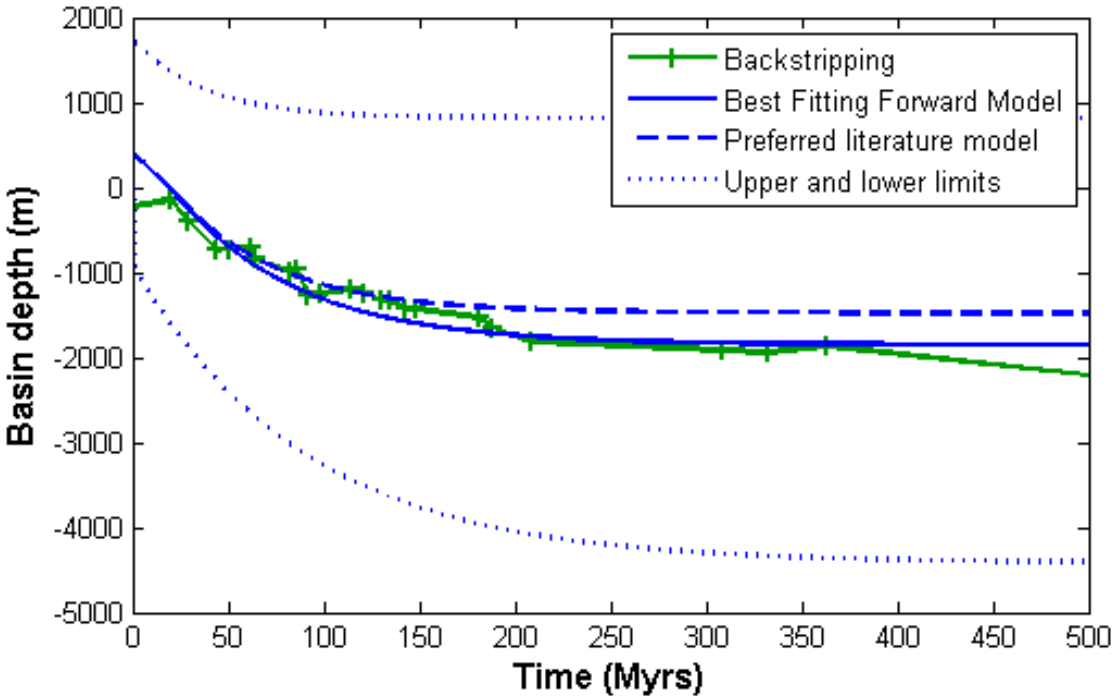

Figure 3.7: Comparison of the subsidence from backstripping the composite well from the Ghadames Basin with a range of forward model runs. The hypothesised subsidence mechanism fits the observed subsidence well

although there is a wide range of subsidence over the possible range of variations in the North African crust as demonstrated by the upper and lower limits.

Four forward model runs are shown on the diagram. One of which uses the best estimates for the crustal assemblage, thickness and plate thickness from the literature, one which is the best fit to the backstripping and then two runs which show the maximum and minimum subsidence for reasonable variations of the properties of the North African crust.

The forward model curves are smooth unlike the backstripped subsidence curves. This is because North African crust has experienced periods of uplift, and the forward model does not include these complexities. However, the forward model fits the broad shape of the backstripped subsidence curve very well. Both have a concave up shape, and the timescale and magnitude of subsidence are very similar. When the crustal thickness, final lithosphere thickness and heat production used are taken from the best estimates of the North African crust in the literature (Fig. 3.5), and therefore are independent of the backstripping, the forward model curve only underestimates the subsidence slightly, by <500 m in 350 Myrs. The discrepancy at 500 Myrs is ~700 m, because of the Mesozoic and Cenozoic subsidence of the Ghadames Basin. This is a separate tectonic event, related to Tethyan opening and evolution (Guiraud and Bosworth, 1999). The best fit model has been fitted iteratively by eye. The input parameters for the best fit model are the same as those from the literature except that the plate is 155 km thick, which results in a final lithospheric thickness of ~124 km. The crust beneath the basins cannot be assumed to be homogenous, in fact because it is accreted from numerous crustal fragments it is likely that it varies across North Africa. The maximum and minimum subsidence based on the variation found in the literature, discussed in section 3.4.2, is shown in Figure 3.7. The upper limit has a 35 km thick crust with 30 km of upper crust and 5 km of lower crust, a heat production of 1.6 mWm^{-3} in the upper crust and 1.0 mWm^{-3} in the lower crust, a potential temperature of 1280 °C and plate thickness of 120 km. The lower limit has 25 km thick crust, where the top 5 km is upper crust and the rest is lower crust, a heat production of 1.0 mWm^{-3} in the upper crust and 0.6 mWm^{-3} in the lower crust, a potential temperature of 1380 °C and a plate thickness of 180 km.

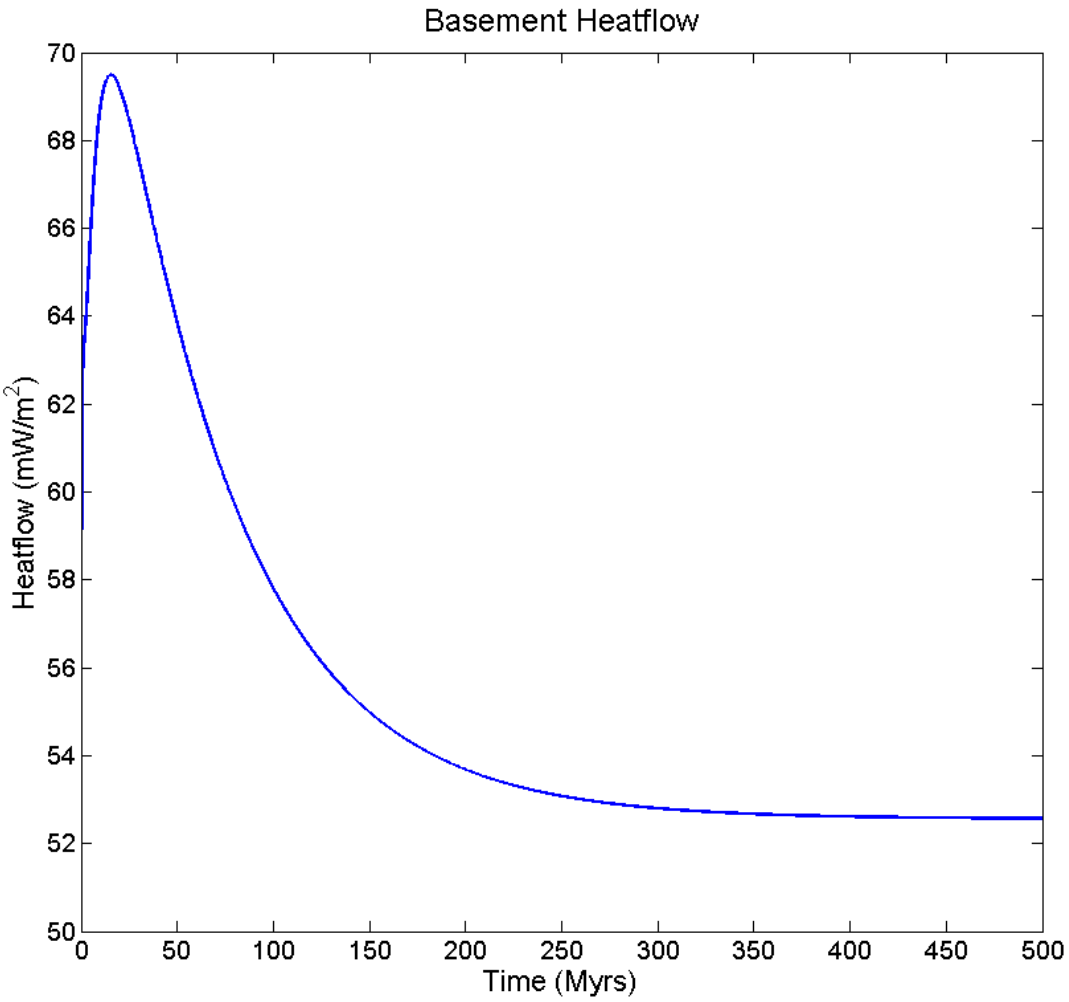

Figure 3.8: Heat flow from the basement produced by the best fitting model for the subsidence in the Ghadames basin as shown in Figure 3.7.

The heat flow produced by the best fitting model from Figure 3.7 (Fig. 3.8) shows a similar decay to the subsidence. This is slightly offset with the heat flow from the basement initially rising. This is an artefact of the model due to the simple initial temperature conditions imposed upon the model (Fig. 3.5). The model as whole is cooling, but the initial temperature gradient through the crust should be higher so the crustal heat flow begins by rising while the temperature gradient equilibrates before it falls in line with the cooling of the model as a whole. The maximum heat flow from the basement of 70 mWm^{-2} is similar to that found in the back arc region of present day accretionary orogens such as the North American Cordillera (75 mWm^{-2}) (Hyndman and Currie, 2011). This shows the starting conditions of the model, though simple are close to those found in modern day regions of accretion.

There are a number of assumptions in both the modelling and backstripping. Both are oversimplified versions of the real situations and processes. The problem has been simplified to be one dimensional, whereas the basins are three dimensional features. This assumes that the basins are large enough features that it is possible to remove effects of marginal uplift from the sedimentary record by choosing wells away from the basin flanks, or constructing composite wells. This allows the basins to be treated as one dimensional features. Another assumption is that North African crust resembles the starting conditions outlined in the hypothesis. This is difficult to test as there is no newly assembled accretionary orogenic belt on the North African scale that can be used as an analogue. However, the building blocks of accretionary crust are available to study. It seems reasonable that North African crust formed through subduction would share the thin lithosphere of its component island arcs and accretionary wedges. When North African crust is modelled using these starting conditions it produces a good fit to the subsidence. As mentioned in the hypothesis as long as the crust is of near normal thickness and has a thin mantle lithosphere these results still apply. The two North African basins have been chosen as case studies, but we propose that the lithosphere cooling and thickening hypothesis is applicable to all the Palaeozoic basins on the accretionary crust of North Africa and Arabia, and to other basins on accretionary crust around the world, such as the Mesozoic cover of the Scythian and Turan platforms of SW and Central Asia (Natal'in and Şengör, 2005), the Mesozoic cover of the Tasmanides of Eastern Australia (Gallagher et al., 1994) and the late Palaeozoic platform cover over the Altaid orogenic collage in Central Asia (Cook et al., 1994).

3.5.2 Discussion of other potential subsidence mechanisms

The good fit between modelled and backstripped subsidence curves do not prove that lithosphere thickening and cooling is the cause of the subsidence. Other authors have suggested that the Palaeozoic basins in North Africa formed by rifting (Lüning et al., 1999), orogenic collapse (Ashwal and Burke, 1989) and dynamic topography (Heine et al., 2008). Lüning et al. (1999), compared the Al Kufrah Basin to pull apart basins in Oman and Saudi Arabia, and suggested that the Najd fault system may extend north into the Al Kufrah Basin and be reactivated as a rift during the Precambrian. Seismic lines of the south of the Al Kufrah Basin do indeed have features which have been interpreted as rifts. However, they are only found in a small area of the basin and the synrift subsidence accounts for a sixth of the overall subsidence (Ghanoush and Abubaker, 2007). The Ghadames Basin has very similar stratigraphy

to Al Kufrah, but shows no evidence of rifting. Rifting is not widespread or large enough to cause the subsidence across all the Palaeozoic basins in North Africa. This also means that orogenic collapse is an unlikely subsidence mechanism, given that this is a special case of rifting on thickened continental crust. Armitage and Allen (2010) suggest that these basins can still form due to extension, but when stretching is occurring at low strain rates the strain might not localise along faults. It is hard to distinguish between their model and the model proposed in this paper on the grounds of rifting. Subsidence due to extension at low strain rates produces a prolonged period of constant subsidence rate during stretching producing a straight line on a graph, followed by decreasing subsidence during the thermal sag phase. Whereas cooling of a thin lithosphere produces subsidence which decreases smoothly throughout time. The latter model fits the backstripping results better (Fig. 3.4), which do not have a period of constant subsidence, then a kink and a curved section. Instead they are closer to a smooth curve which is predicted by the lithospheric cooling model.

There are problems with using dynamic topography to explain the basins: it has a transient effect and will rebound once the down welling has ceased leading to uplift and erosion. Nor is it possible at present to model whether the basins in North Africa would have been affected by mantle down-welling during the Palaeozoic. Thermal subsidence on the other hand explains the lateral extent of the subsidence as the lithosphere would be thin across most, if not all, of the accretionary crust. These results show that it is long lasting, fits the magnitude of the observed subsidence and is able to cause subsidence over a wide range of terranes.

Thermal subsidence has a number of important implications. It suggests that one of the fundamental properties of accretionary crust is that, in the absence of other competing tectonic forces, it will subside after its formation. This will alter the overall composition of the crust, adding several kilometres of sediments to crust made up largely of island arc and oceanic material. It also predicts that the lithosphere beneath accretionary crust is not depleted by the melting events which produced the crust, but is compositionally no different to upper mantle. This is because the lithosphere is initially thin and what composes the lithosphere following subsidence is upper mantle which has cooled, similar to the oceanic lithosphere. This will make the lithosphere more susceptible to thermal erosion as it does not have compositional buoyancy and also affect the character of melts originating in it or passing through it. Ashwal and Burke (1989) also noted that this fits the geophysical measurements of the thickness and seismic properties of the lithosphere and with the geochemistry of Cenozoic volcanism in North Africa.

3.6 Conclusions

This chapter has shown that results from backstripping wells in two North African basins and numerical modelling, are consistent with a basin forming mechanism of lithospheric cooling and thickening, underneath relatively juvenile, accretionary crust. The backstripping revealed that the Ghadames and Al Kufrah basins have experienced their highest rates of subsidence, (22.2 m/Myr and 10.1 m/Myr, respectively) at the start of the Palaeozoic, declining to almost zero at the end of the Palaeozoic. There is almost no tectonic subsidence during the Mesozoic and Cenozoic. The forward modelling shows that thermal subsidence of accretionary crust provides a viable explanation for the formation of the Palaeozoic basins of North Africa, fitting the available data better than previously suggested mechanisms.

This suggests that thermal subsidence following accretion would be expected in other areas of accretionary crust, and could have influenced the rifted West Siberian Basin. It also predicts that accretionary crust is underlain by fertile mantle lithosphere which may explain why Cenozoic volcanism in North Africa and Arabia seems to originate from a fertile source (Ashwal and Burke, 1989).

Declaration of authorship

A version of this chapter was published as a journal article in Tectonophysics in 2010 (Holt et al., 2010). While it was written by myself, it was aided by editing and discussion of the ideas, methods and results with my supervisors. Therefore they are included as authors on the published paper. Philip Allen and an anonymous reviewer also suggested expanding the discussion to look at a wider variety of subsidence mechanisms which could produce these basins and also consider the evolution of the Sirte basin to the north and to outline any trade off between parameters in greater detail. The paper however, lacked any mention of the heat flow data because Statoil did not wish this to be published.

Chapter 4 – A global study of subsidence upon accretionary crust

4.1 Introduction

The accretionary crust of North Africa, which formed during the Neoproterozoic (Caby and Monié, 2003; 1994) experienced broad scale subsidence during the Palaeozoic (Bumby and Guiraud, 2005; Guiraud and Bosworth, 1999). Study of the basins formed upon this crust led to the proposal of a new formation mechanism (Chapter 3), which proposed that the subsidence was a direct consequence of the properties of juvenile accretionary crust. In summary, the accretionary crust inherits the thin lithosphere of many of its constituent building blocks (island arcs, accretionary wedges and young oceanic crust) and as this thickens following tectonic assembly it causes subsidence as an isostatic response.

Other subsidence mechanisms have been suggested for these basins and other intercontinental basins around the world. Recently, it was suggested that many intercontinental basins form due to stretching of the continental lithosphere at low strain rates for long periods of time (50 – 100 Myrs) (Armitage and Allen, 2010). This produces a subsidence profile that begins with a straight line during the stretching phase, and then has a slight kink followed by a curved section caused by cooling acting over the stretched area. It has also been suggested that subsidence is due to orogenic collapse following an accretionary orogen because the mantle lithosphere undergoes delamination (Ashwal and Burke, 1989). This scenario envisions a high density of rifts, similar to the Basin and Range province, followed by a period of broad scale uniform subsidence with an exponential decay as the delaminated lithosphere is replaced by cooling upper mantle. There are many other mechanisms which have been suggested for individual basins, such as simple rifting (Oliveira and Mohriak, 2003) or back arc extension (Thomas et al., 1999), dynamic topography (Gallagher et al., 1994) and flexure to create a foreland basin (Catuneanu, 2004; Milani and De Wit, 2008).

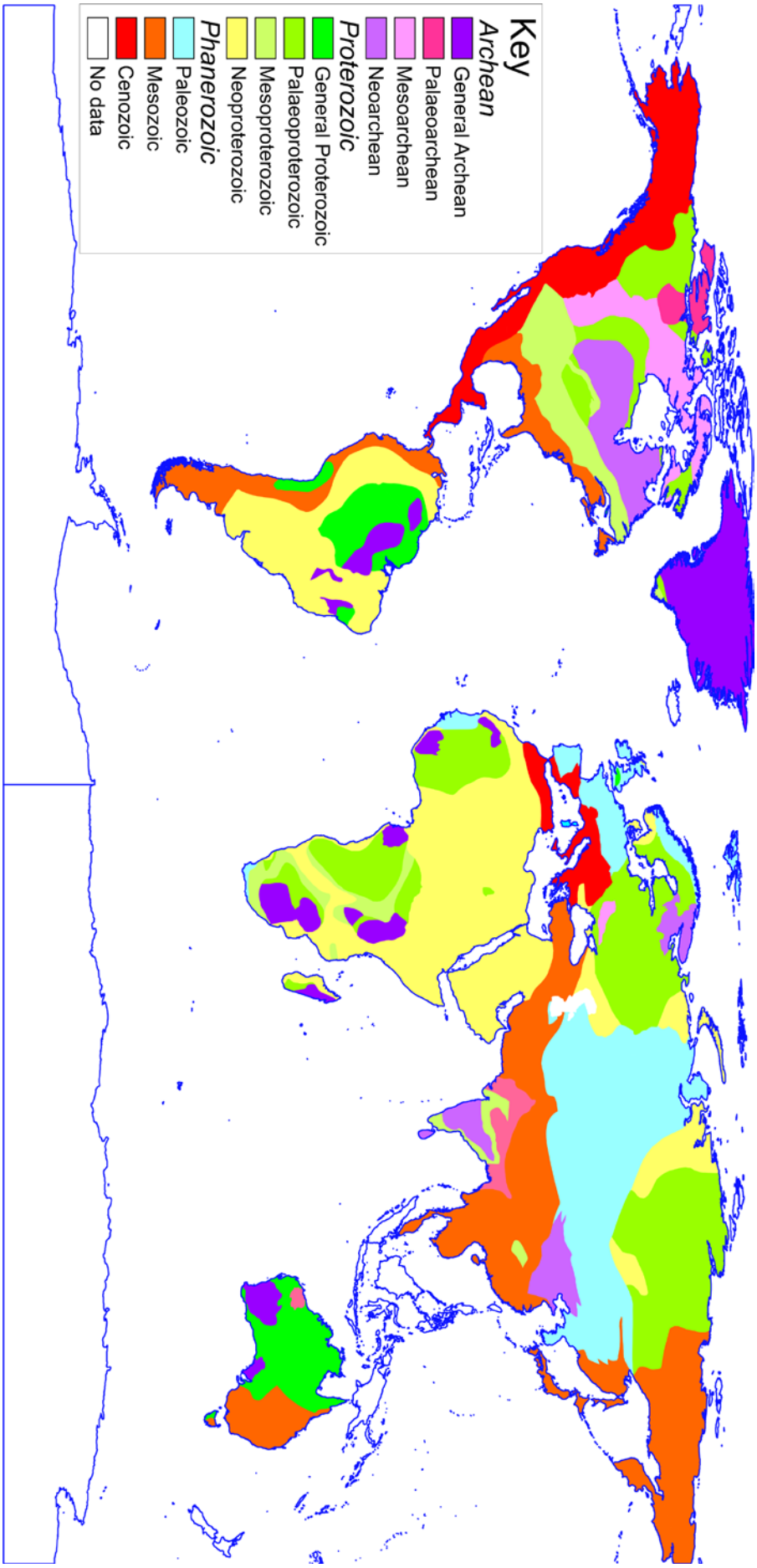
Key
Archean
General Archean
Palaeoarchean
Mesoarchean
Neoarchean
Proterozoic
General Proterozoic
Palaeoproterozoic
Mesoproterozoic
Neoproterozoic
Phanerozoic
Paleozoic
Mesozoic
Cenozoic
No data

Figure 4.1: This map shows the age of assembly for the continental crust. It is important to note this is not necessarily the age of the units within each area, but the age at which that region of crust was assembled as a unit. This is a compilation of data from numerous publications. From South America (Almeida et al., 2000; Milani and De Wit, 2008), for North America (Canil, 2008; Williams et al., 1991), for Europe (Gee and Stephenson, 2006), for Africa and Arabia (Begg et al., 2009; Van Hinsbergen et al., 2011), for Asia (Şengör and Natal'in, 1996) and for Australia (Debayle and Kennett, 2003).

Chapter 3 showed that the platformal subsidence in North Africa fitted well with thickening and cooling of the lithosphere. However, it has not yet been proven if it is an inherent property of accretionary crust and therefore more widely applicable. This chapter aims to test this by looking at a global overview of the subsidence patterns from a number of regions of accretionary crust. The major areas of accretionary crust are shown in Figure 4.1. The majority of these do indeed have large, intact, platformal sequences upon them although there are a few notable exceptions such as the Altaids in central Asia. This is likely to be a consequence of ongoing involvement in the India-Asia collision. There are also areas of platformal sediments that are not covered in this study, such as the Scythian platform, where it was not possible to find suitable data. The West Siberian Basin is not included because the subsidence is complicated by the influence of a plume head (Chapter 5). The areas covered in this study have been accreted at various times ranging from the Neoproterozoic to the Mesozoic and situated all around the world.

Each region is looked at in turn considering both the accretion history of the area and the subsidence record from the basins formed on the crust. It is not the intention to review each region in exhaustive detail, rather the aim is to give an overview, and compare the subsidence in as many regions as possible to the proposed formation mechanism. This will allow further comparison and evaluation against the other suggested causes of subsidence. This also allows comparison of the subsidence records from different regions and a discussion of what causes variation between different regions.

4.2 Methodology

The first step in assessing the cause of the subsidence in each region is to backstrip the sedimentary record to get the tectonic subsidence of the region. This can then be compared to subsidence produced by a numerical forward model of thickening and cooling of the mantle lithosphere.

Backstripping is the process of computing the tectonic subsidence from a sedimentary column. The theory behind this is common place and follows that of Watts and Ryan (1976), which is outlined in detail in Chapter 2 of this thesis. The first step taken was to see if there are any backstripped subsidence curves available in the literature. This is beneficial because it avoids repeating work and often the authors have access to detailed well data, which they are not able to make public, but they are allowed to publish the subsidence curves. In other areas where the well data are available, but no subsidence curves are published, the backstripping was carried out using the methodology outlined in Chapter 2. Where neither of these are available published records of the stratigraphy are used. These range from regional cross sections constructed using seismic data, to regional stratigraphic columns based on thicknesses from fieldwork studies of the outcropping sediments. In each region as many different data sources are used as are available to allow comparison between subsidence curves calculated from different data sets. Likewise, where there is disagreement in the literature as to the ages of the sediments, a subsidence curve is calculated for each conflicting interpretation.

The subsidence produced by thickening and cooling of the lithosphere beneath accretionary crust is calculated using a numerical forward model described in detail in Chapter 2. This model calculates the conductive heat flow through a column of crust and upper mantle material and then the resultant subsidence of the column. The subsidence calculated is water loaded tectonic subsidence and therefore is directly comparable to that calculated from the backstripping. The modelled subsidence is most sensitive to variations in the thickness of the crust and the final thickness of the lithosphere, which is controlled by the model thickness (plate thickness). Therefore these are varied to find the column of lithosphere and crust which best fits the subsidence for each region. The 1200 ˚C isotherm is used as an indication of lithospheric thickness (Turcotte and Schubert, 2002). Throughout this chapter, when discussing the lithosphere thicknesses used in the modelling it is the depth of the 1200 ˚C isotherm that is being referred to not the model thickness. This can then be compared to measurements of the crustal and lithospheric thickness from other sources to see if those used in the model are realistic. This provides another check to the model parameters other than how well the subsidence produced fits the observed subsidence from the basin.

This chapter provides a broad brush study of a range of locations across the world. It uses a wide range of data sources and provides a good global verification of the theory. An in depth

study of each region would be ideal, but is beyond the scope of this thesis. However it would be a good avenue for further work and allow additional details to be teased out.

4.3 Regional analysis of the observed and modelled subsidence

4.3.1 South America – Geological background

The first region considered is the accretionary crust of South America. Much of western Brazil and Argentina are made up of crust accreted in the Brasiliano orogeny. Before the formation of the Atlantic this formed a continuous band of accretionary crust with that formed in the Pan African orogeny (Bumby and Guiraud, 2005). The assembly of the North African accretionary crust appears to have finished marginally earlier with the final phase of accretion occurring ~600 Ma dated using orogenic granites (Liégeois et al., 1994). The similar batholiths found in the Brasiliano collage occur between 590 and 500 Ma (Almeida et al., 2000). The crust is not exclusively made up of juvenile terranes, but includes numerous older Proterozoic and even some Archaean blocks (Brito Neves, 2002). However, these are reworked during the orogeny and should not affect the initial conditions of a thin lithosphere suggested in the model.

There are a number of basins situated in this region, such as the Parnaíba basin, the Paraná basin and its extension into Argentina, the Choco-Paraná basin, shown in Figure 4.2. The Paraná basin is situated in southern Brazil and covers an area of over 2 million km^2 (Fig. 4.2). The earliest sediments within it date from the late Ordovician, and the sedimentary succession continues through to the Jurassic where it is capped by lavas of the Serra Geral related to rifting in the Atlantic. Detailed descriptions of the sedimentary fill are given in Zalán et al., (1990) and Eyles et al., (1993). The earliest sequence is known as the Silurian sequence though strangely it starts with continental sandstones and conglomerates from the Mid to Late Ordovician (Zalán et al., and Eyles et al., disagree as to exactly when) which change gradationally into shales and siltstones in the Silurian, and back to shallow marine sandstones at the end of the Silurian. There is a period of erosion during the Early Devonian, followed by deposition of the Devonian sequence. Again, this shows a complete transgressive – regressive cycle beginning with transgressive sandstones fining up into marine shales, which are overlain by deltaic sandstones. This is followed by another hiatus and further erosion, which lasts for much of the Carboniferous. Sedimentation begins again with continental redbeds at ~ 270 Ma. This is followed by deposition of glacial marine sediments and another transgressive – regressive cycle during the Permian. There is some disagreement between different authors;

Eyles et al., (1993) show continuous sedimentation through to the base of the lavas, whereas Zalán et al., (1990) report a hiatus during the Lopingian (end Permian) and Early Triassic. Both authors agree the Triassic sediments are entirely continental, consisting of lacustrine, fluvial and Aeolian sediments until the Jurassic. These then intermingle with the lavas above.

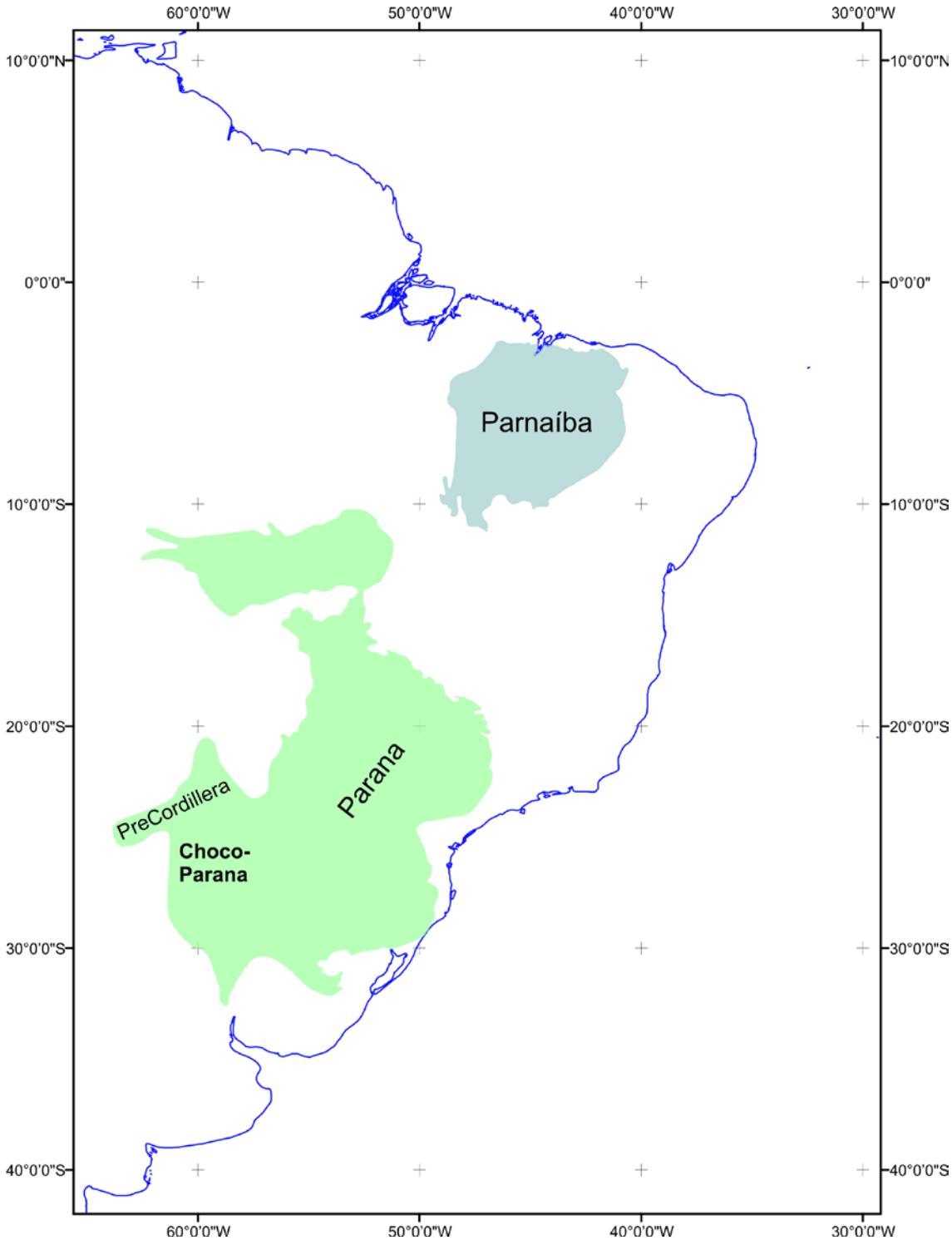

Figure 4.2: Location map of the Palaeozoic basins in South America. The Parnaíba basin is not backstripped, but has a very similar infill to the Paraná basin so is shown as another potential basin

formed in this way. The exact location of the wells from the Paraná basin and PreCordillera are not shown because they are not included in (Milani and De Wit, 2008).

4.3.2 South America - Results

Backstripped curves for the Paraná basin and PreCordillera were published by Milani and De Wit, (2008). These are taken from unpublished well data. However, because there is also a published cross section through the Paraná basin (Zalán et al., 1990), this was backstripped as well. This was done to get a comparison of subsidence curves produced by detailed analysis of well data and those taken from a cross section which is a more rough and ready approach. This provides a gauge of the accuracy of results from cross sections in other regions studied. The cross section was backstripped with both of the conflicting age estimates for the sediments (Eyles et al., 1993; Zalán et al., 1990). To my knowledge no backstripped subsidence curves or detailed cross sections which cross the depocentre are available from the Parnaíba basin. The chronostratigraphy shown in Oliveira and Mohriak, (2003) indicates it has a similar basin infill, but without subsidence data it is not possible to explore this further. The results for the three subsidence curves from the Paraná basin and the PreCordillera are shown in Figure 4.3, alongside the best fitting foreword model curve.

Firstly, it is evident that while the backstripped subsidence curves from the well data and the cross section differs in detail, they are broadly consistent in the magnitude and timing of subsidence. When they are compared to the modelled subsidence curve, the first 150 Myrs shows subsidence similar to a model curve with a 36 km thick crust and a final lithospheric thickness of 130 km. The fit is not perfect in part because there are periods of uplift and erosion, which shows up in the backstripping, but not the forward modelling. However, until 311 Ma the subsidence is broadly consistent with the model. After 311 Ma there is sudden increase in the subsidence rates. This coincides with collision of the Gondwanides along the Western margin of South America (see Fig 4.1). Therefore it has been suggested the Paraná may become a foreland basin at this point causing a renewed phase of subsidence (Milani and De Wit, 2008). The subsidence in the PreCordillera begins ~ 100 Ma earlier and may reflect earlier accretion and cratonisation of the crust beneath this basin before it docked with the rest of South America. This collision at the end of the Ordovician is said to be the reason for the increased subsidence observed after 400 Ma (Milani and De Wit, 2008). It is fitted best by a model with a 30 km thick crust and a 130 km thick lithosphere. The fit to the model is remarkable for the first 150 Ma. The results show that lithospheric cooling of accretionary crust can explain a lot of the subsidence seen in the basins in this region of South America, but

they are both then affected by a later period of subsidence proposed to be due to flexure in a foreland basin setting. The crustal thickness used for both basins is consistent with the results of Feng et al., (2007) who measure the Moho varying between 35 and 40 km depth beneath Paraná, and between 25 and 35 km depth beneath the PreCordillera.

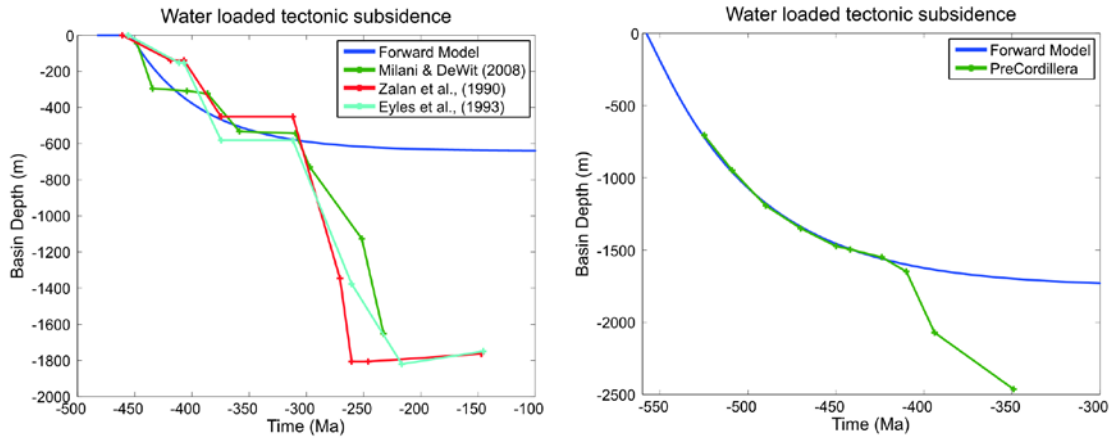

Figure 4.3: The backstripped subsidence curves for the Paraná basin and the PreCordillera compared with the best fitting forward model. The sources of the three curves from the Paraná basin are explained in the text. The best fitting model for the Paraná basin has a 36 km crust and a model thickness of 130 km. The PreCordillera is best fitted by a model with a 30 km thick crust, but the same model thickness

4.3.3 South Africa – Geological background

The Cape Fold Belt and the Karoo Basin in southern African have similar sedimentary fills to the South American basins described in the previous section. The subsidence patterns are also similar, leading to a number of correlations being suggested (Milani and De Wit, 2008). However, unlike South America the basins are not entirely underlain by accretionary crust (Fig. 4.1). The Cape Fold Belt is largely underlain by Neoproterozoic accretionary crust of the Damara Belt, which forms part of the same mobile belt as the South American accretionary crust. The Cape-Karoo Basin to the north is underlain by Mesoproterozoic basement, and its western side is floored by Archean basement of the Kaapvaal craton (Milani and De Wit, 2008). If the subsidence mechanism suggested formed the Cape-Karoo basin then the older crust must have been remobilised by the Pan African orogeny. This is supported by evidence from the Mesoproterozoic basement flanking the Damara belt which has been rejuvenated (Frimmel and Frank, 1998). Also the basement of the combined Cape-Karoo Basin is intruded by A-type granites from the Cambrian indicating involvement in the accretion process. A similar situation is seen in the North African accretionary crust, where there is evidence of a

Palaeoproterozoic cratonic block which has been reworked during the Pan African and yet has no discernible effect on the subsidence patterns (Abdelsalam et al., 2002). This suggests the accretion process can lead to thinning of neighbouring crust in the right circumstances. This could be because during the accretion there is an intervening ocean subducting beneath the older crust, thinning the lithosphere through corner flow or back arc stretching (Arcay et al., 2006; van Keken, 2003).

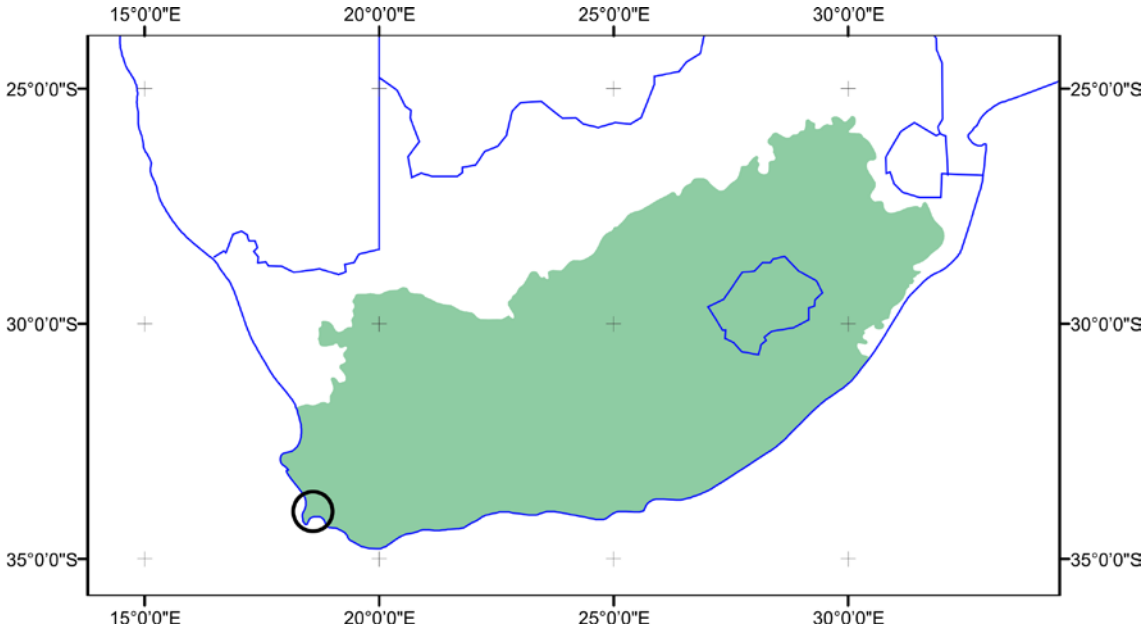

Figure 4.4: The extent of the Cape-Karoo basin of South Africa taken from (Tankard et al., 2009). The location of the outcrop sections used to make up the subsidence curve for the Cape fold belt are shown by the bold circle. Again the location of the wells used by Milani and De Wit (2008) are not shown because they do not appear in the original publication. However, the text suggests one is located to the north of the outcrop sections and the other is more centrally located in the Cape-Karoo basin.

The sedimentation in both the Cape Fold Belt and Cape-Karoo Basin began with a succession of mature continentally derived siliciclastic sediments. Deposition began sometime in the mid Cambrian, though this is difficult to date, and continued until the Devonian. Strata show glacial influence during the Ordovician, followed by shales representing maximum flooding of the Ordovician to Silurian transgressive – regressive cycle (Turner et al., 2011). Unlike the Paraná Basin, there is no significant hiatus before the Devonian cycle. The sedimentation is similar in character to the Paraná showing a transgressive – regressive cycle with silt and mudstones representing the maximum flooding which shallow upwards to lacustrine sediments. This sequence is the last preserved sediments in the Cape Fold Belt, which terminates in the early Carboniferous (Turner et al., 2011). In the Cape-Karoo Basin they are overlain by glaciogenic sediments made up of diamictites and rhythmites, which continued until the early Permian.

These are followed by black mudstones grading into deltaic sands. There is some debate as to whether the glaciogenic sediments and those following are deposited into a marine or lacustrine environment (Milani and De Wit, 2008). At the end Permian there is deepening of the basin as black shale is deposited. There is then a gradual shallowing with distal turbidites passing upwards into coarser turbidites and ultimately shoreline and fluvial deposits. From this point on the sediments are terrestrial represented by desertification throughout the Triassic. The sequence is terminated by the eruption of the Karoo Large Igneous Province in the Jurassic. A more detailed overview of the sedimentary history of the Cape Fold Belt can be found in Turner et al., (2011) and for the Cape-Karoo Basin in Milani and De Wit, (2008).

4.3.4 South Africa - Results

The subsidence curves for the Cape-Karoo Basin are from Cloetingh et al., (1992) and the curve for the Cape Fold Belt is from Turner et al., (2011). The data from Turner et al., (2011) are taken from outcrop data measuring the thickness of each unit in the field, and therefore is a composite thickness for the region. Both subsidence curves for the Cape-Karoo Basin are fitted well with by a model with a crustal thickness of 27 km and a final lithospheric thickness of 122 km (Fig. 4.5). However, the second Cape-Karoo curve is fitted slightly better by a 29 km thick crust with a 139 km thick lithosphere. Regionally, a 122 km thick lithosphere fits better, as the subsidence of the Cape Fold Belt is matched most closely by a 23 km thick crust and a 122 km thick lithosphere. However to achieve this match an unusually thin initial lithopshere of only 27 km thickness is required. If a thicker initial lithosphere was used the shape of the curve would remain the same, but the first part of it would be missing as it would start below sea-level. Although this is an unusual starting condition compared to the parameters used for modelling other basins it is still consistent with geochemical indications of the lithospheric thickness beneath island arcs where garnet does not play a role in the fractionation of basalt, which suggest they fractionate beneath a lithosphere < 35 km thick (Macpherson, 2008). Because island arcs form the basic building blocks of the accretionary crust, this is not beyond the range of possible starting parameters, but instead may represent an endmember of natural starting conditions. The results also show that to explain the greater subsidence in the Cape Fold Belt a thinner crust is required. This agrees with the crustal thickness which thins towards the south from ~30 km to 25 km (Pasyanos and Nyblade, 2007). The regional best fitting lithospheric thickness is also in good agreement with the lithospheric thickness measured using shear wave tomography, which is 120 km (Priestley and McKenzie, 2006). The

model provides a good fit to the subsidence curves in South Africa using parameters which match those published in the literature. Similar to South America there is a phase of renewed subsidence, which has again been attributed to growth of the Gondwanides (Milani and De Wit, 2008).

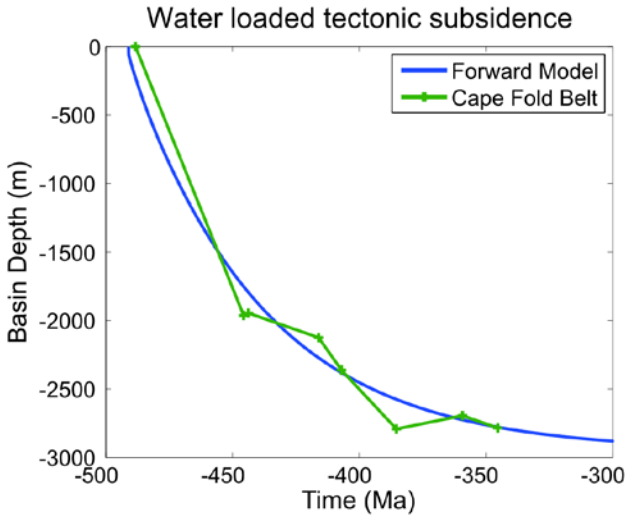

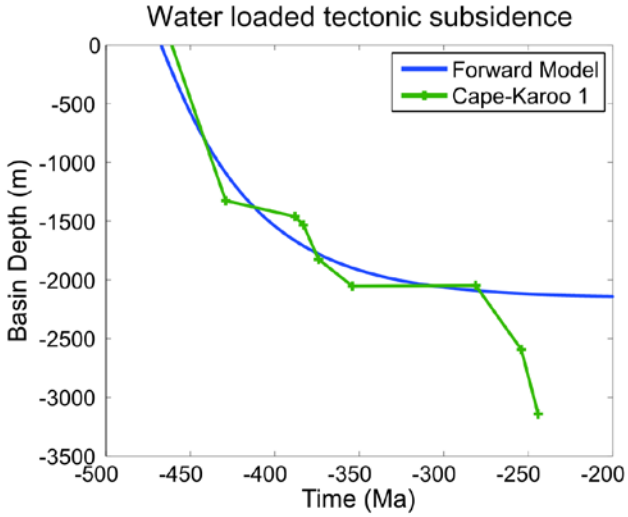

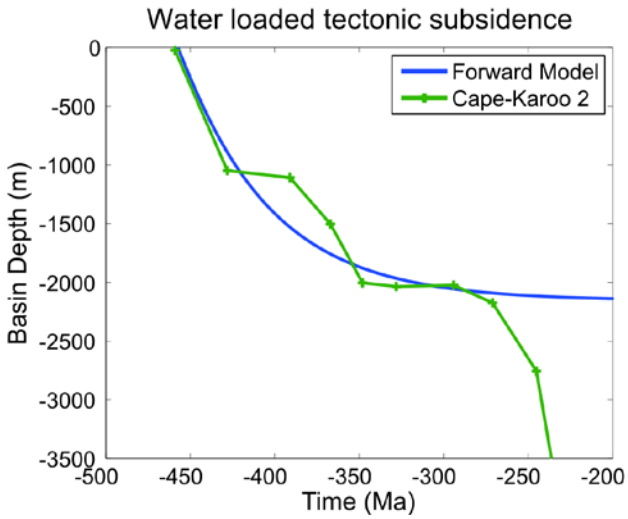

Figure 4.5: Backstripped subsidence curves from the outcrop data in the Cape Fold belt and from the wider Cape-Karoo basin. The best fit forward models to each of these subsidence curves are shown alongside the backstripping. All the best fit models have a final lithospheric thickness of 122 km. The Cape Fold belt is fitted by a 23 km thick crust and the wider Cape-Karoo by a 27 km thick crust.

4.3.5 Arabia – Geological background

The Arabian crust also forms part of the accretionary crust formed during the Pan African orogeny. The basement is particularly well exposed along the flanks of the Red Sea due to flank uplift. Therefore it provides good insight to the makeup and assembly process of accretionary crust. The crust is composed of numerous terranes sutured together along shear zones. Many of the terranes are island arcs dating between 870 – 690 Ma (Stern, 1994). There are also ophiolitic terranes, accretionary wedges (not to be confused with accretionary crust) and older terranes from the Meso-Palaeoproterozoic. In his area of study Stern, (1994) described roughly 2/3 of the crust as juvenile. The geochemistry of xenoliths brought up from the lower crust and mantle by Miocene and younger volcanics in Syria, Jordan and Saudi Arabia confirm that regions with sedimentary cover are also underlain by juvenile basement made up of Neoproterozoic island arc terranes (Al-Mishwat and Nasir, 2004). The accretion is a gradual process with some terranes colliding with each other to form composite terranes before colliding in the main accretionary orogen. The date of the final phase of accretion is ~550 Ma in the east of Arabia, but gets progressively younger westwards, and is ~500 Ma on the flank of the Red Sea.

Apart from where the basement is exposed alongside the Red Sea most of Arabia is blanketed by Palaeozoic sediments as shown in Figure 4.6. The earliest sediments are continental clastics which are Cambrian in age. These were deposited in the north and east, but are not seen in the southwest of Arabia. During the Ordovician the marine influence spread inland, and the area of deposition expanded to the southwest. Even so, Early Ordovician sediments are mostly sandstones except along the fringes of the platform. These were overlain by fine grained clastics in the Mid Ordovician. The Late Ordovician saw a period of glaciation with widespread erosion inland and glaciogenic deposition near the edges of the platform. This was followed by filling of the glacial topography with coarse clastics and then a widespread transgression during the Silurian. In the Early Silurian shales were deposited, which are an important source rock for hydrocarbons in some areas. The sediments then record the transgressive phase of the cycle coarsening upwards into shoreface and deltaic sandstones. More detail is available in Garfunkel (2002), who notes that the same sedimentary patterns are seen across much of

North Africa and therefore concludes that it formed a 2000 km wide platform. As Figure 4.6 shows, later sediments are not as well preserved and have a patchier distribution.

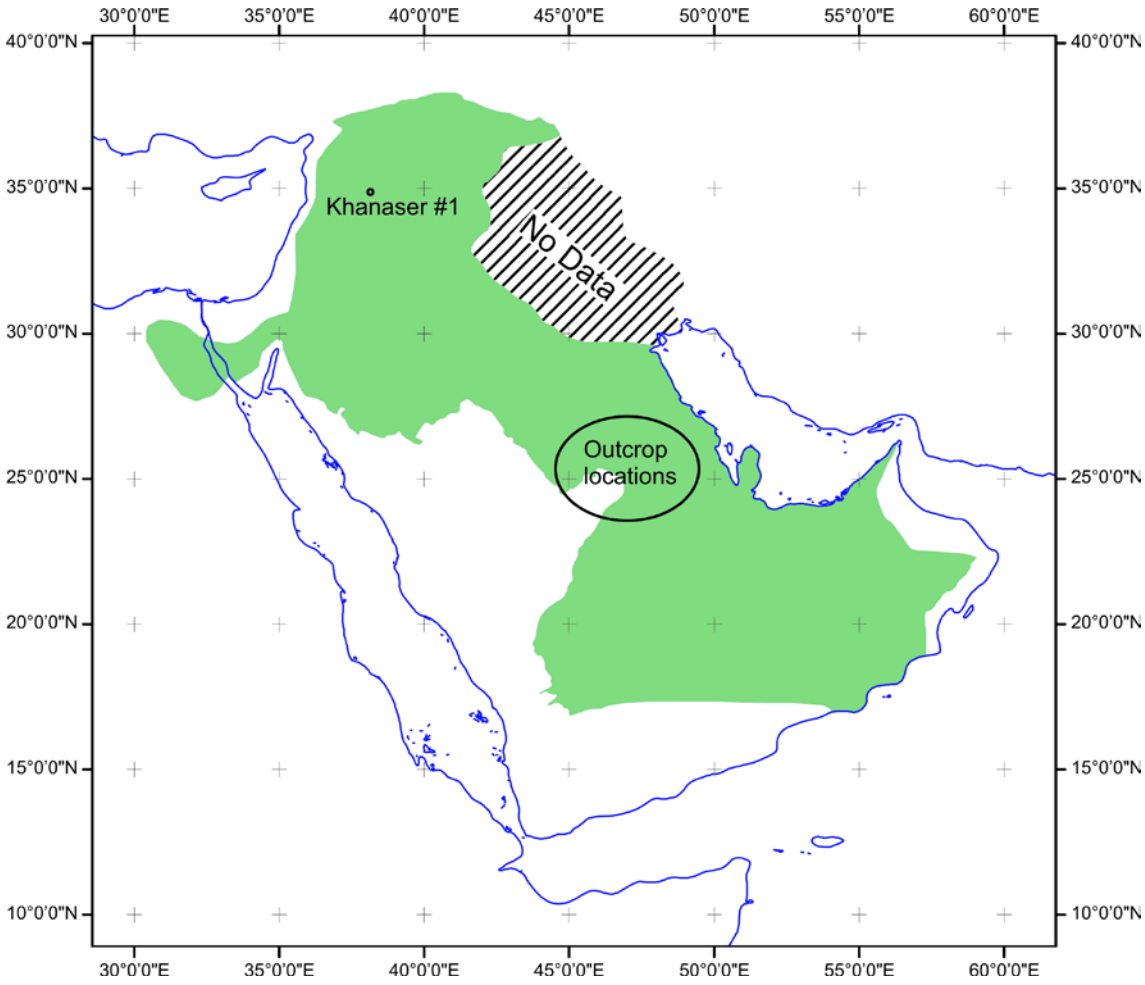

Figure 4.6: The extent of sediments beneath the Hercynian unconformity (Late Carboniferous, 311 Ma) across Arabia. The location of the Khanaser #1 well in Syria and the outcrop study used for the backstripping are both located upon the map.

There was then a hiatus in sedimentation, which resumed in the Middle Silurian in central Arabia (McGillivray and Husseini, 1992), but did not begin until the Late Silurian further north in Syria (Best et al., 1993) or Iraq (Al-Juboury and Al-Hadidy, 2009). This hiatus was related to the "Caledonian orogeny", which is seen across North Africa as well. The quotation marks are advisable: this deformation is Early Palaeozoic in age, and for this reason commonly termed "Caledonian", but there is no simple correlation with the orogeny of that name in northwest Europe and conjugate parts of North America.

Sedimentation renewed in the Devonian in central Arabia, with a transgressive to regressive cycle that began with fluvial sediments. These rocks pass into marine sandstones with minor

carbonates in the Emsian, then back into shoreface sandstones. In the north of the platform the hiatus lasted until the end of the Mid Devonian. The sequence deposited afterwards is mainly siltstones and shales, with some sandstones and minor carbonates, and the youngest rocks are from the end of the Mississippian. In both areas the top of the sediments is marked by an erosional surface referred to as the Hercynian event – with a similar caveat about the use of this term to "Caledonian". This has cut down to the Silurian sediments in some areas, so extensive section may be missing. Both areas experience subsequent phases of subsidence. However the modelling results suggest that the effect of cooling and thickening of lithosphere should be negligible by this point (> 200 Myrs after accretion has finished). Therefore subsequent episodes of subsidence are likely to be caused by other mechanisms. This illustrates the polyphase nature of many of these basins. In Arabia, the later phases are much better studied because they host the majority of the discovered hydrocarbons (Guiraud and Bosworth, 1999).

4.3.6 Arabia - Results

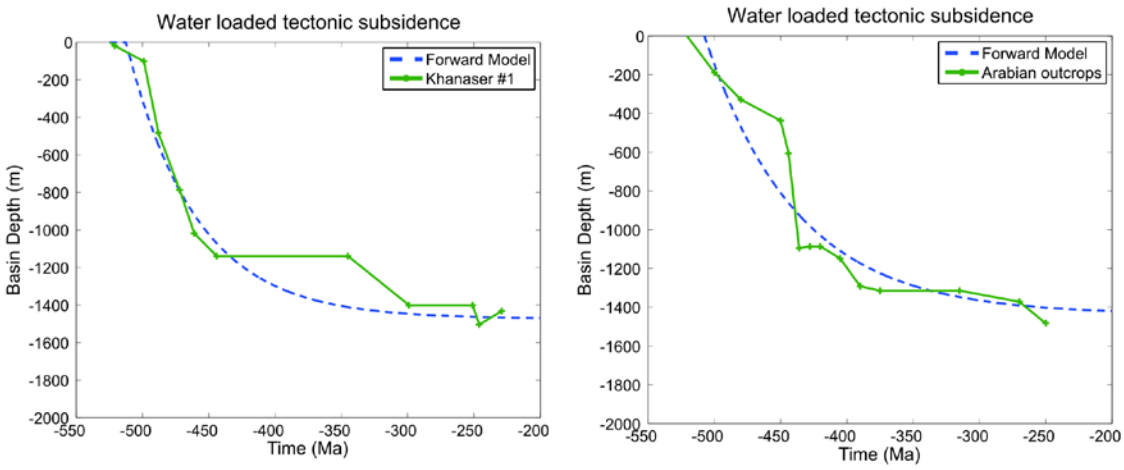

Figure 4.7: The Palaeozoic sediments of Arabia contain a number of eroded sections which shows in the backstripped subsidence curves. The best fitting subsidence curves from the forward model are shown alongside the backstripping. The Khanaser #1 well is fitted best by a 30 km thick crust and 122 km thick final lithosphere. The outcrops are fitted best by a 33 km thick crust and a 139 km lithosphere.

Finding good wells to use for backstripping or published tectonic subsidence curves is very hard to find for the region because much of the data are economically sensitive, and are never published. McGillivray and Husseini, (1992) published a number of wells through the Palaeozoic section in Syria. Of these two penetrate crystalline basement and one finishes in

the Cambrian, however all three are missing section from the Devonian and Early Mississippian. The most complete in terms of sedimentary units is the Khanaser #1 well therefore this is presented here (Fig. 4.6). Well data from central Arabia are even sparser, therefore thicknesses from outcrop have been used instead (Best et al., 1993). Figure 4.7 shows the fit of the modelled subsidence to the backstripping. The outcrop data from central Arabia is fitted best by a 33 km thick crust with a 139 km final lithospheric thickness. The model parameters used to acquire the best fit for the Khanaser #1 well are a 30 km thick crust with 122 km thick lithosphere. The crustal thicknesses are both broadly in agreement with the 38 km inferred by Al-Mishwat and Nasir (2004) when the sedimentary cover is added. The slightly thinner crust in the north would also provide a neat explanation for the earlier onset of sedimentation than in the south of the platform. Comparison with the present day lithospheric thickness is not viable because it has been affected by later events, such as the collision between Arabia and Asia in the north (Priestley and McKenzie, 2006) and the rifting of the Red Sea in the South West (Pasyanos, 2010). In both cases the proposed subsidence mechanism provides a reasonable fit to the backstripping, but there is a lot more variance from the predicted subsidence curves taken from the modelling than in other regions. This may be because of the greater amount of erosion experienced by these sections than in other regions in this chapter. However, there is still a good temporal link between the accretion and the subsidence as well as a broad fit to the subsidence curves, despite the problems with erosion.

4.3.7 Scythia and Turan – Geological background

The platforms of Scythia and Turan formed upon part of a band of accretionary crust which collided on the northern side of the Palaeo-Tethys Ocean (Fig. 4.1). The location is unique amongst the regions studied in that it is not on the margin of Gondwana. The previous study areas all finished accreting around the Precambrian-Cambrian boundary. The basement of the Scythia and Turan region is penetrated by numerous boreholes. These contain a mixture of granitoids, mafic, felsic and intermediate volcanics of Carboniferous to Triassic age. All those that have undergone geochemical analysis have been shown to be subduction related. The terranes which make up the basement are mostly paired forearc and arc units. The terranes show an en-echelon stacking pattern interpreted from magnetic, seismic and gravity data alongside the borehole data. This has led the suggestion that the crust is formed from a single arc, which was stacked up by strike slip arc slicing faults and arc shaving faults (Natal'in and Şengör, 2005). These are known to form in transpressional subduction zones (see Figure 1.2 in

Chapter 1). Amalgamation finished during the mid-Triassic in Turan. However, the southern margin of the region remained a subduction zone until the continental collision with Arabia. The initial subsidence history of the basin is complicated by rifting related to back arc stretching, and localised pull apart basins related to strike slip motion during accretion.

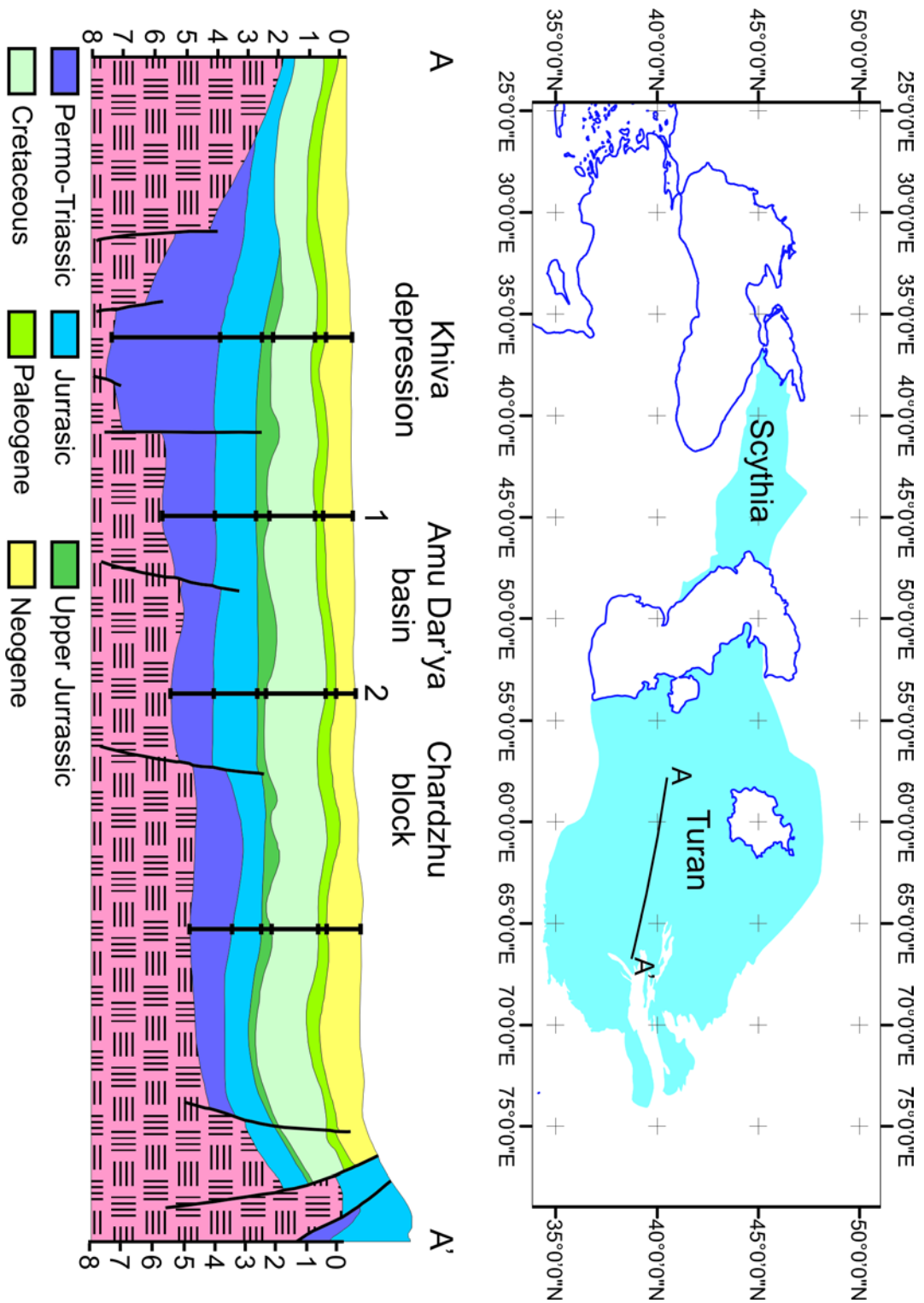

Figure 4.8: A map of the sedimentary cover over the Turan and Scythian platforms take from (Natal'in and Şengör, 2005; Thomas et al., 1999). There is no well data so instead a cross section (Thomas et al., 1999) has been used as input for the backstripping. The location of the cross section is shown on the map. The 4 'pseudo wells' from the cross section are marked.

The initial sediments overlap in age somewhat with the final phase of accretion. Only a summary of the geological evolution is given here. Greater detail for the Scythia and Turan platforms can be found in Nikishin et al., (2001) and Thomas et al., (1999) respectively. Sedimentation began on the Turan platform in the Permian with continental sediments. The platform was then submerged and sedimentation switched to marine clastics which continued into the Triassic. The Permo-Triassic sediments are thickest in the south (Fig. 4.8 cross section). Thomas et al., (1999) do not further divide the Permo-Triassic, neither do they show when during the Permian or Triassic the earliest sediments occur, though they note the main extension phase seen across the region is Late Permian – Early Triassic. The extension is interpreted to be caused by back arc stretching. During the Late Triassic there was a period of compression with some erosion in the north of the platform.

The earliest sedimentation on the Scythia platform is Early Triassic. There are a number of N-S trending rifts with reefs preserved on the intervening highs and deeper carbonates deposited in the troughs (Nikishin et al., 2001). During the Late Triassic – Early Jurassic there was a period of compression as the Alborz terrane collided to the south. This led to erosion, which obscures the original extent of the Triassic sediments. The Scythian platform remained above sea-level during the Early Jurassic. In the Mid Jurassic the east of the platform was flooded and a sequence of sandstones, siltstones and shales were deposited. The western side of the platform remained above sea-level at this time. On the Turan platform, the Early Jurassic sediments to the north and east were fluvial and deltaic, whereas in the southwest shallow marine sandstones fined upwards into silts and shales. These patterns were repeated in the Late Jurassic where a regression causes evaporites to be deposited to the north and east, but in the southwest carbonates were deposited instead. There was then a major transgression across the whole platform during the Cretaceous, and marine sediments were deposited across the platform. The type of marine sediment is not specified (Thomas et al., 1999). To the west on the Scythian platform there was subsidence across the platform and extensive shallow water chalks were deposited. This was followed by gentle folding during the Early Palaeocene before sedimentation resumes across the platform. There was a regression on the Turan at this time leading to a brief hiatus. This was followed by the deposition of shallow marine sediments on a slowly subsiding platform during the rest of the Palaeocene and Eocene. Sedimentation

terminated on the Scythian platform during the Eocene because of the Caucasus orogeny to the west. In Turan there was a final pulse of subsidence caused by compression on the southern margin during the Oligocene to late Pliocene related to the collision between Arabia and Asia. The sediments deposited at this time are clastics being shed from the rising mountains and the basin takes on the characteristics of a foreland basin.

4.3.8 Scythia and Turan - Results

The sedimentary thicknesses for the Turan platform are taken from Thomas et al., (1999). They carried out a study of the isopachs of each layer using regional seismic data constrained by 500 wells. These were used to create a number of cross sections across the platform, one of which was used to provide the inputs for the backstripping. Four columns were backstripped from the cross section to look at the difference across the platform (Fig. 4.8).

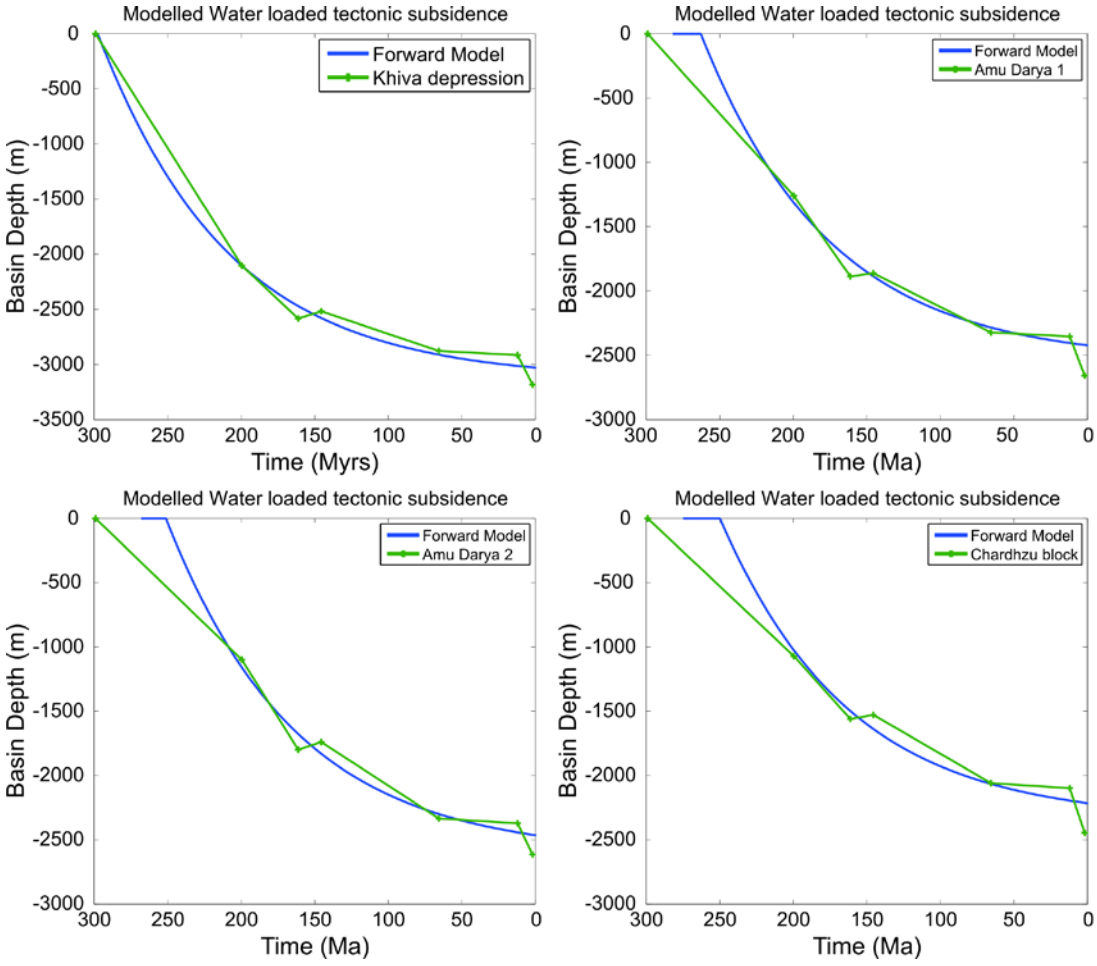

Figure 4.9: The results of the backstripping from the four wells in the Turan platform. The best fitting models for each well all have a final lithospheric thickness of 155 km. The best fitting crustal thickness

for the Khiva depression is 28 km, 30 km is used for both Amu Dar'ya 1 and 2 and a 31 km thick crust is used for Chardhzu.

The fit between the forward model and backstripping are shown in Figure 4.9. The deepest sequence in the Khiva depression is fitted very well by a 28 km thick crust and a 155 km thick final lithosphere. For the other 3 columns the fit is good except for the first point. As mentioned previously the first layer of sediment is not divided beyond Permian and Triassic, which has been followed in the backstripping. Therefore the timing for the start of subsidence has the greatest uncertainty. Equally the area was still being influenced by accretion and rifting until the mid Triassic, which could also affect the poor fit to the start point. The other points fit well with lithospheric cooling with the reduced subsidence being explained by a slight increase in the crustal thickness to 31 km in the east. This fits with the observations of Natal'in and Şengör, (2005) who note that the forearc terranes, which are floored by oceanic crust coincide with the deepest sedimentary cover. The lithosphere thickness was kept constant across the Turan platform and is within the range of variation suggested for the region (120-180 km) (Pasyanos, 2010; Priestley and McKenzie, 2006).

4.3.9 Eastern Australia – Geological background

This final region studied is the Tasmanides of Eastern Australia shown in Figure 4.10. They were accreted from the Mid Cambrian to the Permian, which is on a similar time scale to the accretionary crust in Arabia and North Africa. There is a mix of terrane types including older Proterozoic crustal fragments, island arcs, accretionary complexes and ophiolitic terranes. The region provides a particularly good study of the accretionary process because it has been well studied over a long period of time and there is abundant data available. A comprehensive review of the current understanding of the region is given by Glen (2005). The accretionary crust formed over five distinct orogens which are marked by a period of collision of new terranes onto the margin. This phase was followed by a period of extension while subduction continued along the margin of the region. This shows the change from an advancing to a retreating orogen (Chapter 1). This may explain why the lithosphere remained thin until the accretion has terminated because it was being stretched after each collision phase. The earlier orogens were originally thought to contain a greater proportion of older crust, but this has been recently revised based on dating of basement from new wells (Glen, 2005). Again, many of the Proterozoic microcontinents were rejuvenated during accretion and are penetrated by syn-orogenic and post orogenic granites.

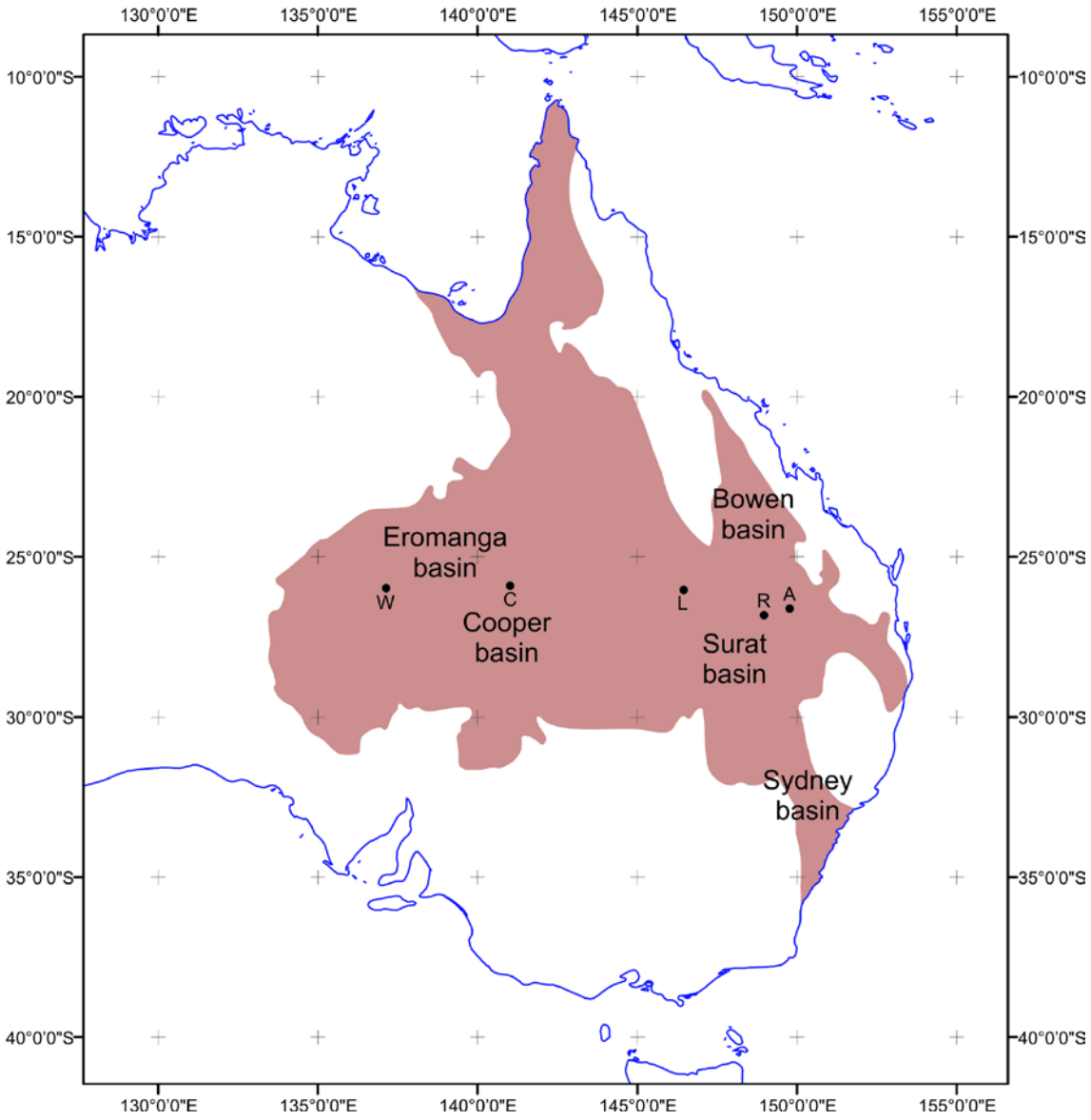

Figure 4.10: The Mesozoic-Cenozoic cover of Eastern Australia. The extent of the sedimentation is taken from Gallagher et al., (1994). The location of the depocentres mentioned in the text and the wells used in the backstripping are shown on the map. The abbreviations for each of the wells are as follows. W = Walkandi 1, C = Cook North 1, L = Lowood 1, R = Redwood 1 and A = Arlington 1.

Much of the Tasmanides (10^6 km^2) are covered by platformal Mesozoic to Cenozoic sedimentary cover (Fig. 4.10). The earliest sediments are Early Permian and found in the Eromanga and Cooper basins in the west of the Tasmanides and the Bowen-Surat-Sydney basin which stretches N-S in east. These sediments are shallow marine clastics in the east and continental clastics (fluvial and lacustrine sediments) in the west. In the Mid Permian sedimentation ceased and there was a brief period or erosion across the platform before continental clastics were deposited across the region during the Triassic. During the Late Triassic there was another period of erosion which was more severe towards the east. In the

Jurassic a fining upwards succession passing from coarse sandstones to shales was deposited across the entire platform and is interpreted to be a fluvial environment changing into a lacustrine environment. The sediments contain progressively more volcanically derived material in the east suggesting there was a volcanic margin to the east of the basin. In the Early Cretaceous the basins were connected to the sea and sediments fluctuate between shallow marine and deltaic sediments in both the Eromanga and Surat basins. There was a regression in the east around 110 Ma , and during the Cenomanian continental sediments were deposited. In the west there is a brief period of increased subsidence at 100 Ma. Sedimentation ceased shortly afterwards. A fuller description of the evolution of the platform can be found in Gallagher et al., (1994).

4.3.10 Eastern Australia - Results

Gallagher et al., (1994) also review the different suggested subsidence mechanisms. They dismiss a thermal cause and argue that the subsidence is caused by downward pull from the subducting slab. Their argument for this is that there is greater subsidence in the east closer to the subduction zone and that the backstripped subsidence does not show a distinct curve. Considering the data they present there are a number of problems with this theory. Firstly when looking at the backstripping data, one well from the east, e.g. Arlington 1 (Fig. 4.11) does show greater subsidence however, other wells from the east and west of the platform (the Walkandi 1 and Red Cap 1 wells) have almost identical subsidence profiles until 100 Ma despite being over 1000 km away from each other. The sedimentary cover is even more extensive than that covered by the wells and is remarkably uniform when seen in cross section (see Figure 1 from Gallagher et al., (1994)). It does not show increased subsidence in the east nearer to the active margin. It is difficult to see how a subduction zone could exert such a wide ranging and uniform subsidence pattern. Equally, the subsidence patterns are consistent with the subsidence produced by cooling of the lithosphere as proposed in this thesis rather than flexure caused by a subduction zone. The backstripped subsidence does fit the subsidence from the model well for most of the subsidence history.

The wells in Figure 4.11 are ordered from east to west and the best fitting models show a trend of a thicker final lithosphere in the west (154 km – Walkandi 1) than the east (122 km – Arlington 1). This agrees with the trend seen in surface wave tomography (Fishwick et al., 2008). Their results suggest a lithosphere of 150-200 km in the west which is in good agreement with the results of this study, however they only have a ~100 km thick lithosphere in the east which is thinner than the 120 km used in the best fitting model. However, it may be

that a later event caused thinning beneath eastern Australia. The crustal thicknesses used in the model also fit reasonably well with those measured. The Moho depth beneath the Eromanga basin is between 36-40 km (38 km – Walkandi) and 34-36 km beneath the Surat basin (34 km – Red Cap 1, 32 km – Arlington 1) (Collins et al., 2003). While the modelled subsidence does not explain the increased subsidence rates seen in the Late Cretaceous it does provide a good fit up to this point.

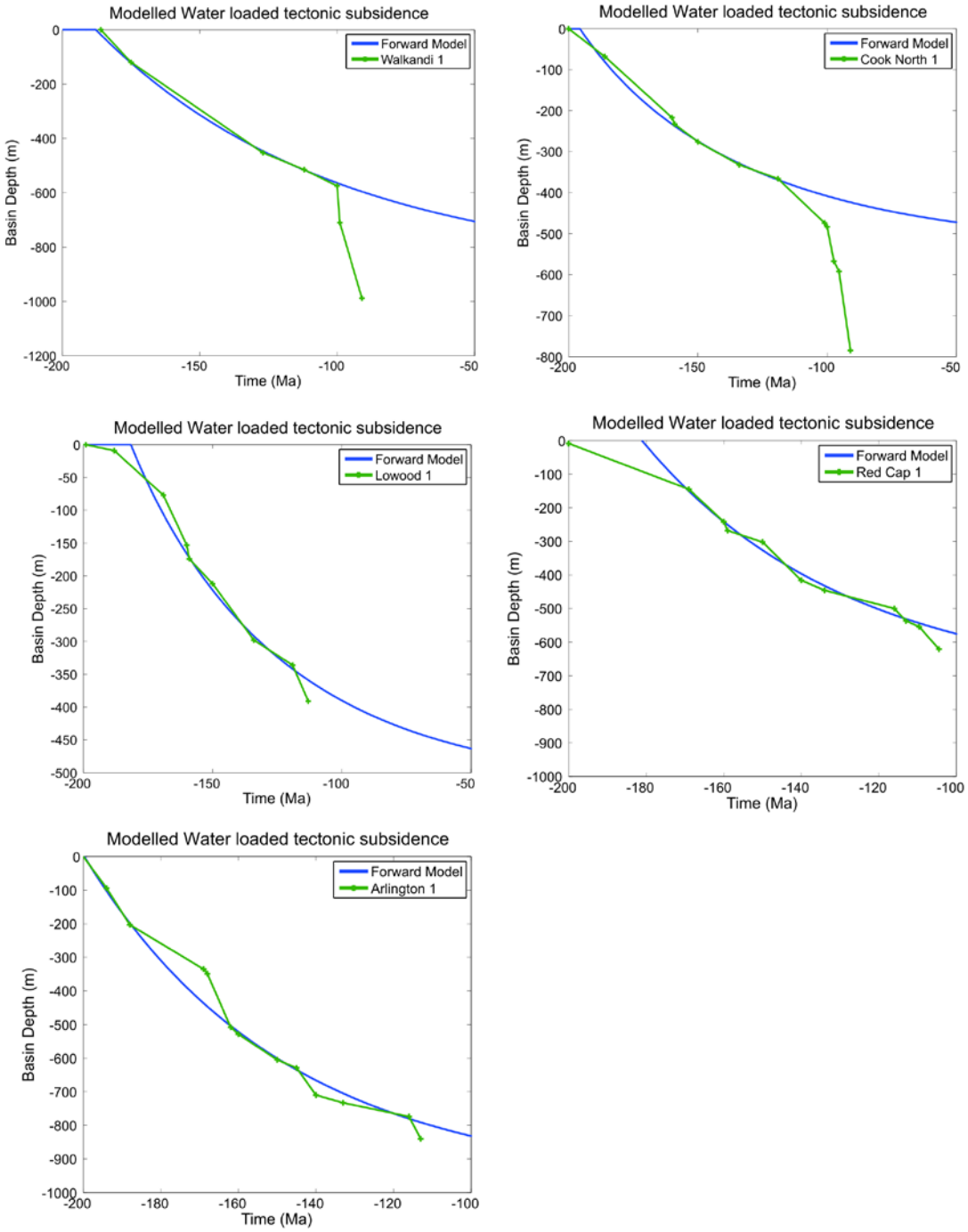

Figure 4.11: The backstripped subsidence curves from the platformal succession of Eastern Australia compared to the curves produced by the best fitting forward model. The locations of the wells are shown on Figure 4.10. The best fitting model varies from Walkandi 1 well in the west which is fitted best by a model with a 154 km thick lithosphere and a 38 km thick crust. The best fitting crust gets thinner as does the lithosphere to the east with the Arlington 1 well being fitted best by a 32 km thick crust and a 122 km thick final lithosphere.

4.4 Discussion

The results of the study demonstrate that cooling and thickening of the lithosphere provide a good explanation for the subsidence seen across many areas of accretionary crust on a global scale. Chapter 3 and Holt et al., (2010) showed that this mechanism provided a good fit to the subsidence of two North African basins in a detailed case study. This chapter provides further evidence supporting this subsidence mechanism, but also shows it applies more broadly and is likely to be an inherent property of accretionary crust on a global scale, when other forces such as continental collision are not affecting the crust. Equally the range in basin ages shows that this mechanism has occurred throughout the Palaeozoic and quite likely as long as the accretion process has been acting. Interestingly a study into what causes the elevation of the more recently accreted American Cordillera suggested a very similar situation to the starting parameters of the model used here. Hyndman and Currie, (2011) propose that the lithosphere for 100s of km behind the active arc may remain thin (~ 60 km) even though the crust is of a normal thickness. Once the subduction terminates this could potentially be a region of future subsidence.

4.4.1 A comparison with other suggested basin forming mechanisms

However, numerous alternative mechanisms have been suggested to explain the formation of these basins. Rifting in some form has been suggested for the basins in North Africa (Lüning et al., 1999), South America (Oliveira and Mohriak, 2003), Turan (Thomas et al., 1999) and Australia (Korsch et al., 1988). In many of these regions there are indeed rifts visible on seismic data in some of the basins. The subsidence profiles themselves are not always detailed enough to clearly distinguish whether there is a rift phase. In many cases, especially in the older basins, the earliest part of the subsidence suffers from poor dating and consequently the time span taken to deposit the first layer may only be confined to a period or epoch. This means it is often ambiguous as to whether it would better fit a rift or cooling and lithospheric growth. Yet the rift sequences generally only form a small proportion of sediments within the basins and

are seen in some basins in the region, but not in others despite the sedimentary sequences in each basin sharing remarkable similarities (Chapter 3). Even in basins where rifts are clearly imaged they tend to be localised and cannot explain the subsidence across the whole basin. It is possible that the rifts have not been discovered yet. However, many of the basins considered are producing oil or are actively being explored and good seismic data exists across the basins so it is unlikely this is the case. The two mechanisms do not have to act in isolation. In fact the initial conditions of a normal thickness crust, underlain by a thin lithosphere would tend to favour rifting as the warm conditions would weaken the crust, which may then add to the overall subsidence.

Another argument against these being solely rift basins is the timescale the subsidence occurs for (over 200 Myrs). This led to the mechanism of 'slow rifting' being put forward where the stretching occurs at low strain rates over a long period of time (Allen and Armitage, 2011; Armitage and Allen, 2010). This produces a subsidence pattern which is initially linear during the slow stretching phase, then there is a kink when stretching ceases and this is followed by a decaying curve due to the thermal relaxation phase. When the first points are poorly dated it is often difficult to distinguish between this mechanism and the one investigated in this thesis. This is the case in South Africa and for the Turan platform. However, in Australia the dating is good enough to show that the subsidence profiles are curved throughout for wells Arlington 1 and Walkandi 1. The composite well from the Ghadames basin backstripped in Chapter 3 also has good age resolution for the first points and is curved throughout. Therefore subsidence patterns alone are not sufficient to distinguish between the mechanism proposed by Armitage and Allen (2010) and the one put forward in this thesis.

However, the argument that applies to rifting also applies to this mechanism; there is a lack of imaged rifts in many of the basins. Armitage and Allen, (2010) argue that slow rifting may result in deformation being spread over numerous small faults, which is why they are not imaged. This does not agree with the results from analogue models of rifting which show that lower strain rates lead to increased localisation of strain on fewer large faults (Bellahsen et al., 2003). The same is observed at mid ocean ridges, where faster spreading ridges have a more homogenous distribution of strain over lots of smaller faults whereas slower spreading ridges have a more heterogeneous distribution of strain with fewer larger faults (Carbotte and Macdonald, 1994). Similar trends are seen from studies of active continental rifts, such as the East African rift, where differing strain rates lead to the bimodal volcanism observed (Mazzarini et al., 2004). Fast strain rates lead to more faults which provide a larger number of

pathways for magma to reach the surface. This means it has less time to differentiate. Slow strain rates produce fewer faults impeding the ascent of magma resulting in differentiation at depth and the eruption of more evolved magmas. The results of these studies contradict Armitage and Allen's explantion for the absence of rifts. Therfore the lack of sufficient rifting is a strong argument against their suggested basin forming mechanism. It is more conclusive than comparing the fit of the two proposed subsidence mechanisms to the backstripping results from many of the basins

Armitage and Allen, (2010) link the formation of these basins to periods of supercontinent breakup. They suggest that before and during breakup large areas of the continent are under tensional stress which causes the slow stretching. This scenario could fit for eastern Australia where rifting from India occurs at ~ 156 Ma and a deep sea passage has been established between Australia and Antarctica by 116 Ma (Veevers, 2004). However, this would suggest that the continent is under tension until around 116 Ma, which would result in a linear subsidence history until this point. The subsidence data from the Arlington, Red Cap 1 and Walkandi 1 wells do not show this, but fit the thermal subsidence calculated from my forward modelling. The Cook North 1 and Lowood 1 subsidence could both fit a straight line or a curve as shown in Figure 4.11. The timing of the subsidence on the Turan platform also fits with the breakup of Pangea, but it is on the northern margin of the Neo-Tethys and far from any rifted margins where tensional stresses are concentrated. The basins in Arabia, North Africa, South America and South Africa form after the amalgamation of Gondwana and during the formation of Pangea (Veevers, 2004). This does not fit with the timing of basin formation proposed by Armitage and Allen. However, the timing of subsidence in each of the basins fits much better with the accretion age of the underlying crust (Table 3.1). Finally slow rifting also requires the basin to be under tension for long periods of time whereas many of the basins show periods of compression in their history. This does not present a problem for cooling and thickening of the lithosphere because it acts in the background and certain times in the basin's history may be dominated by other forces, but when these cease the subsidence will continue.

Dynamic topography has also been suggested as a potential mechanism for forming these basins (Heine et al., 2008). The main problems with this mechanism are that the subsidence patterns it would produce are not known and models of which areas of the crust were experiencing negative dynamic topography only go back ~ 70 Myrs. This is too young to say whether any of the basins considered in this study may have been affected. Another weakness of this model is that Heine et al., (2008) show that at present the basins of North Africa and

South America should be experiencing negative topography, but both are currently continental platforms above sea-level and neither are major sites of sediment accumulation.

4.5 Conclusions

This study worked from the hypothesis that accretionary crust begins with thin lithosphere which is a property of its constituent terranes. Then cooling and growth of the lithosphere causes subsidence as an isostatic response. This had been shown to be a viable formation mechanism for the Palaeozoic basins of North Africa in Chapter 3, providing a good fit to the backstripped subsidence curves. This chapter shows that the modelled subsidence from this mechanism fits the subsidence from a wide number of basins formed upon accretionary crust from around the globe. This further indicates that the mechanism is generically applicable to accretionary crust. The basins formed at different times throughout the Palaeozoic shortly after the end of the accretionary process. Some overlap the final stages of accretion, but generally deposition of sediments starts 25-50 Myrs after accretion has ceased. The basins follow a curved subsidence pattern where the subsidence rate decays through time. There are undoubtedly different stories mixed in with the subsidence pattern of each individual basin related to periods of compression, climatic effects or other complimentary subsidence mechanisms which could be teased out in in-depth studies of each region.

However, a global study like this is still able to raise interesting points. It demonstrates the predictive capabilities of the model to help constrain the lithospheric thickness beneath the basins from the observed subsidence. It also has possible implications for the evolution of continental crust if a natural property of juvenile accreted crust is to subside and therefore accrue a sedimentary cover. It also allows for a global comparison with other subsidence mechanisms which have been suggested to form intracratonic basins. This study shows that cooling and growth of the lithosphere is much better at explaining a large number of features seen or not seen within these basins.

Declaration of Authorship

The backstripping results for the Cape fold belt were published as part of a paper in Sedimentary Geology (Turner et al., 2011). This was my contribution to the paper and as such I was third author. The other authors were responsible for the sedimentology and isotope analysis. As such when referring to results from the sedimentology within this chapter I reference the paper as I would any other paper in this work.

Chapter 5 – Subsidence of the West Siberian Basin: Effects of the impact of a mantle plume

5.1 Introduction

The West Siberian Basin (WSB) is one of the largest intra-continental rift basins in the world, with an area of roughly 3.5 million km^2, including prolongations in to the Yenisey-Khatanga Trough and the Kara Sea (Fig. 5.1). The basin is associated with the Siberian Traps, which form the largest Phanerozoic continental flood basalt province. Eruption took place at the Permian-Triassic boundary (~250 Ma; (Reichow et al., 2009)), with a plausible connection between the magmatism and the end Permian environmental crisis (Wignall, 2001). These events are commonly interpreted to be the result of the impact of a mantle plume head at the base of the Siberian lithosphere (Richards et al., 1989).

An important feature of the WSB is the regional delay on the order of 60-90 Myrs, in the onset of sedimentation after the initial rifting (Saunders et al., 2005). The cause of this delay has been inferred to be decay of uplift generated by the thermal effect of a mantle plume (Campbell and Griffiths, 1990; Saunders et al., 2005), but so far this hypothesis has not been quantified. The subsidence patterns within the WSB also present an ideal opportunity to examine the generic spatial extent of spreading plume material beneath the lithosphere. Previously this has only been estimated from the aerial extent of volcanism (d'Acremont et al., 2003), which is complicated by erosion, lack of exposure and the distance flood basalts flow from the eruptive vent, and numerical models of plume head spreading (Campbell, 2007). By comparing subsidence patterns predicted by a 1-D conductive heat flow model, this chapter provides 1) a quantitative explanation for the cause of the subsidence delay after initial rifting, 2) independent estimates of the lateral

extent of the Siberian mantle plume head beneath the lithosphere, and 3) new constraints on mantle plume head dynamics.

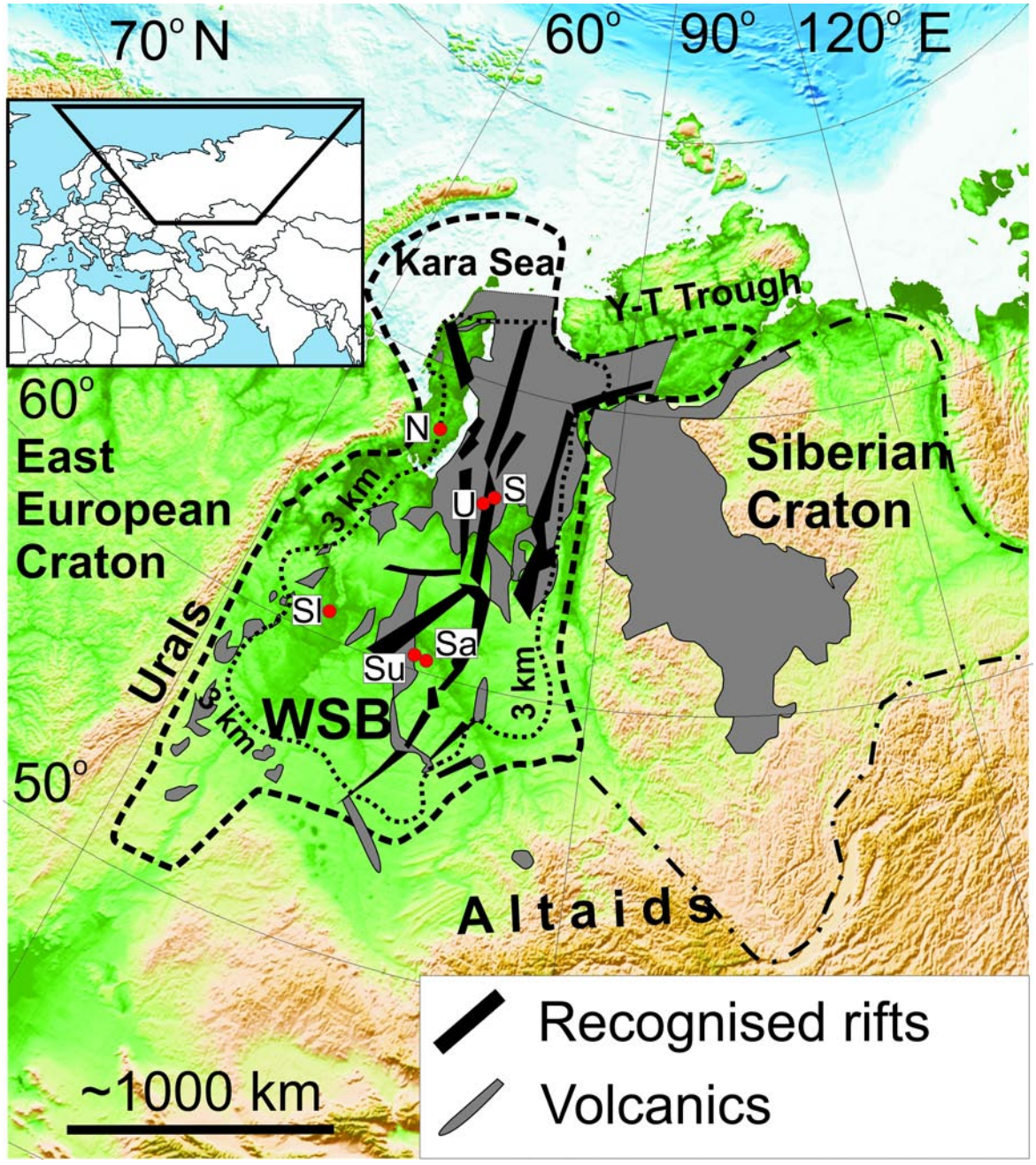

Figure 5.1: Location of the West Siberian Basin (dashed line), the 3 km sedimentary thickness contour (dotted line) and the neighboring Siberian Craton (dot dash line). Red dots mark backstripped wells from Saunders et al. (2005). N=Novoporto-130, S=SG-6, Sa=Samotlar-39, Sl=Salym-184, Su=Surgut-51, U=Urengoy-414, Y-T Trough=Yenisey-Khatanga Trough. Modified from Allen et al. (2006).

5.2 Geological Background

The Geology of Siberia and the WSB are reviewed in depth in a few papers (Peterson and Clark, 1991; Vyssotski et al., 2006). Therefore within this chapter I focus on the data pertinent to understanding the cause of the subsidence in the basin and important when choosing the right parameters when modelling this.

5.2.1 Tectonic and geological evolution

The basement beneath the WSB is formed from segments of island arcs, oceanic crust, Proterozoic micro-continents and other terranes. These were accreted to the margins of the Siberian Craton and Baltica during the Palaeozoic as the Khanty-Mansi Ocean closed between these two older continental blocks and the smaller Tarim block to the south (Aplonov, 1995). These events formed part of the Altaid orogeny, also known as the Central Asian Orogenic Belt. There was localised deposition of Palaeozoic sediments over the more stable micro-continents (Peterson and Clark, 1991). This period in the evolution of western Siberia predates the formation of the WSB, but is important to consider when setting the initial conditions and input parameters for composition of the crust in the numerical model.

At the end of the Permian (250 Ma) the stress affecting the west Siberian area changed from compression to extension, possibly with a component of right-lateral shear between the Siberian Craton and Baltica (Allen et al., 2006). This led to rifting within the WSB which was associated with eruption of the Siberian flood basalts. The location and extent of the rifts within the WSB basin varies between authors. Aplonov, (1995), Saunders et al. (2005) and Allen et al. (2006) all have different structural maps. Part of the problem is that authors use different datasets; the rifts are identified from gravity, magnetic and seismic data. Vyssotski et al. (2006) compared the lineaments from magnetic and gravity data with the basement depressions visible on seismic data. They showed that there is good agreement in the north of the basin with rifts identifiable on all three datasets; however, in the south of the basin the presence and locations of rifts is much more uncertain. Based upon this, Vyssotski et al. (2006) divided the basin into a rifted zone and a passively subsiding zone using the 64^{o} N line of latitude. Figure 4.1 shows the locations of rifts which are agreed by all the authors above. The rifting precedes and continues during the eruption of the Siberian flood basalts between 254 and 248 Ma. The basalts have been found from wells

drilled across the WSB, though they are not found everywhere. They are thicker within the rift systems and sometimes absent from uplifted fault blocks, whether this is due to erosion is not clear. Radiometric dating and magnetostratigraphy show the basalts in the basin erupted at the same time as those outcropping across West Siberian Craton (Reichow et al., 2009; Westphal et al., 1998) and to have a similar geochemical signature to the Noril'sk suite found in outcrop (Reichow et al., 2005). The basalts reach a maximum thickness of 3 km on the neighbouring Siberian Craton. The maximum thickness penetrated in the basin is 1km in well SG-6, however the well was terminated within the basalt pile and seismic data suggests that there is a further 1-2 km beneath this (Reichow et al., 2005). An average thickness of 2 km is used by Braitenberg and Ebbing (2009) in their gravity modelling who say that it is an upper estimate. Most authors agree that the basalts in the WSB are erupted sub-aerially (Saunders et al., 2005; Saunders et al., 2007; Vyssotski et al., 2006; Westphal et al., 1998) and therefore it is likely that the basin was uplifted at the time, although there is some dispute regarding this (Elkins Tanton and Hager, 2000).

As rifting occurred coarse grained, non-marine sediments were deposited within the rifts. During the Triassic sediment deposition continued within the rifts at a reduced rate, but there was no deposition (or at least preservation) outside the rifts. In areas adjacent to the major rifts, sedimentation began in the Early Jurassic (200 Ma). The first basin wide transgression did not occur until the Callovian (~160 Ma) in the late Jurassic (Peterson and Clark, 1991; Vyssotski et al., 2006). This is when the earliest sediments are recorded in the Novoporto-130, Samotlar-39, Salym-184 and Surgut-51 wells from Saunders et al. (2005) and it is visible in their backstripped subsidence curves (see Fig. 5.4). The sedimentation throughout the rest of the Mesozoic and Cenozoic is largely marine, siliciclastic and is strongly influenced by changes in the global sea-level. There is a general trend from a sediment starved basin to an overfilled basin during this time (Peterson and Clark, 1991). A more in depth review of the Mesozoic and Cenozoic basin fill can be found in Peterson and Clark (1991) and Vyssotski et al. (2006). There is little further tectonic activity within the basin after the rifting, just gentle subsidence and some minor block reorganistion until the Tertiary when there is a period of very minor compression or transpression, resulting in the inversion of older normal faults and an absence of significant Miocene-Quaternary deposition (Vyssotski et al., 2006). This has not resulted in significant uplift or erosion in the basin and a near complete sedimentary record is found across the basin. The sediment thickness

underlying the structures in Figure 5.2 A is reproduced from Aplonov (1995) and is created from older seismic data from Kunin and Ioganson (1984).

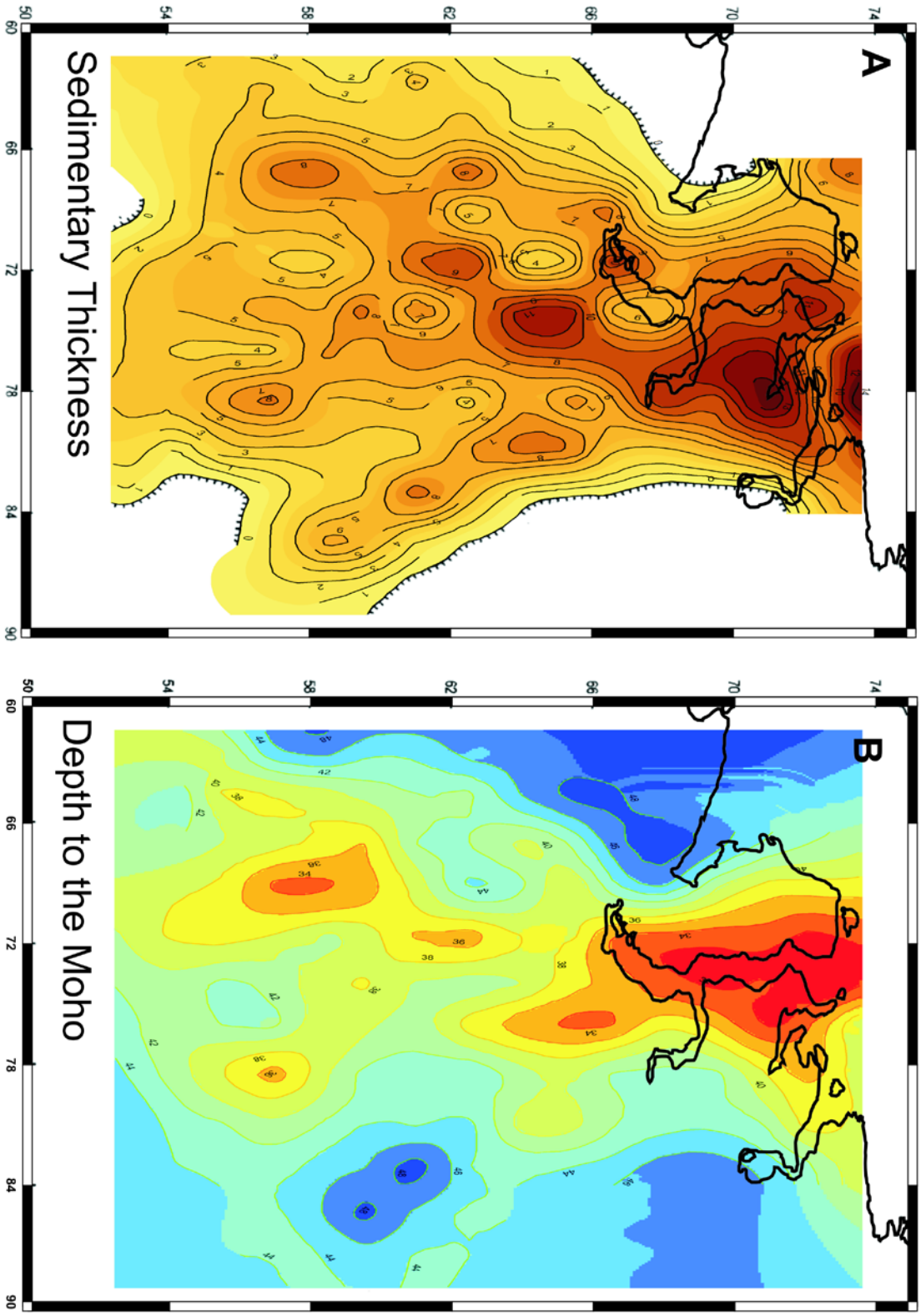

Figure 2: **A**. Map of the total sediment thickness within the basin including sediments predating the main basin forming phase. **B**. Map the Moho depth across the basin. The contours are given in km. Both are digitised versions of the maps from (Aplonov, 1995) in turn produced from an earlier study by (Kunin and Ioganson, 1984). They show some correlation with the rifts in Figure 5.1 in the north of the basin.

The differences between this and other sediment maps demonstrates the uncertainty in the exact sediment thicknesses (Braitenberg and Ebbing, 2009; Peterson and Clark, 1991).

5.2.2 Present day crust and lithosphere structure

The crustal and lithospheric thickness are both important parameters when modelling subsidence (Chapter 3). There are a number of Moho maps published for the WSB. Figure 5.2 B shows the Moho map from Aplonov (1995) which is differs from the one shown in Vyssotski et al. (2006). They are produced from different data which may in part explain the discrepencies. Both show the crust beneath the WSB is thinner than either that of the Urals to the west or the Siberian Craton to the east. In the WSB Vyssotski et al. (2006) shows the Moho depth ranging from 36-44 km whereas Aplonov (1995) has a range of 32-44 km. Individual features from either map do not match up; one area where Aplonov (1995) shows an area of thinned crust (34 km) Vyssotski et al. (2006) have an area of thickened crust (40 km). The general thicknesses agree with 2D surveys such as the QUARTZ profile (Morozova et al., 1999) and the CRATON profile (Li et al., 2007), which also show a variation in crustal thickness of 36-42 km. However, aligning relatively shallow geological features such as rifts with features in the Moho thickness maps has a high degree of uncertainty, especially away from the 2D deep seismic lines.

Measurements of the thickness of the lithosphere beneath the WSB also differ. The QUARTZ profile showed a low velocity zone in the upper mantle at ~ 150 km depth, however beneath this a layer with a normal velocity for lithospheric mantle is followed by a second low velocity zone at ~ 200 km depth (Morozova et al., 1999). Artemieva and Mooney (2001) used heat flow data to model the geothermal gradient taking the 1300 ˚C as the base of the lithosphere and calculated a thickness of ~ 125 km across the WSB. In comparison, Priestley and McKenzie (2006) who used shear wave velocities to calculate the thickness of the lithosphere reached a thickness of ~180 km under the WSB. This is similar to Pasyanos (2010) who used surface wave dispersion to model the lithospheric thickness.

5.2.3 Temperature, thickness and depth of a potential plume head

For the purpose of modelling it is important to assess the viable range of possible temperatures, thicknesses and depths of a plume head acting on the base of the WSB lithosphere. The temperature can be estimated from the composition of the volcanic rocks erupted. Elkins Tanton et al. (2007) estimate that temperatures between 1550 and 1700 ˚C at a depth of ~ 150 km are required to produce the primary melts of the youngest volcanic rocks outcropping on the Siberian Craton. This is slightly hotter, but still broadly consistent with the 1500-1600 ˚C estimated for the Hawaiian plume (Ribe and Christensen, 1999; Watson and McKenzie, 1991). A global review by Herzberg et al. (2007) showed an ambient mantle temperature between 1280-1400 ˚C with thermal anomalies 200-300 ˚C above this. This gives a plume temperature between 1480 and 1580 ˚C for mantle with a potential temperature of ~ 1280 ˚C.

The Gd/Yb ratio of the Siberian flood basalts, which can be used as an indicator of the influence of garnet in the residue and therefore the depth of melting, decreases over time from values overlapping those of Hawaiian basalts to ratios approaching the MORB field in the later basalts. Saunders et al. (2005) suggest this is evidence for a decrease in the depth of melting from > 100 km to 100-50 km. We interpret this to show that the plume thins the lithosphere, potentially to a thickness of only 50 km or heats it up to this depth. A similar trend in melting is seen in the North Atlantic Tertiary LIP (Kerr, 1994). This is also consistent with models of the Hawaiian plume which show that the swell cannot be supported by buoyancy of the depleted materials alone and requires thermal buoyancy of the lithosphere and asthenosphere (Ribe and Christensen, 1999). Estimates for the thickness of the lithosphere beneath the Hawaiian islands vary from 89 km (Ribe and Christensen, 1999) calculated from numerical models and 50-60 km measured using S-wave receiver functions (Li et al., 2004). Numerical models of plume head and lithosphere interactions also show evidence for thinning of the lithosphere, however they disagree over the amount. Nyblade and Sleep (2003) argue that only the rheological boundary layer is removed and the lithosphere is not thinned significantly because secondary convection is suppressed. The model of Moore et al. (1999) disagrees and shows secondary convection for excess temperatures of only 100 ˚C and rapid lithospheric thinning. When the lithosphere and crust are treated as having brittle and plastic rheologies (a feature not included in most models) then the lithosphere is thinned mechanically due to stress as well (d'Acremont et al., 2003).

The thickness of a plume head spreading out beneath continental lithosphere was also investigated by Nyblade and Sleep (2003) who calculated a thickness in the order of 10s of km and subsequently used a thickness of 40 km in their model. In contrast the model of Campbell (2007) which models plumes from origination at the core mantle boundary to spreading beneath the lithosphere show that the plume head will have a thickness of 175 ± 25 km. In many models the size of plume is arbitrarily defined in the starting conditions of the model (Farnetani and Richards, 1994). Even when allowed to form within the model their size is dependent on the Rayleigh number used for the convecting mantle (Zhong, 2005).

5.3 Methodology

A 1-D forward thermal model was used to examine whether the cooling of the proposed thermal anomaly could cause the subsidence in the WSB. The model was written to investigate the subsidence of accretionary crust. An in-depth description of the model is included Chapter 2. Therefore, I only summarise the underlying physics used in the model below and then outline the starting parameters, before looking at the effect of varying parameters relevant to the WSB.

5.3.1 Model construction

The model is a 1-D finite difference code written in Matlab to solve conductive heat flow through the lithosphere and upper mantle and then calculate the subsidence of the column. The code calculates the temperature *T* of each individual element at its respective depth *z* over time *t* by combining Fourier's law for conductive heat flow with conservation of energy and including the heat produced by radioactivity in each element *A* to give the equation

$$\frac{\partial T}{\partial t} = \frac{1}{C_p \sigma}\{\frac{\partial}{\partial z}(k\frac{\partial T}{\partial z})\} + A \qquad (5.1).$$

Each element of the model has a specific heat C_p related to the rock type and a density ρ which is dependent on the temperature and rock type as shown in equation 5.2.

$$\rho = \rho_0(1 - \alpha(T - T_0)) \ (5.2).$$

The reference density ρ_0 is the density of the material at the reference temperature T_0. The coefficient of thermal expansivity α and ρ_0 both vary with the rock type. The temperature is

calculated through time numerically using the forward Euler method. The temperature profile through the model (the geotherm) is then used to calculate a density profile through the column from the reference density for each grid point. From this the height of the column relative to sea-level is calculated with isostacy by comparing it to a column of mid ocean ridge material made up of 2.7 km of water overlying a 7 km basaltic-gabbroic crust above a peridotitic upper mantle. If the height calculated for the column drops below sea-level then the 'basin' is filled to sea-level with water. This means the subsidence produced by the model is equivalent to water loaded tectonic subsidence calculated from backstripping. In order to compare the model to the observed Moho depths the model is also run with sediment loading. However, the Moho depths from the literature are those observed today and not the initial conditions, so the model was run to produce a final crustal thickness, including sediments deposited in the basin, which matches the present day crustal thicknesses.

The temperature at the top of the model is fixed to 0 °C whereas the temperature at the bottom is fixed at 1381.3 °C, which is calculated by following an adiabat of 0.3 °C/km down from a potential temperature at the surface of 1330 °C to the base of the model (170 km). A detailed description of the model including how it was benchmarked is shown in Chapter 2.

The initial conditions of the model are set up to match our current knowledge of the WSB as closely as possible. The crust is composed of a layer of basalt at the surface above a granitic upper crust and a lower crust of with a density corresponding to granulite and mafic intrusions related to the volcanics at the surface. The thickness of the crust is varied, as are the basalt thickness and the upper/lower crust ratio to model the changes seen in these parameters across the WSB. The crust is underlain by mantle lithosphere down to the top of the plume head. The initial temperature profile through the crust and mantle lithosphere is a linear gradient from 0 °C at the surface which intersects the mantle adiabat at the top of the plume head. The initial temperature of the plume head, its thickness and position are varied. Below the plume head, the temperature follows the mantle adiabat down to the base of the model at 170 km depth. This model thickness results in the base of the lithosphere settling at ~ 150 km (using the 1200 °C definition of Stein and Stein (1992)), which is an intermediate value of the various estimates of present-day lithospheric thickness (Artemieva and Mooney, 2001; Morozova et al., 1999; Pasyanos, 2010; Priestley and McKenzie, 2006).

5.4 Results and discussion

5.4.1 Model sensitivity and the standard model

The effect of varying the relevant parameters within the ranges seen in the WSB on the modelled subsidence was investigated. The sensitivity of the model to variation of the crustal thickness, composition, potential temperature, final lithospheric thickness and radioactive heat production are shown in Chapter 3. Large variations in the mantle potential temperature and radioactive heat production were shown to have little effect on either the total subsidence or the shape of the subsidence curve and therefore are not considered. However, the composition and thickness of the crust and the final lithosphere thickness both cause large variations in the subsidence produced.

Chapter 3 did not look at conditions specific to the WSB or investigate the effect of a plume head. Therefore in this chapter the sensitivity of the model to variations in crustal thickness and basalt thickness in the WSB, and different plume scenarios is studied. In each case one of the parameters is varied while the rest are kept constant in a standard set up which has an 18 km thick lower crust, a 15 km thick upper crust and a 2 km thick basalt layer. The thermal anomaly begins at 50 km depth and is 50 km thick, with a temperature of 1500 °C. This set up is referred to as the Standard Model from here on in this Chapter.

5.4.1.1 Crustal thickness

Crustal thickness varies across the WSB. The Moho depth varies from greater than 45 km at the edge of the basin to 34 km in the rifts although throughout most of the basin the crust is between 36-40 km thick (Fig. 5.2). Model runs carried out at the two extremes of a 46 km thick crust and 34km thick crust, and for an intermediate value of 38 km are shown on Figure 5.3a. All the other parameters are kept as standard. The presence of a hot layer in the lithosphere beneath a 46 km thick crust causes an elevation of about 2.5 km to begin with, which subsides as the anomaly decays away. It does not result in a basin as the crust never drops below sea level so is unlikely to become a depocentre for sediments. For a final crustal thickness of 38 km, including sediments, the crust starts with an elevation of 1400 m, which then subsides, dropping below sea-level after 88 Myrs. The shape of the curve changes as sedimentation begins and reaches a final water loaded

subsidence of 1000m. When the model is run for the thinned crust with a final crustal thickness of 34 km the initial elevation is 360 m and the model drops below sea-level after 14 Myrs. The final water loaded tectonic subsidence is 2850 m.

In Figure 5.3b the effect of variation in the thickness of the basalts is investigated. To test the effect of different possible basalt thicknesses present in the WSB, the model was run with no basalt on the surface through to a 4 km basalt layer. All the other parameters are kept as standard. The results show that as the basalt layer is thickened the initial elevation and the length of time above sea-level decreases, but the total amount of subsidence increases (see Fig. 5.3b.). Thickening the basalt layer by 1 km increases the final water loaded subsidence by 66 m because basalt is denser than the granite it replaces (the total thickness of the crust is kept constant). However, the limit of possible variations in basalt thickness in the WSB has a much smaller effect on the subsidence of the basin than that of other parameters, such as the crustal thickness.

5.4.1.2. Plume head conditions

There is a large degree of uncertainty in the conditions of the plume head. As discussed in more detail in section 5.2.3 there is a lot of debate about the temperature, depth and thickness of a possible plume head. Using the model it is possible to see whether cooling of a thermal anomaly could cause the uplift and delayed subsidence seen in the WSB. The first parameter investigated was the temperature of the plume head. A range of temperatures from 1400 – 1600 °C were chosen to cover the range of possible plume temperatures following melting and thinning of the lithosphere. The model runs were carried out at intervals of 50 °C. The results are shown in Figure 5.4c and reveal that a hot plume results in more initial uplift and increases the length of time before a basin begins to form. A thermal anomaly with a temperature of 1400 °C produces a model with an initial elevation of 1200 m which starts forming a basin after 81 Myrs whereas a plume head with a temperature of 1600 °C uplifts the crust to 1550 m and the crust does not drop below sea-level until after 95 Myrs. In all model runs, the final temperature profile, and therefore the final subsidence, is the same.

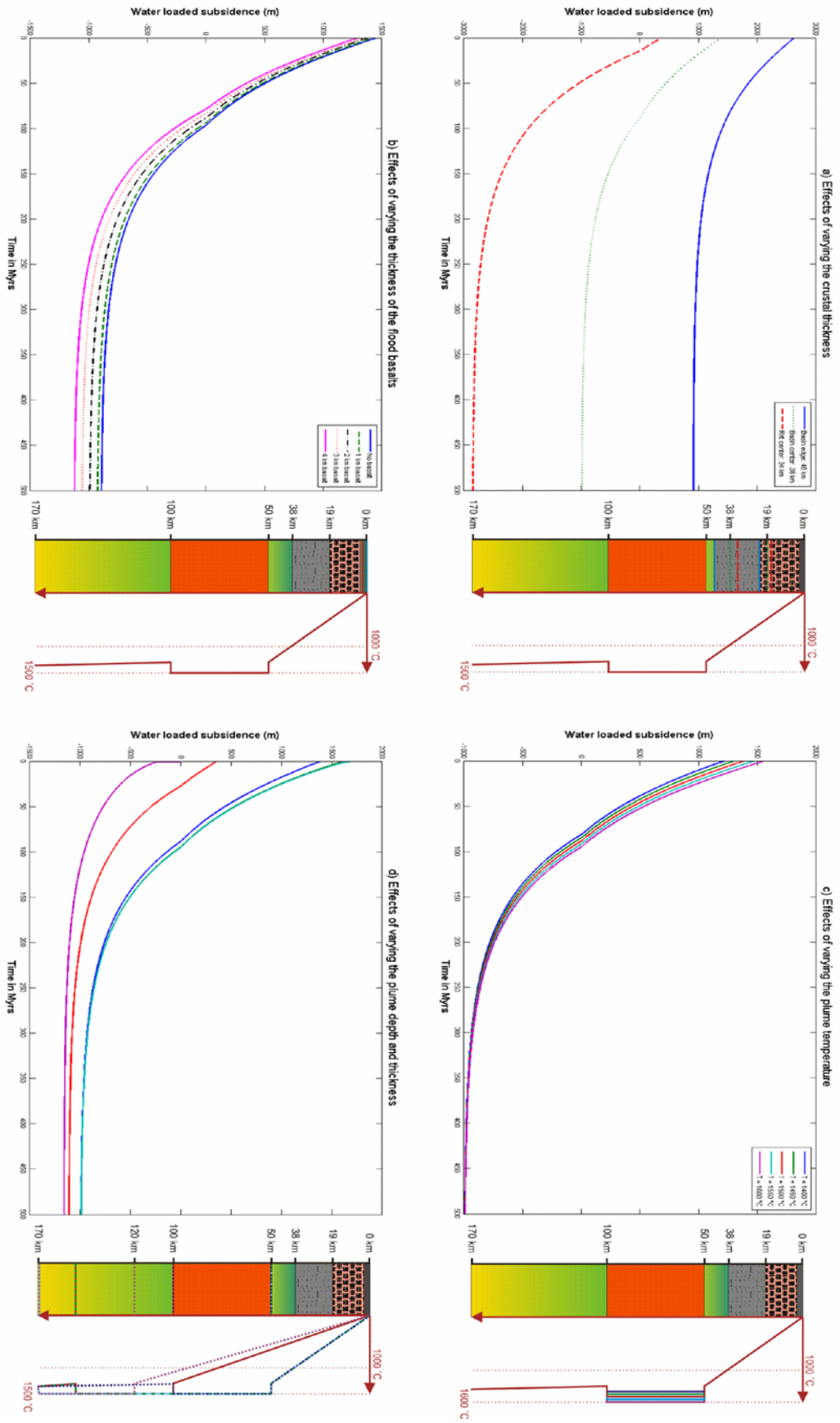
Water loaded subsidence (m)
Time in Myrs
a) Effects of varying the crustal thickness
Basin edge: 48 km
Basin centre: 36 km
Rift centre: 24 km
0 km
19 km
38 km
50 km
100 km
170 km
1000 °C
1500 °C
Water loaded subsidence (m)
Time in Myrs
b) Effects of varying the thickness of the flood basalts
No basalt
1 km basalt
2 km basalt
3 km basalt
4 km basalt
0 km
19 km
38 km
50 km
100 km
170 km
1000 °C
1500 °C
Water loaded subsidence (m)
Time in Myrs
c) Effects of varying the plume temperature
T = 1400 °C
T = 1450 °C
T = 1500 °C
T = 1550 °C
T = 1600 °C
0 km
19 km
38 km
50 km
100 km
170 km
1000 °C
1600 °C
Water loaded subsidence (m)
Time in Myrs
d) Effects of varying the plume depth and thickness
0 km
19 km
38 km
50 km
100 km
120 km
170 km
1000 °C
1500 °C

Figure 5.3: The sensitivity of the model to a) the thickness of the crust, b) the variation in the basalt thickness, c) the temperature of the plume head and d) the depth and thickness of plume head. In each case only one parameter is varied while the rest are kept as a standard model described in the text. The column to the right of the water loaded subsidence curves schematically represents initial set up of the model.

Analyses of the lavas suggest that the lithosphere may have been thinned to as little as 50km (Saunders et al., 2005), however others suggest that the lavas are produced from a deeper source without the need for such lithospheric thinning (Elkins Tanton and Hager, 2000). Studies of modern hotspots and modeling of plumes provides further variation on possible plume head scenarios, as described in section 5.2.3. To test the effect of the depth of the plume the model was run for a thin plume head (only 50 km thick) situated between 50-100, 100-150 and 120-170 km depth. Then the model was run with a plume head between 50-150 and 50-170 km depth to see what effect the plume head thickness has. The results in Figure 5.3d show that for all the model runs where the plume starts at a depth of 50 km the crust starts significantly above sea-level. For a 120 km thick plume the initial elevation is 1700 m whereas a 50 km thick plume only has an initial elevation of 1400 m and the onset of sedimentation is hastened. However, there is little difference when compared to the initial elevation of deeper plumes. If a 50 km thick plume begins at 100 km depth then its initial elevation is 350 m above sea-level whereas if the plume is 20 km deeper then the initial elevation of the plume is 250 m below sea-level. The results show that the subsidence curve is much more sensitive to the depth of the plume than the thickness of the plume. This is because the temperature contrast of the plume with the normal geotherm is greater at shallower depth, which will cause a greater reduction in the density of the material and therefore more initial uplift.

The model predicts that the subsidence in the WSB is most sensitive to the thickness of the crust within the basin and the depth of the plume in the column. Varying the temperature and thickness of the plume and the thickness of the basalts for the ranges observed and expected for the WSB does not significantly alter the subsidence curves.

5.4.2 Thermal subsidence curves

The results of the sensitivity tests on the model show that it is possible for a range of different starting parameters for the cooling of a plume head to produce a sedimentary basin with a delayed onset of sedimentation after rifting similar to that seen in the WSB (Peterson and Clark,

1991; Vyssotski et al., 2006). However, by using what is known of the crustal structure after rifting and flood basalt eruption as input parameters the model can be compared to backstripped subsidence curves from wells within the WSB to test the model further.

An estimate of the initial crustal thickness can be reached by subtracting the present day sedimentary thickness from the present day Moho depth (Fig. 5.2). This indicates an initial crustal thickness of around 28 km in the deepest rifts and 32-36 in the wider basin. The variation in the basalt thickness is not known, so we assume the basin is covered by an average thickness of 2 km as used by Braitenberg and Ebbing (2009) in their gravity modeling. There is far greater degree of uncertainty in the make-up of the lithosphere and upper mantle. The present day lithospheric thickness does not help to show to what depth the plume penetrated, whether the plume head spread out across the entire basin and if it was the same temperature, thickness and depth across the entire basin. To keep the model simple the plume head was assumed to be present across the entire basin at the same depth and temperature as the standard model. The model was set up to mirror the real situation as closely as possible.

Backstripped wells from Saunders et al. (2005) were used to test the models as they cover a broad range of locations geographically from around the WSB, but also different crustal thicknesses and sedimentary thicknesses. The locations of the 6 wells are shown on Figure 5.1. The backstripping analysis showed earlier onset of sedimentation in the rifts, around 250 – 240 Ma, and a greater amount of subsidence than the wells from the wider basin, which show the onset of sedimentation between 200 and 160 Ma. The backstripped wells are shown alongside the modeled subsidence in Figure 5.4. The Standard Model with a 36 km crust underestimates the tectonic subsidence compared with the all the wells. However, it produces a final crustal thickness including sediments of 38.05 km which fits observations of the present day Moho in the wider basin, outside the rifts. When a slightly thinner initial crust of 34 km is used (the 'Basin model' in Fig. 5.4) then the subsidence from the model fits the wells outside the rifts (N, Sa, Sl, Su), giving a final crustal thickness (including the sediments) in the wider basin of 37 km thick. This is within the range of Moho depths seen in the basin, but is on the low side. Both the Standard and Basin model have an equal thickness of upper and lower crust. If the proportions of upper crust and lower crust are varied in the model, then it is possible to fit both the observed Moho values and backstripped subsidence curves from the WSB ('Thin upper crustal model' Fig. 5.4). The standard rift model has a 14 km lower crust, 12 km of granite and 2 km of basalt. This gives an initial crustal thickness of 28

km which aims to mirror the initial conditions in the rifts. However, it overestimates the subsidence when compared to the backstripped well logs from the Urengoy rift system (S and U). It does produce a good match to the final crustal thickness (34 km) which includes a sedimentary thickness of 6 km, like that seen in deep well SG6. If the initial crustal thickness is increased to 30 km the final crustal thickness is ~35 km which is slightly larger than observed values, but the tectonic subsidence produced by the model provides a much better fit to the backstripping from the wells. This is the 30 km rift model from Figure 5.4. The starting set up for the five model runs shown in Figure 5.4 are summarised in Table 5.1.

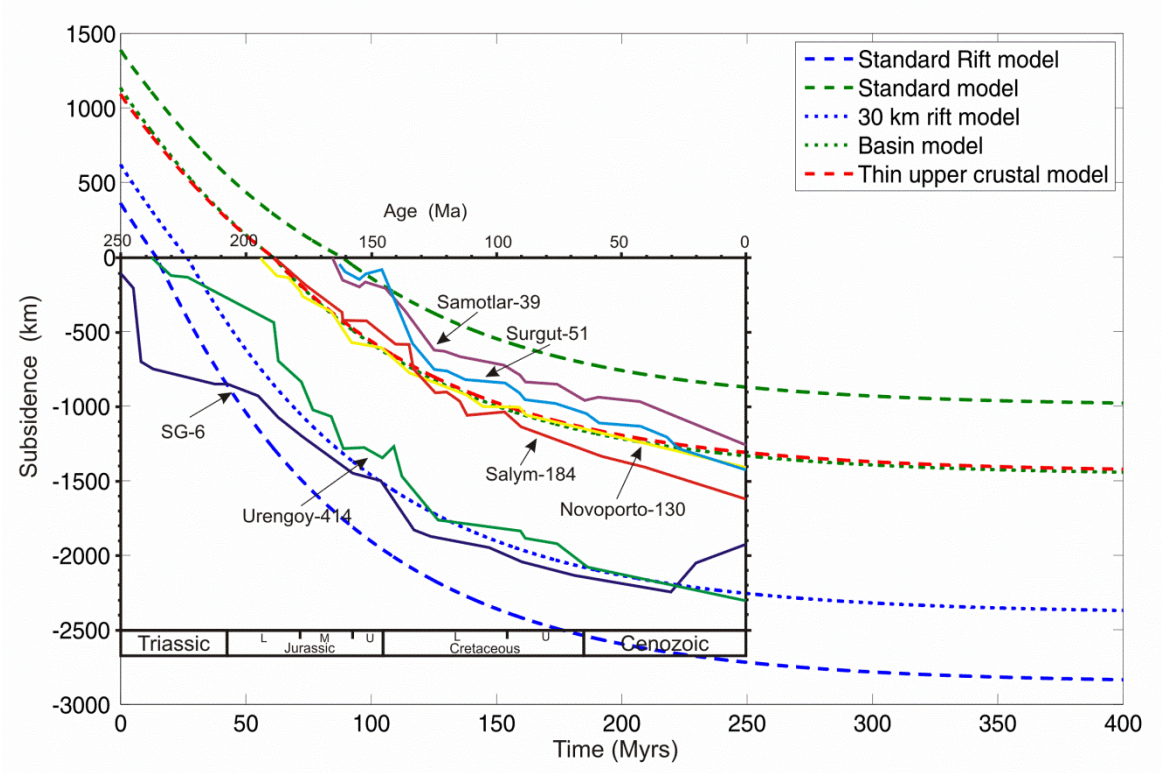

Figure 5.4: Backstripped water-loaded subsidence from wells across the basin (Saunders et al., 2005) is compared to the subsidence produced by the forward model. The wells within the rifts are fitted best by a model with a 30 km thick crust. This does not fit the rift phase of SG-6 well because rifting is not included in the model, however it is a close fit to the thermal subsidence phase. The standard rift model has a thinner initial crustal thickness of 28 km. The delayed onset in sedimentation seen from the wells outside the rifts can be matched equally well by a model with an initial crustal thickness of 34 km with the lower crust forming 14 km of this or a 35 km crust where the lower crust is 21 km thick. In each of the above models the plume lies at 50-100 km depth and has an initial temperature of 1500 ˚C. The standard model is shown for comparison.

	Basalt Thickness (km)	Upper Crustal Thickness (km)	Lower Crustal Thickness (km)	Depth to Top of plume (km)	Plume Thickness (km)	Model Thickness (km)
Standard rift model	2	12	14	50	50	170
Standard Model	2	15	17	50	50	170
30 km rift model	2	13	15	50	50	170
Basin model	2	14	16	50	50	170
Thin upper crustal model	2	12	21	50	50	170

Table 5.1: A summary of the starting models used in Figure 5.4 for comparison with the backstripped well results.

5.4.3 Discussion

Changes in the initial crustal thickness alone are sufficient to fit both the subsidence observed in the rifts and in the wider basin. This is the parameter which shows the most variation across the basin while other parameters such as the initial thickness of the lithosphere and plume temperature would be expected to be constant. To cause subsidence in each of the wells the plume head must cover the area of the wells which gives a minimum areal extent of 220 000 km^2. However, there is no suggestion that the area covered by the well data is not representative of the entire basin. Using the 3 km contour of sediment thickness from Vyssotski et al. (2006) as a proxy for regional subsidence (Fig. 5.1) on the scale described above the plume head may have covered an area of 2 645 000 km^2 with little variation in depth to the top of the plume head.

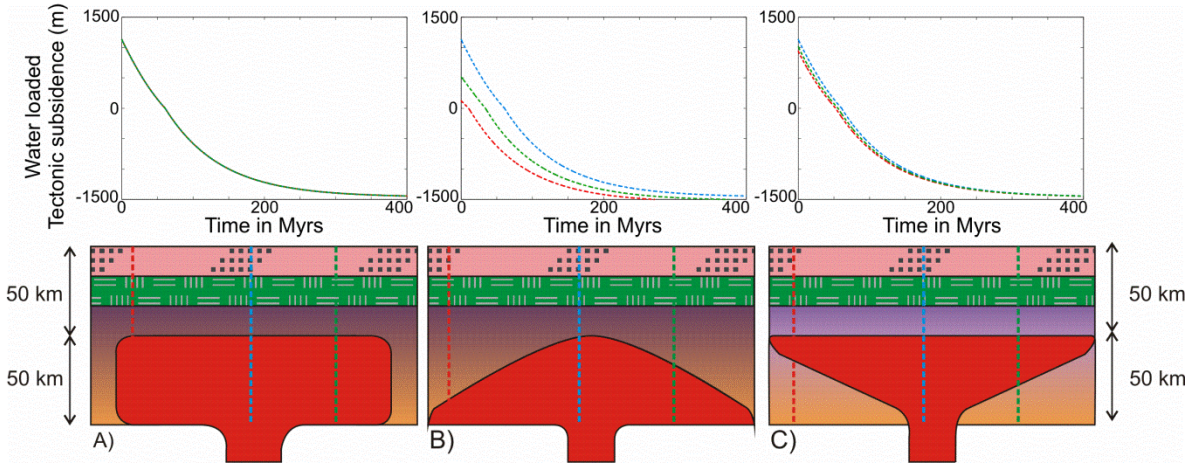

Figure 5.5: The effect of three end member shapes of possible plume heads on subsidence patterns across the basin are shown in A, B and C. In each case the crust is kept at a constant thickness. They demonstrate

that the amount of thinning or rejuvenation of the lithosphere is more important than the thickness of the plume material.

The subsidence patterns can also be used to investigate the shape of the plume head beneath the lithosphere. Three alternative end members are shown in Figure 5.5. There is very little difference in the subsidence across the basin for case A and C or between A and C because the subsidence is much more sensitive to the depth of the plume rather than its thickness. Plume head B shows the largest delay in the onset of sedimentation is in the centre of the basin where the plume material is thickest and closest to the surface. This is the opposite to the pattern of subsidence seen in the basin. However, A and C do not match the subsidence pattern from the WSB either. Changes in the initial crustal thickness must also occur as shown in Fig 5.4. It is not possible to differentiate between case A and C based on the subsidence patterns observed. Both predict significant lithospheic thinning is necessary to create the subsidence seen in the WSB. The validity of this can be further tested using the melting model of Iwamori et al (1995) where dry mantle at 1500 °C brought to 50 km depth would produce a melt column of 6-7 km which is consistent with a 2 km thick basalt pile and 4-5 km of intrusives located deeper in the crust.

This does not necessarily require a plume head; however, this would seem the simplest method of supplying hot material to the base of the lithosphere. Other mechanisms such as edge-driven convection (King and Anderson, 1998) or lithospheric foundering (Elkins Tanton and Hager, 2000) could potentially create the same initial conditions. However, lithospheric foundering does not provide the prolonged uplift evidenced from the wells outside the rifts. Edge-driven convection would be driven by the step up from the thick cratonic lithosphere to the thinner lithosphere beneath the accreted crust underlying the WSB, which could be amplified by the rifting. However, it requires an unusually low solidus to explain why the material did not melt earlier as the rising material only originates ~ 200-300 km deeper. It is also inconsistent with the temperature conditions estimated from the basalts (Elkins Tanton et al., 2007).

Uplift has been suggested in conjunction with the eruption of a number of other large igneous provinces (LIP's) including the Emeishan traps, the Deccan traps, the North Atlantic LIP and Yellowstone (Saunders et al., 2007). Our modeling shows that if the lithosphere is significantly thinned or heated, then isostasy alone will be enough to cause the uplift seen. This is in agreement with the recently proposed isostatic cause for the abnormal elevation seen in the American Cordillera (Hyndman and Currie, 2011) although the reason for the temperature anomaly is

markedly different in each case. We have not included dynamic uplift in our model as it is a transient effect only acting while the plume was beneath the basin. Whether a plume can thin lithosphere, as our results indicate, is matter of debate both for active plumes such as Hawaii and in numerical models. Ribe and Christensen (1999) calculated that the majority of the Hawaiian swell could be accounted for by dynamic uplift with only minor thinning of the lithosphere to 89 km. Likewise in the model of Nyblade and Sleep (2003) there is some lithospheric thinning, but it limited to the rheological boundary layer at the base of the lithosphere. In contrast Li et al., (2004) showed that seismic data indicates that the lithosphere beneath Hawaii is only 50-60 km thick. Similarly the model of d'Acremont et al., (2003) that focus on implementing a realistic crust and mantle lithosphere rheology shows that strain rate and stress weakening of the lithosphere enhances its erosion by a plume head. Our study provides another line of independent evidence supporting thinning of the lithosphere. Geochemical evidence from the North Atlantic LIP (Kerr, 1994) shows such thinning is associated with other flood basalt provinces. The areal extent that the lithosphere is thinned over will likely vary somewhat between LIP's as the volumes of flood basalts do. d'Acremont et al (2003) use the extent of flood basalts visible at the surface to estimate that the plume head thins the lithosphere over an area ~3 million km^2. Our method, using the subsidence patterns to give an indication of this, is preferable as flood basalts can flow large distances from where they are erupted whereas the subsidence is more directly linked to the state of the lithosphere beneath it.

5.5 Conclusions

Subsidence curves from well logs within the WSB (Saunders et al., 2005) and mapping from seismic data (Peterson and Clark, 1991) show that outside the Urengoy rift sedimentation does not begin for 60-90 Myr after the eruption of the flood basalts. This delay was suggested to be caused by uplift due to a plume head. This chapter used a 1D numerical conductive heat flow model to investigate the validity and model parameter sensitivity of this hypothesis.

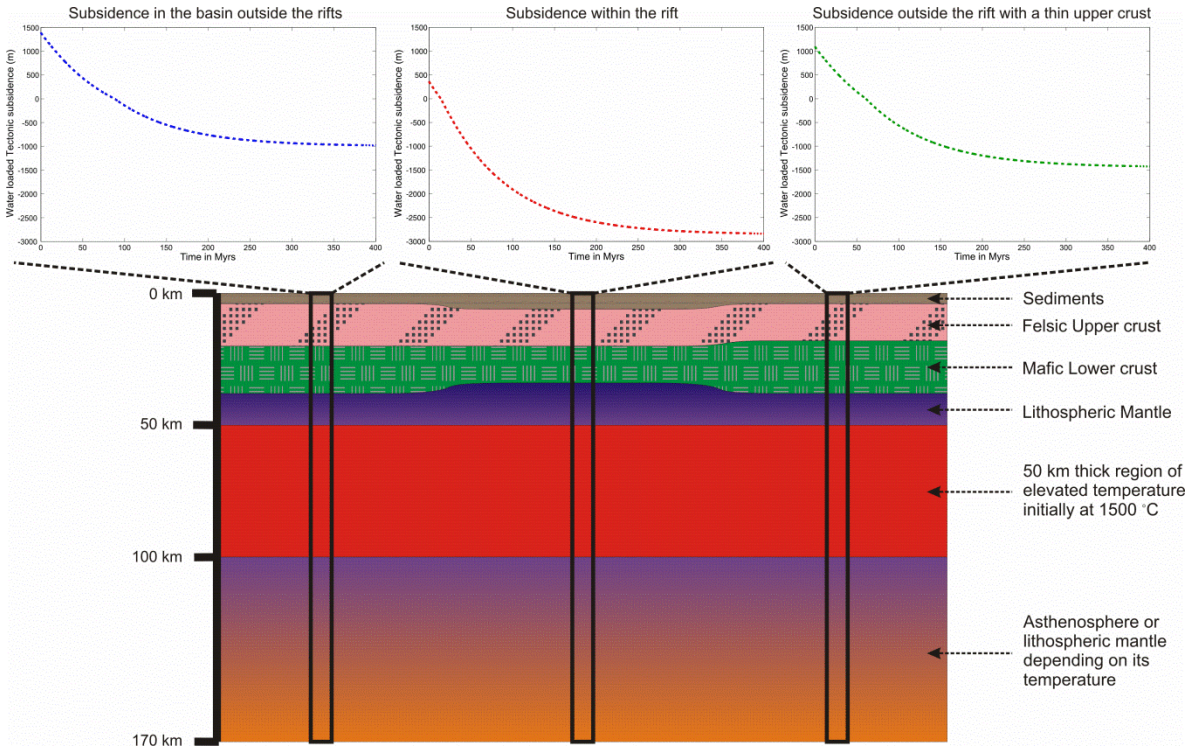

Figure 5.6: A schematic cross section across the WSB illustrating the way crustal structure can control the subsidence patterns. The subsidence patterns are not unique to one crustal thickness as variations in the relative proportions of upper and lower crust can also alter the subsidence pattern.

Comparing thermal subsidence curves from numerical heat flow models with backstripping results illustrates that the West-Siberian Basin subsidence is well explained by a 1500˚C, 50-km-thick plume head, impinging on a overlying lithosphere that is ~50 km thick after plume head emplacement with a 30 km thick crust in the rifts and a 34 km thick crust in the wider basin (Fig. 5.6). The plume head spreads out beneath the entire basin eroding the lithosphere across the basin covering an area of over 2.5 million km^2. The shape of the lower surface of the plume head is less well constrained because the subsidence is not sensitive to this parameter.

The fit of the model allows me to propose that the post-rift subsidence of the West Siberian Basin formed due to the decay of a thermal anomaly which had thinned the lithosphere to about 50 km. The most likely cause of the thermal anomaly is a plume head impacting the base of the lithosphere beneath the WSB at the end of the Palaeozoic, causing melting and eruption of the Siberian flood basalts which flowed across the WSB and the Siberian craton, and progressively thinned of the lithosphere. The plume caused uplift of the WSB except in the rifts, where the synrift subsidence counteracted the uplift caused by the plume, and therefore remained at, or

below sea level. This was then followed by cooling and thickening of the lithosphere as the supply of hot material ceased. This resulted in subsidence across the WSB. However, because areas outside the rifts were uplifted, sediments were not deposited until the crust subsided to sea-level, resulting in a depositional hiatus across the basin except in the rifts. From the Jurassic onwards the whole basin was below sea-level and continued to deepen with gradually decreasing subsidence rates. The rifts experienced greater subsidence because the thinned crust reduced the buoyancy of these areas. This chapter therefore concludes that quantitative comparison between modeled and observed subsidence of continental flood basalt provinces is a fruitful way to provide tighter constraints on the volume, lateral extent, and thermal erosion effects of mantle plume heads.

Declaration of authorship

A shortened version of this chapter has recently been accepted for publication in Geology. The paper was returned with changes from the reviewers. Interestingly they asked for more detail on the modeling which is already included in the methodology chapter of the thesis. They also suggested a fuller discussion of other mechanisms proposed to explain the flood basalts which was cut from the manuscript to fit it into Geology's page limit. My supervisors are second and third author for their helpful discussion, for the idea of using the model in this way and for helping to edit the paper, especially to cut it down.

Chapter 6 – Discussion: implications for lithosphere thickness and evolution, and potential future avenues for research.

6.1 Introduction

There are a number of common research themes which run throughout this thesis which benefit from a broader discussion than is included at the end of each chapter. Chapters 3 and 4 look directly at the question of what forms intracratonic basins upon accretionary crust in the absence of widely recognised subsidence mechanisms such as rifting or flexure. Chapter 5 may seem slightly out of place because it looks at subsidence following lithospheric thinning caused by a plume head rather than inherited from accretionary crust. Even though the West Siberian Basin is floored by accretionary crust, this does not directly control its evolution. However, all the basins considered share a genetic link because the driving force for the subsidence is the isostatic response to cooling and growth of the lithosphere. This means that they have similar subsidence patterns and consequently similar sedimentary fills. This has been discussed in detail in earlier chapters. However, what the formation of these basins is able to tell us about the evolution and present day make-up of the lithosphere has not been considered thus far. Therefore the aim of this chapter is to discuss a number of broader implications and look at ideas for further study which have come up as the research has been carried out.

6.2 The effect of lithospheric growth on subsequent volcanism

While writing the third chapter an interesting topic for further work arose which would provide another test of the model. The subsidence mechanism hypothesised is driven by cooling and subsequently growth of the lithosphere as the asthenosphere cools and becomes rigid therefore becoming part of the lithosphere. This would mean that a large proportion of

the lithosphere would be compositionally similar to the asthenosphere. This is demonstrated schematically in Figure 6.1.

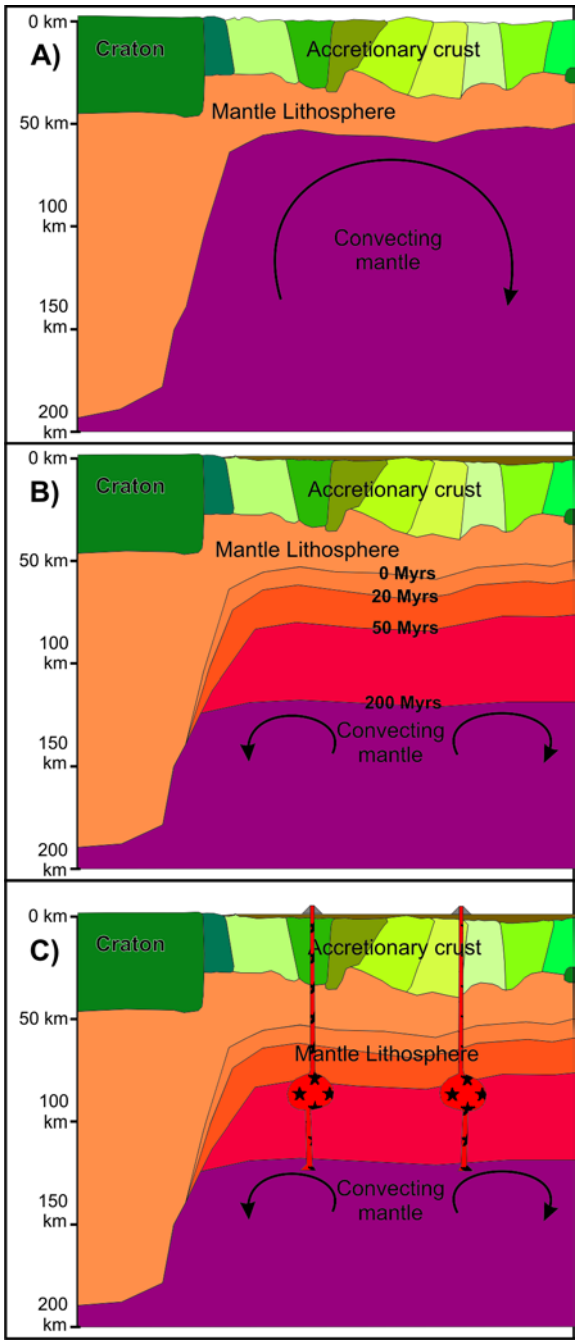

Figure 6.1: Testing the proposed subsidence mechanism using subsequent volcanism. **A)** Following the accretion of the basement beneath the basins the accretionary crust has a thin lithosphere, which means the convecting asthenosphere is much closer to the surface than beneath neighbouring cratons. **B)** The lithosphere then thickens as the asthenosphere beneath cools and becomes part of the lithosphere. This gives the lithosphere beneath the accretionary crust a different composition to the neighbouring craton which has a lithosphere made of buoyant residue from the melting which formed the crust. **C)** The accretionary crust has a lithosphere which is compositionally similar to the

asthenosphere, which should be evident from lithospheric xenoliths brought up by intraplate magmatism.

Unlike the classic model of continental lithosphere it would not be composed of the residue from the melts which formed the crust, but would be similar to the lithosphere beneath the oceans. Although it would be depleted upper mantle this is still more fertile than lithosphere beneath the older cratons and this may be visible in the chemistry of volcanism which originates from melting of the lithosphere or melts which pick up xenoliths from the lithosphere as they rise. The model predicts the lithosphere reaches its final thickness after ~ 200 Ma. Therefore the volcanism studied would need to postdate the accretion of the crust by at least this length of time. In North Africa there is some evidence from Cenozoic volcanism that this is indeed the case (Beccaluva et al., 2007). They suggest that the lithosphere has been rejuvenated, but do not consider the compatibility of their work with the model from this thesis. Future work could attempt to date the formation of the lithosphere in North Africa as this would distinguish between a later rejuvenation event and lithosphere formed by cooling shortly after accretion. Any future work of this nature should look more widely than just North Africa and consider volcanism from the regions looked at in Chapter 4 and 5 as well. This would be particularly useful in the West Siberian Basin where it could provide further evidence to support thinning of the lithosphere by a mantle plume.

6.3 Growth of the lithosphere and the final thickness

There a number of implications related to the growth of the lithosphere which follow from the subsidence mechanism proposed in this thesis. The best fit models are all reached by varying the crustal thickness and final lithospheric thickness. The previous chapters show that the values used in the modelling are consistent with other measurements, but equally the subsidence pattern recorded in the sedimentary fill could be inverted to predict these parameters. This would work particularly well when one of either the crustal or final lithospheric thickness is well constrained, but the other is less well known, which often the case with current data sets. The thickness of the crust is generally relatively well known from seismic measurements of the Moho, but the lithospheric thickness is not as easily measured (Priestley and Tilmann, 2009).

What actually compromises the lithosphere is a matter of debate. The modelling in this thesis uses a thermal definition of the lithosphere, which refers to the region of the earth where

conduction is the main process for transferring heat energy, rather than convection. However, this is also affected by the composition of the material. A depleted hazburgite will begin convecting on geological timescales at a different temperature than a fertile peridotite (Priestley and McKenzie, 2006). When residues from melts are also present this complicates matters yet further as this is less dense than the underlying mantle and will naturally adhere to the base of the lithosphere. This has been suggested as the underlying cause of the thick lithospheric roots beneath Archean cratons (Rudnick et al., 1998). However, the building blocks that make up accretionary crust are mainly formed in a subduction zone. The asthenosphere beneath the island arc will be depleted by melting, but because the mantle is constantly being replenished by corner flow (Arcay et al., 2006; Kincaid and Sacks, 1997) it will remain mostly fertile peridotite. Therefore temperature used to define the lithosphere-asthenosphere boundary in this study is taken from peridotite (Turcotte and Schubert, 2002).

There are numerous different tomography datasets and different techniques that can be used to study the thickness of the lithosphere. In general they are consistent in mapping areas of thick and thin lithosphere, but vary in the absolute values by 10s of km. For example compare the differences from estimates in Priestley and McKenzie (2006), Pasyanos (2010) and Artemieva and Mooney (2001) for the lithosphere beneath the West Siberian Basin. Some, such as the method used by Priestley and McKenzie (2006), have much poorer resolution when looking at relatively thin lithosphere (less than 140 km). Many of the results from this study lie in this range. To further test the validity of using the predictions from the best fitting models to constrain the thickness of the lithosphere, a comparison with another data set was sought. The model results show that an equilibrium point is reached where the lithosphere ceases growing. Theoretically this should be controlled by the temperature regime beneath the lithosphere. Areas of hotter asthenosphere should lead to the equilibrium point being shallower and vice versa. This could be used to indicate areas of upwelling and downwellling in the upper mantle. Therefore the lithosphere thicknesses predicted from the subsidence patterns were compared to a P wave tomography model (Zhao et al., 1997) and a hybrid tomography model utilising the full waveform known as the Voigt average shear velocity (Lekic and Romanowicz, 2011) at depths of 290 and 250 km respectively. These depths were chosen to sit a little below the base of the lithosphere. As Figure 6.1a shows there is no correlation between either of these data sets and the lithospheric thickness. There are numerous reasons why this may be the case. Firstly the velocities of seismic waves in the mantle are affected by composition as well as temperature. The lithospheric thickness could be also be controlled by composition rather than temperature. However, the most likely reason is illustrated in Figure 6.1c. The two

extremes of lithosphere thickness predicted by the model are 122 km and 155 km. The base of the lithosphere corresponds to the same temperature in each case (1200 ˚C) then the temperature increases along the mantle adiabat (~0.3˚C/km) beneath the lithosphere. Therefore a difference in lithospheric thickness of 33 km only equates to a temperature difference of 9.9 ˚C in the asthenosphere beneath which is far too small to image in the tomography data sets.

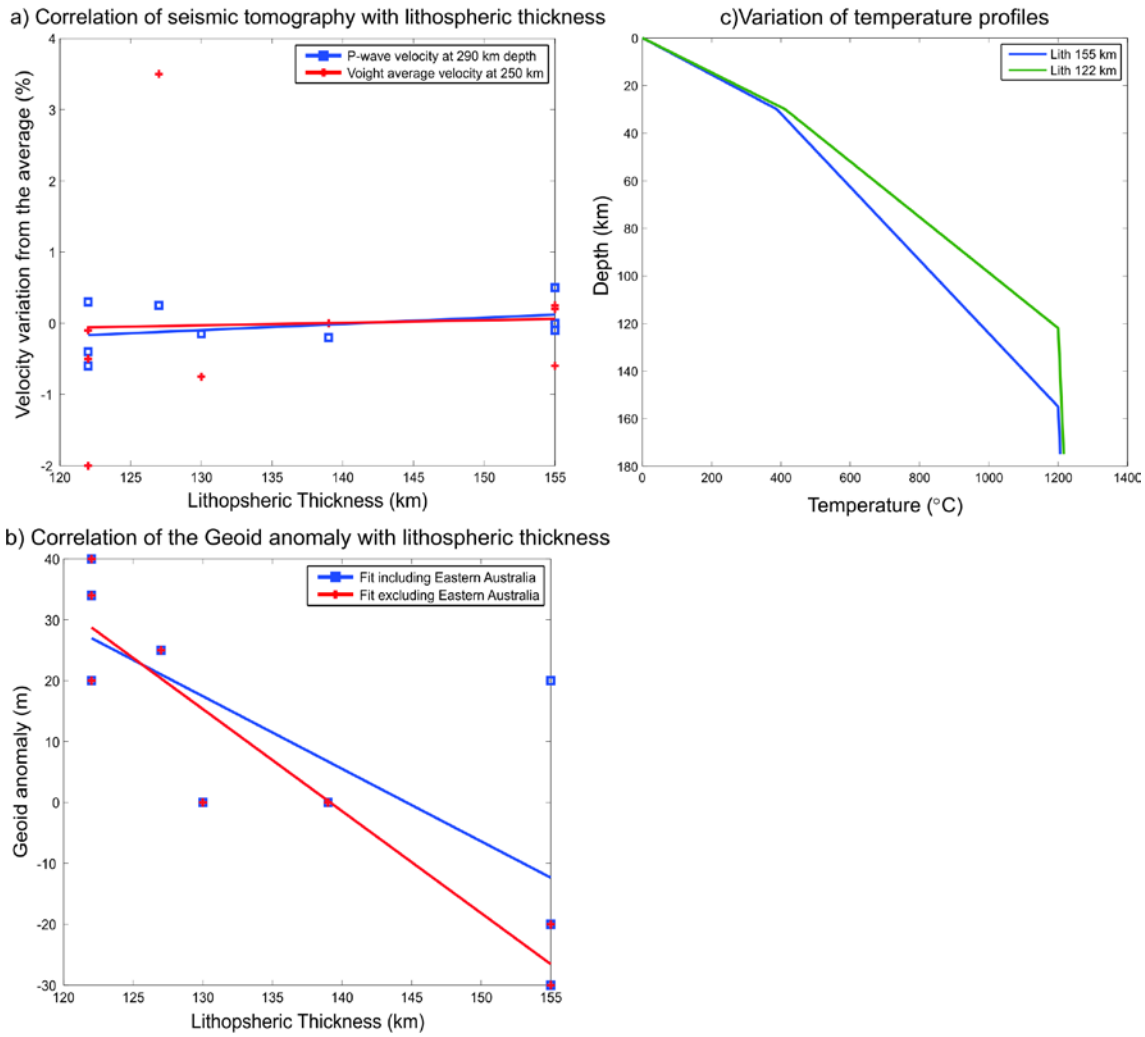

Figure 6.1: Testing what causes the variation in lithospheric thickness and what assertions can be made from this. A) shows that the variation in lithospheric thickness shows no correlation to the velocity of the underlying upper mantle. B) on the other hand shows that the thickness of lithosphere beneath the basins correlates with the geoid anomaly. C) explains why the temperature variation between a 155 and a 122 km thick lithosphere effects the gravity signal, but would have little effect on the temperature of underlying mantle and therefore how it transmits seismic energy.

However, the temperature profiles (Fig. 6.1c) do show a significant divergence at depths less than 155 km depth. This means that the density of the material will differ significantly (>200 kgm^{-3}) therefore an effect should be seen on the gravity signal. The effect of cooling and

thickening of the lithosphere in the oceans on the geoid has been previously demonstrated both theoretically and from observations (Lister, 1982). When the best fitting lithospheric thicknesses from each basin from Chapters 3-5 are plotted against the geoid anomaly there is a much clearer correlation with a R^2 value of 0.55. This is fairly good considering the geoid provides an indication of the total gravity field without any correction for topography and or other excess masses within the crust. The eastern Australian basin is close to the largest positive geoid anomaly in the world (centred over Papua New Guinea) and therefore is likely to be affected by this. If it is left out of the data set the correlation improves even more to a R^2 value of 0.88. To a first order the final lithosphere thicknesses do correlate with the geiod measurements and supporting their use as a predictive tool.

The good correlation of the geoid with the best fitting lithospheric thickness used in the modelling increases the confidence that these reflect real variation. This leads to the question 'What causes this variation?' The results from each of the basins suggest it is not small scale convection because it acts on a regional scale with a wavelength at least as large as the basins (500-1000 km). Even though the predicted temperature variations are too small to be imaged upon seismic tomography data the variation could still indicate the shallow signature of mantle flow. However, if this is so they should correlate to models of dynamic topography such as Heine et al., (2008), which are also controlled by upwelling and downwelling in the mantle, but there is no match. It does not appear to be controlled by the age of accretion of the crust either. North Africa which finished accreting at the start of the Paleozoic (~550 Ma) has a thinner lithosphere (122 km) than the Turan Platform (155 km) which did not finish accreting until the Triassic (~250 Ma). Western Australia, which also finished accreting around the Late Triassic (Glen, 2005), has a variation in lithospheric thickness from 155-122 km across the region. The temperature variations could be as a result of a heating under a tectonic lid in which case locations further from plate boundaries and closer to stable cratons might be expected to have thinner crust. This would seem to fit with Africa which predominantly has thinner lithosphere (122 km in North and South Africa), but does not hold up for the West Siberian basin which is flanked by two old and stable cratons and not near any subduction zones yet has thick lithosphere (155 km). Another possibility is that the variation in the subsidence patterns could be caused by heterogeneity in the upper mantle that cools and becomes part of the rigid lithosphere over time. This sort of compositional variation in the final lithosphere is not included in the model, but could also explain the geoid anomaly. Equally if it is a result of small temperature variations these could be chaotic or affected by regional controls not considered here. Unfortunately from a cursory comparison with these data sets it

is not possible draw any conclusions. There was not time in the course of the thesis to fully investigate these problems. Therefore the discussion above is only my preliminary thoughts on the issue.

To determine what causes the apparent variation in lithosphere thickness would require an in-depth study of the seismic datasets used to estimate lithosphere thickness to see exactly what they are observing alongside other methods to determine the lithosphere composition such as geochemical analysis of lithospheric xenoliths from the different regions.

6.4 Evolution of the continental crust

Another implication of the subsidence mechanism proposed in this thesis concerns how it affects the evolution of continental crust. The mechanism that produces continental crust has long been a subject of debate and is generally concluded to be a combination of formation at island or continental arcs and intraplate volcanism followed by accretion (Rudnick, 1995). A major problem with this is that island arcs and intraplate volcanism have a bulk basaltic composition whereas the continents as a whole have a more evolved bulk andesitic composition. What causes this evolution is the subject of yet more debate. One common mechanism suggested is that the lower crust once contained a layer of mafic or ultramafic cumulates which have been removed by delamination. Delamination of the lithosphere has been shown to occur in some locations such as beneath part of the North China craton (Gao et al., 2008), but these occurrences do not appear to be universal and do not mean that the mafic part of the crust must also have been lost. For example lithospheric delamination has been shown to occur beneath the north of the North China craton, but not the southern part (Liu et al., 2011).

The subsidence mechanism presented here provides an alternative possible explanation for this evolution. It shows that an inherent property of accretionary crust is that it will subside following accretion accumulating a sedimentary cover of 3-4 km thickness on average. This will be broadly siliciclastic though may have periods of carbonate deposition. It is made up of the eroded products of the surrounding crust, which have been mechanically sorted by sedimentary processes to produce a rock with a much more evolved silicic chemical signature. The system of erosion and transport in rivers breaks down the mafic minerals which tend to be weaker (Allen and Allen, 2005). They either dissolve or bypass the basins because of their small size and end up in the oceans. However, the quartz and feldspar which are more durable

remain as larger grains and therefore are deposited in in the basins. This enriched layer then can be mixed back into the crust during metamorphism occurring in continental collisions. For this to be the case, the mechanism needs to act over a long period of time to go through the full process. Time is not in short supply over the course of geological history and many older crustal areas show evidence of metamorphism in orogenies.

Sedimentary processes have previously been suggested as a possible method for evolving the crust (Rudnick, 1995). Work has been done to look at the chemical effects of erosion, but little has been done to look at the mechanical effects of erosion or to look at the materials deposited with a view of how they might affect the evolution of the crust. It has previously been dismissed as playing too minor a role with sediments said to only compose 3 % of the crust (Rudnick, 1995), however a 3-4 km thick sedimentary layer within a 30 km thick crust is ~ 10% of the crustal thickness and once it has been metamorphosed and stacked up within the upper crust through collision it may play a more significant role than previously envisioned.

At present this is only a theory and no work has been done to test it. This would require a detailed study of the bulk composition of the sediments found within these basins to identify their major and minor element abundances as well as the trace element patterns. This could then be combined with similar studies of the crystalline upper crust in accretionary areas and studies of the composition of abyssal sediments. These would allow box modelling to be carried out to see if reasonable combinations of the three reservoirs can produce the correct evolution of continental crust. This would focus on what proportions of upper crust and sediments would be needed to approach a bulk continental crust. It would also identify whether other reservoirs are needed and how much of a role other processes such as orogenic volcanism, which would accompany metamorphism, play in the process. This could be further verified with field studies of older exposed orogenic belts such as the Grenville Orogeny or Lewissian of northwest Scotland to see whether the predictions of the model are borne out in the proportions of metamorphosed sediments and crystalline basement present. Careful field studies could also help constrain the amount of tectonic interlayering between the crystalline upper crust and the overlying sediments and therefore what thickness of the continental crust is altered by this process. These studies could also look at the affects fluids have on chemical interaction between the crystalline crust and the sediments during the process. Finally they could determine the importance of orogenic granites in this process.

6.5 Summary

The evidence from the subsidence data presented throughout this study shows that the subsidence mechanism proposed provides a good explanation for the formation of basins upon accretionary crust, but like any theory, further work that tests its compatibility with other data sets is valuable. Using the geochemistry of volcanism that samples the lithosphere in some way could be a useful tool in this respect. In Chapter 4 it was argued that cooling and thickening of the lithosphere not only fits the available data, but fits it better than other subsidence mechanisms proposed. Therefore it is possible to look at possible implications from this. Looking at all the regions together helps to understand the growth of lithosphere and possibly the evolution of the continental crust as well. It is amazing that a study which primarily aimed to look at the subsidence of intracratonic basins can have such far reaching implications and can provide evidence for much longer term and deeper processes going on in the earth.

Chapter 7 - Summary and Conclusions

The main aim of this thesis was to determine what causes the subsidence of intercratonic basins upon accretionary crust. Cross sections through the Palaeozoic basins of North Africa suggest that the accretionary crust underwent platformal subsidence which was then modified into separate basins by the uplift of intervening arches (Craig et al., 2008). This is shown by the continuity of the sediments between different basins and the lack of onlap onto the intervening highs. When the sediments from the Ghadames and Al Kufrah basins were backstripped their subsidence profiles further supported this. They showed similarities in shape especially in the older sections although there was some variation due to erosion of the younger sediments in Al Kufrah. All of this points toward a common subsidence mechanism which acted across all the basins. The basins are all situated on crust which was accreted or rejuvenated during the Pan African orogeny at the end of the Proterozoic (Guiraud and Bosworth, 1999). This led to the hypothesis that accretionary crust forms with a thin lithosphere because its building blocks have thin lithosphere. The lithosphere remains thin while the accretion process is ongoing (while it is in the back arc region of the subduction zone where accretion is taking place). When accretion ceases the lithosphere is then able to cool and thicken, which in turn leads to subsidence. A forward model was used to test this subsidence mechanism against the subsidence data from the basins. The results showed that the subsidence from the Ghadames basin was fitted best by a model with a 30 km thick crust which has an initial lithospheric thickness of 50 km. This then cools to give a final lithospheric thickness of ~124 km. This is consistent with measurements of the present day lithospheric and crustal thickness. Variation of these parameters within the range found in the crust of North Africa fits the variation in subsidence seen in other basins from the region.

This subsidence mechanism was then tested for basins formed on regions of accretionary crust from around the world. The Paraná basin in South America, the Cape-Karoo in South Africa, the Palaeozoic sediments of Arabia, the Turan platform and the basins of eastern Australia were used. These are found on crust which finished accreting at different times ranging from the end of the Proterozoic to the Early Triassic. They all show an onset of subsidence at or shortly after accretion finished and the model produces a good fit to the subsidence patterns from the basins. Though there is significant variation in the magnitude of subsidence from the different basins these are fitted well by using the different crust and final lithosphere thicknesses from each region. Better age data with an increased number of divisions of the sedimentary column (especially in the older sediments) would be useful to constrain the shape of the subsidence curves further. This would help to discriminate between the subsidence mechanism proposed in this thesis and other suggested mechanisms, particularly slow strain rate stretching (Armitage and Allen, 2010). However, in the basins with more detailed stratigraphy, the subsidence curves do fit a model of subsidence due to a cooling and thickening lithosphere better than stretching at slow strain rates.

The West Siberian Basin provided a study which applied the computer model to a different situation with very different starting parameters. Saunders et al., (2005) observed that the subsidence outside the rifts has a delayed onset of sedimentation, which they proposed was caused by the thermal support of a plume head. The model developed in this thesis was used to test this and to investigate the extent of the plume head, the thinning of the lithosphere and the temperature of the plume material. It was found that a 50 km thick thermal anomaly of 1500 ˚C, which is placed between 50 and 100 km depth, produces the delayed subsidence patterns observed in the wider West Siberian Basin. The variation in subsidence can be explained by the variations in the crustal thickness across the basin. The sensitivity of the model was investigated and the depth of the plume head was the primary control on the subsidence. The temperature of the plume head and its thickness both had smaller affects on the subsidence patterns.

The evolution of these basins on a global scale presents an interesting possible explanation as to how the continental crust evolves from the bulk basaltic composition of island arc crust into the more evolved composition of bulk continental crust.

There are a number of conclusions which can be drawn from this work

1. The basin forming mechanism proposed within in this thesis fits the subsidence data and provides a good explanation for the formation of large basins and platformal sediments upon accretionary crust.
2. It provides a good fit for a variety of basins situated around the world which suggests such subsidence is a global property of accretionary crust inherited from its constituent building blocks or during its formation process.
3. The basins formed subside slowly over hundreds of millions of years. This means in general sedimentation keeps pace with subsidence so the basin fill is strongly affected by eustatic sea level variations.
4. The basement heat flow associated with this mechanism is at its maximum during the deposition of the earliest sediments and decays exponentially during the first 200 Myrs to average crustal heat flows. This reflects the subsidence history.
5. Other processes may also contribute to formation of the basin. Cooling and growth of the lithosphere effectively forms a background control on the subsidence which acts continually, but may be overprinted by periods of compression or accelerated subsidence due to other tectonic forces. This can be seen in the subsidence patterns observed in the basins. For example the Al Kufrah basin has a small rift succession in the south of the basin which locally affects the sediment fill.
6. The formation of the West Siberian Basin is consistent with the thermal decay of a plume head. This is similar to the cooling and thickening of an initially thin lithosphere, however with anomalously high initial temperatures. A plume head provides a mechanism which is able to explain the rifting, eruption of the Siberian flood basalts and their chemistry as well as the delayed onset of sedimentation in much of the West Siberian Basin.
7. This suggests a plume head is able to thin the lithosphere over a large area and the extent of this may be linked to the subsidence patterns seen at the surface.

Appendix A – Example of the backstripping computer code

```
%Peter Holt - A program to decompact sediments and then backstrip well
%A1NC198
%Modified from Sonia Scarcelli.
%Written on 18/03/2008
%For well A1-NC198


clear
n = 10;
% initial parameters ( actual thicknesses from boreholes)
z = zeros(1,n);
z(1) = 252;         % Thickness of the Continental Mesozoic, in m
z(2) = 215;         % Thickness of the Post Tasselian in m
z(3) = 378;         % Dalma
z(4) = 891;         % Binem
z(5) = 44;          % Tadrart
z(6) = 78;          % Akakus
z(7) = 106;         % Tannezuft
z(8) = 201;         % Mamuniyat
z(9) = 1534;        % PreGlacial Cambro-Ordovician
z(10) = 1;          % Bottom meter of C-O so that the column starts at
zero

% Surface porosity for each formation from Sclater & Christie
fi = zeros(1,n);
fi(1) = 0.50;          % surface porosity of the Continental Mesozoics
sandstones facies;
fi(2) = 0.51;          % surface porosity of the Post Tasselian
sandstones facies;
fi(3) = 0.51;          % surface porosity of the Dalma formation;
fi(4) = 0.55;          % surface porosity of the Binem Formation;
fi(5) = 0.515;         % surface porosity of the Tadrart;
fi(6) = 0.55;          % surface porosity of the Akakus;
fi(7) = 0.61;          % surface porosity of the Tannezuft;
fi(8) = 0.50;          % surface porosity of the Mamuniyat;
fi(9) = 0.49;          % surface porosity of the PreGlacial Cambro
Ordovician
fi(10)= 0.49;          % Bottom metre of C-O


% fi-depth coefficent for each formation
c = zeros(1,n);
c(1) = 0.000280;       % fi-depth coefficent in m^-1 for sandstones of
the Continental Mesozoic;
c(2) = 0.000310;       % fi-depth coefficent in m^-1 for sandstones of
the Post Tasselian;
c(3) = 0.000310;       % fi-depth coefficent in m^-1 for the Dalma Fm;
c(4) = 0.000405;       % fi-depth coefficent in m^-1 for the Binem
formation;
c(5) = 0.000295;       % fi-depth coefficent in m^-1 for the Tadrart
formation;
```

```
c(6) = 0.000420;       % fi-depth coefficent in m^-1 for the Akakus
formation;
c(7) = 0.000485;       % fi-depth coefficent in m^-1 for the Tannezuft
shaley sequence;
c(8) = 0.000280;       % fi-depth coefficent in m^-1 for the Mamuniyat
formation;
c(9) = 0.000270;       % fi-depth coefficent in m^-1 for the PreGlacial
Cambro Ordovician formation;
c(10)= 0.00027;        % Bottom metre

%depth to the top of the formations
y = zeros(1,n);
y(1) = 0;           % Continental Mesozoic Sandstones
y(2) = 252;         % Post Tasselian Sandstones
y(3) = 467;         % Dalma Fm
y(4) = 845;         % Binem Fm
y(5) = 1736;        % Tadrart Fm
y(6) = 1780;        % Akakus Fm
y(7) = 1858;        % Tannezuft shales
y(8) = 1964;        % Mamuniyat Fm
y(9) = 2164;        % Preglacial Cambro-Ordovician sandstones
y(10)= 3699;        % Lowest Metre
yBas = 3700;

% density at the surface conditions
rho_w   = 1030;         % density of the sea water Kg/m-3;
rho_m   = 3300;         % density of the mantle
rho = zeros(1,n);
rho(1)  = 2655;         % grain density of the Continental Mesozoic
Sandstones
rho(2)  = 2660;         % grain density of the Post tasselian Sandstones
rho(3)  = 2660;         % grain density of the Dalma Fm
rho(4)  = 2690;         % grain density of the Binem Fm
rho(5)  = 2655;         % grain density of the Tadrart Fm
rho(6)  = 2680;         % grain density of the Akakus Fm
rho(7)  = 2710;         % grain density of the Tannezuft Fm
rho(8)  = 2655;         % grain density of the Mamuniyat Fm
rho(9)  = 2650;         % grain density of the Cambro-Ordovician
sandstones
rho(10) = 2650;         % grain density of the bottom metre

%The paleosea-levels compared to the present day sea-level taken form the
%Exxon curves
sl(1)   = 205;          % The Cretaceous (Continental Mesozoic)
sl(2)   = 20;           % The Upper Jurrassic (Post Tasselian)
sl(3)   = 20;           % Mississippian (Dalma Fm)
sl(4)   = 105;          % Late Devonian (Binem Fm)
sl(5)   = 175;          % Early-Mid Devonian (Tadrart Fm)
sl(6)   = 105;          % Mid-Late Silurian (Akakus Fm)
sl(7)   = 145;          % Early Silurian (Tannezuft Fm)
sl(8)   = 140;          % Hirnantian (Mamuniyat Rm)
sl(9)   = 165;          % Cambro-Ordovician
sl(10)  = 100;          % Start of the Cambrian
sl = fliplr(sl);

%The Paleobathymetry or water depth.
```

```
Wd(1)  = 0;             % The Cretaceous (Continental Mesozoic)
Wd(2)  = 0;             % The Upper Jurrassic (Post Tasselian)
Wd(3)  = 20;            % Mississippian (Dalma Fm)
Wd(4)  = 40;            % Late Devonian (Binem Fm)
Wd(5)  = 0;             % Early-Mid Devonian (Tadrart Fm)
Wd(6)  = 60;            % Mid-Late Silurian (Akakus Fm)
Wd(7)  = 100;           % Early Silurian (Tannezuft Fm)
Wd(8)  = 50;            % Hirnantian (Mamuniyat Rm)
Wd(9)  = 5;             % Cambro-Ordovician
Wd(10) = 5;             % Start of the Cambrian
Wd = fliplr(Wd);

x = zeros(n,n);             %create an array for the depths to the top of
the units over time

for it = 1:n
    eps = 0.0001 ;
    error = 2*eps ;

    x_top = 0;
    for in = n-(it-1):n
        x_iter = 1;
        eps = 0.0001 ;
        error = 2*eps ;
        while error > eps
            x(in,it) = z(in) - fi(in)/c(in)*(exp(-c(in)*y(in))-exp(-
c(in)*(y(in)+z(in)))) + fi(in)/c(in)*(exp(-c(in)*x_top)-exp(-
c(in)*x_iter)) + x_top;
            error  = abs(x(in,it)-x_iter)/x_iter;
            x_iter  = x(in,it);
        end
        x_top = x(in,it);       % reset for the next layer
    end
end
xu = flipud(x);                  % This creates a matrix with time on the
x-axis and each layer on the z-axis
t = [513 445.6 443.7 440.8 416 386 359.2 318 223.4 97]; %prepare for the
plot

% carry out the backstripping
%calculating the porosity for each layer through time
fi_depth = zeros(n,n);
rho_i = zeros(1,n);
rho_b = zeros(1,n);
tecsub = zeros(1,n);
for it = 1:n
    x_top = 0;
    for in = n-(it-1):n
        fi_depth(in,it) = (fi(in)/c(in)) * ((exp(-c(in)*x_top)-exp(-
c(in)*x(in,it)))/(x(in,it) - x_top));
        rho_i(in) = (fi_depth(in,it)*rho_w + (1-
fi_depth(in,it))*rho(in))*(x(in,it)-x_top)/x(n,it);
        x_top = x(in,it);
    end
    rho_i
    rho_b(it) = sum(rho_i);
```

```
        tecsub(it) = x(n,it)*((rho_m - rho_b(it))/(rho_m - rho_w)) -
sl(it)*(rho_w/(rho_m-rho_w)) + (Wd(it)-sl(it));
end

%Plot of the complete output of the program showing both the decompacted
%subsidence and the tectonic subsidence
figure(1), clf
title ('Subsidence of the Kufrah Basin Well A1-NC198')
subplot (2,1,1)
plot (-t,-xu(1,1:n),'bo-',-t,-xu(2,1:n),'bo-',-t,-xu(3,1:n),'bo-',-t,-
xu(4,1:n),'kx-',-t,-xu(5,1:n),'gx-',-t,-xu(6,1:n),'rd-',-t,-
xu(7,1:n),'rd-',-t,-xu(8,1:n),'c^-',-t,-xu(9,1:n),'y^-',-t,-
xu(10,1:n),'y^-','LineWidth',2)
set (gca,'FontSize',14)
title ('The Decompacted Sedimetary thickness for the Kufrah
basin','FontSize',18)
xlabel ('Time (Ma)','FontSize',16)
ylabel ('Depth of each uncompacted layer (m)','FontSize',16)
%legend ('Cambro-Ordivician','off','off','off','off','off','Black
Shale','Silurian','hide','hide','hide','Devonian','hide','hide','hide','h
ide','Carboniferous','location','SouthWest')

subplot (2,1,2)
plot (-t,-tecsub,'o-','LineWidth',2)
set (gca,'FontSize',14)
title ('Water loaded tectonic subsidence','FontSize',18)
xlabel ('Time (Ma)','FontSize',16)
ylabel ('The Tectonic subsidence (m)','FontSize',16)
axis ([-550 0 -2000 0])
```

Appendix B – Example forward modelling code (WSB)

```
% WSB.m
%
% purpose: solves 1d heat equation to calculate subsidence
% method: finite differences
%         explicit (i.e. forward Euler) time integration

clear

dt = 0.01;                  % timestep in Myrs
nt=ceil(500/dt);            % number of tsteps to reach 100 Ma
secinmyr=1e6*365*24*3600;   % dt in sec
dt=dt*secinmyr;             % unit conversion to SI:

% Set up the spatial extent of the model
h = 1.7e5;                  % height of box: 1.7x10^5 m = 170 km
kappa = 1e-6;               % thermal diffusivity
dz = 1000;                  % discretization step in meters
nz=h/dz+1;
z=0:dz:h;
z_basalt = 2000;
z_basalt = ceil(z_basalt/dz) + 1;
z_conrad = 14000;           % depth of the upper crust in meters
z_conrad = ceil(z_conrad/dz) + 1;
z_bc = 29000;               % depth to the base of the crust in meters
z_bc = ceil(z_bc/dz) + 1;
z_lith = 50000;             % Depth to the base of the initial
lithosphere or top of the plume
z_lith = ceil(z_lith/dz) + 1;
plume_bot = 100000;
plume_bot = ceil(plume_bot/dz) + 1;

%Set up the initial temperatures
pT = 1330;                   % potential temperature in degC
Tm = pT + (0.3*(z_lith+1));  % calculate the temperature at key points
Tpb = pT + 0.3*(plume_bot+1);
Tmb = pT + 0.3*(nz);
Tplume = 1500;               % define the temperature of the plume
Told = Tplume*ones(1,nz);      % initial T=Tplume everywhere ...
Told(1:z_lith-1)= 0:(Tm/(z_lith-2)):Tm;     % ... except above the plume
Told(plume_bot+1:nz)= Tpb:0.3:Tmb;          % ... and the mantle beneath
the plume
Told(nz) = Tmb;
Tnew = zeros(1,nz);        % define empty array for Tnew

k = 3.3*ones(1,nz);        % The k value for the mantle lithosphere
k(1:z_conrad) = 3.1;       % The k value for a granitic crust
k(z_conrad+1:z_bc) = 2.1;  % The k value for the a basaltic lower crust

A = 0.006e-06*ones(1,nz);             % Define the Radioactive heat
production in W/m^3
A(1:z_conrad) = 1.31e-06;
```

```
A(z_conrad+1:z_bc) = 0.8e-06;

% Create a reference density column
refrho = 3300*ones(1,nz);
refrho(1:z_basalt-1) = 2900;
refrho(z_basalt:z_conrad-1) = 2750;
refrho(z_conrad) = 2825;
refrho(z_conrad+1:z_bc-1) = 2900;
refrho(z_bc) = 3100;

alpha = 3.3e-05*ones(1,nz);            % Define the Thermal expansivity
in K^-1
alpha(1:z_conrad) = 2.4e-05;
alpha(z_conrad+1:z_bc) = 1.6e-05;

Cp = 790*ones(1,nz);                   % Define the Specific Heat
Capacity in J/Kg/K
Cp(1:z_conrad) = 790;
Cp(z_conrad+1:z_bc) = 790;

unstable_above = dz^2/(2*(3.3/(2750*790)));

%Define the reference column for the Isostacy. Based on a mid ocean ridge
%column
zw = 3000/dz +1;
zoc = 10000/dz +1;
Tmorb = zeros(1,nz);
Tmorb(zw:zoc+1) = 0:Tm/((zoc+1)-zw):Tm;
Tmorb(zoc+1:nz) = Tm:0.3:Tm+0.3*(nz-(zoc+1));
alpha_m = 3.3e-05*ones(1,nz);
alpha_m(1:zw) = 5e-05;
alpha_m(zw:zoc) = 1.6e-05;

morb_rhoref = 3300*ones(1,nz);
morb_rhoref(1:zw-1) = 1030;
morb_rhoref(zw) = 1965;
morb_rhoref(zw+1:zoc) = 2900;
for im = 1:nz
    rho_morb(im) = morb_rhoref(im)*(1-alpha_m(im)*(Tmorb(im)-0));
end

t=0;                        % set time to zero

% Set up the arrays used in the calculations
base_lithosphere = zeros(1,nt);
baselith = zeros(1,nt);
q = zeros(1,nt);
time = zeros(1,nt);
topography = zeros(1,nt);
wtopo = zeros(1,nt);
old_topography = 1;
wOT = 1;
sediment = 0;
water_depth = 0;
basin_depth = zeros(1,nt);
```

```
wBD = zeros(1,nt);
elevation = zeros(1,nt);
Q = zeros(1,52);

% Plot the initial conditions to check the set up.
figure(1), clf
    plot (Told,-z)
    ylabel('z [m]')
    xlabel('T [^oC]')
    title(['Initial Temperature profile at the edge of the WSB'])

    drawnow
rift29_14_ini = Told;

for it=1:nt

    %  Calculate the numerical solution
    %  internal points:
    for i = 1:nz
        rho(i) = refrho(i)*(1-alpha(i)*(Told(i)-0));
    end
    for i = 2:nz-1
        ka = (k(i)+k(i+1))/2;
        kb = (k(i)+k(i-1))/2;
        Tnew(i) = Told(i) + (dt/rho(i)/Cp(i))*((ka*(Told(i+1)-Told(i))-
kb*(Told(i)-Told(i-1)))/dz^2) + (A(i)*dt)/(rho(i)*Cp(i));
    end



    re = mod(it,10);
    if re == 0

     %plot solution:
    tma=floor(t/secinmyr);
    figure(2), clf
    plot (Told,-z)
    ylabel('z [m]')
    xlabel('T [^oC]')
    title([' T after ',num2str(tma),' Myrs'])

    drawnow
    end

    %  boundary points:
    Tnew(1) = 0;
    Tnew(nz) = Tmb;
    rho(nz) = refrho(nz)*(1-alpha(nz)*(Told(nz)-0));

    rho_m=3300;  % rho_m = rho_mantle is density at T=T_mantle=T(nz)
    rho_w=1030;  % rho_w = rho_water
    rho_s=2200;  % rho_s = the density of the sediments filling the basin

    %Calculate the Topography or bathymetry of the crust
    if old_topography < 0
```

```
        sediment = sediment - old_topography;
    end
    if wOT < 0
        water_depth = water_depth - wOT;
    end

    basin_depth(it) = sediment;
    wBD(it) = water_depth;
    a = 0;
    b = 0;

    for ia = 1:zoc-1
        a = a + ((((rho_morb(ia) - rho_m*(1-alpha_m(ia)*(Tmorb(ia)-0))) +
(rho_morb(ia+1) - rho_m*(1-alpha_m(ia+1)*(Tmorb(ia+1)-0))))/2)*dz)/rho_m;

    end
    for ib = 1:nz-1
        b = b + ((((rho_m*(1-alpha_m(ib)*(Tmorb(ib)-0)) - rho(ib)) +
(rho_m*(1-alpha_m(ib+1)*(Tmorb(ib+1)-0)) - rho(ib+1)))/2)*dz)/rho_m;

    end
    cs =((rho_m-rho_s)*sediment)/rho_m;
    cw =((rho_m-rho_w)*water_depth)/rho_m;

    topography(it) = a + b + cs;
    wtopo(it) = a + b +cw;

    % elevation (find the topography/basin depth as one parameter)
    if topography(it) > 0
        elevation(it) = topography (it);
    else
        elevation(it) = -wBD(it);
    end

    for i = 1:nz
        if Tnew(i)>1200
            break
        end
    end

    %To find the base of the lithosphere very simply

    baselith(it) = z(i) - ((z(i)-z(i-1))*(Tnew(i)-1200)/(Tnew(i)-Tnew(i-
1)));


    %Calculate the heatflow from the surface of the crust
    q(it) = 1000*k(1)*((Told(2)-Told(1))/dz);


    % prepare for next time step:
    Told = Tnew;
    t=t+dt;
    old_topography = topography(it);
```

```
    wOT = wtopo(it);
    time(it) = t/secinmyr;

    re = mod(it,1000);
    if re == 0
        Q(it/1000) = q(it);
    end
end

rift29_14 = elevation;
save ('rift','rift29_14','rift29_14_ini','-append');

%Plot
figure(2),clf
set(gcf,'Units','centimeters','Position',[10 7 28 17])
plot (time,elevation,'r--',time,-basin_depth,'LineWidth',2)
set (gca,'FontSize',8)
title('West Siberian Basin Subsidence','FontSize',14)
ylabel('Basin depth (m)','FontSize',12,'FontWeight','b')
xlabel('Time in Myrs')
legend('Topography','Location','NorthEast')
%axis([0 500 -4500 2000])

figure(3),clf
plot (time,baselith)
xlabel('Time (Myrs)')
ylabel('Depth (m)')
title('Depth to the base of the lithosphere')

figure(4),clf
plot (time,q,'LineWidth',2)
set (gca,'FontSize',14)
xlabel('Time (Myrs)','FontSize',16)
ylabel('Heatflow (mW/m^2)','FontSize',16)
title('Heatflow from the crust','FontSize',18)
legend('Numerical solution','Location','NorthEast'
```

Appendix C – Ghadames composite well cross section

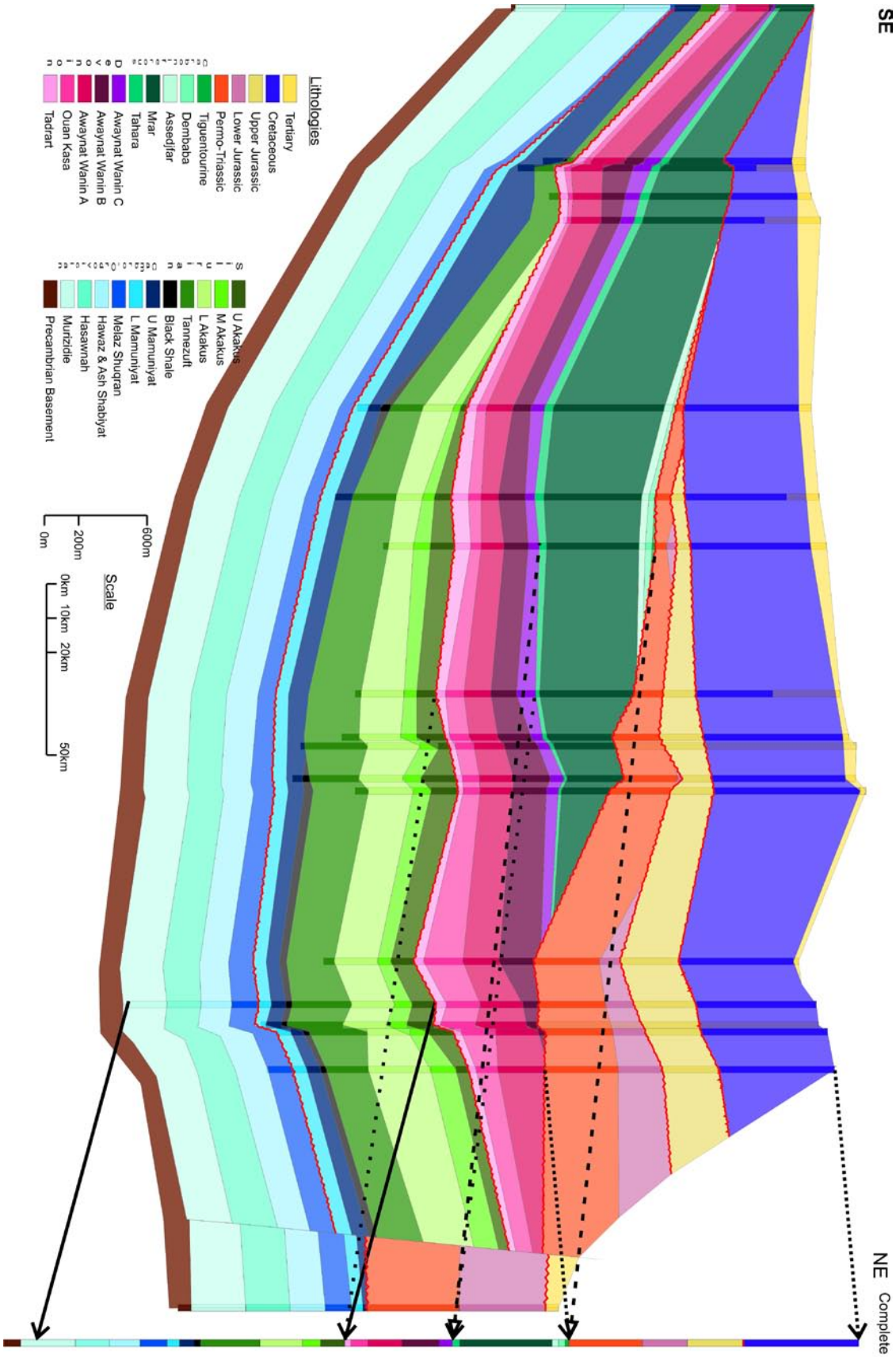

Bibliography

1994, Encyclopaedia Britannica: London.

Abadi, A.M., van Wees, J.-D., van Dijk, P.M., and Cloetingh, S.A.P.L., 2008, Tectonics and subsidence evolution of the Sirt Basin, Libya: AAPG Bulletin, v. 92, p. 993-1027.

Abdelsalam, M.G., Liégeois, J.P., and Stern, R.J., 2002, The Saharan Metacraton, *in* Fritz, H., and Loizenbauer, J., eds., 18th colloquium of African Geology Journal of African Earth Sciences: Graz Austria, Elsevier, p. 119-136.

Al-Juboury, A.I., and Al-Hadidy, A.H., 2009, Petrololgy and depositional evolution of the Paleozoic rock of Iraq: Marine and Petroleum Geology, v. 26, p. 208-231.

Al-Mishwat, A.T., and Nasir, S.J., 2004, Composition of the lower crust of the Arabian Plate: a xenolith perspective: Lithos, v. 72, p. 45-72.

Allen, M.B., Anderson, L., Searle, R.C., and Buslov, M.M., 2006, Oblique rift geometry of the West Siberian Basin: tectonic setting for the Siberian flood basalts: Journal of the Geological Society of London, v. 163, p. 901-904.

Allen, P., and Armitage, J.J., 2011, Cratonic Basins, *in* Busby, C.J., and Pérez, A.A., eds., Tectonics of sedimentary basins: Recent Advances: Cambridge, Wiley-Blackwell Science, p. 602-620.

Allen, P.A., and Allen, J., 2005, Basin Analysis: Principles and Applications: Oxford, Blackwell Publishing.

Almeida, F.F.M.d., Brito Neves, B.B.d., and Carneiro, C.D.R., 2000, The origin and evolution of the South American Platform: Earth Science Reviews, v. 50, p. 77-111.

Aplonov, S.V., 1995, The tectonic evolution of West Siberia: an attempt at a geophysical analysis: Tectonophysics, v. 245, p. 61-84.

Arcay, D., Doin, M.-P., Tric, E., Bousquet, R., and de Capitani, C., 2006, Overriding plate thinning in subduction zones: Localised convection induced by slab dehydration: Geochemistry Geophysics Geosystems, v. 7, p. 26.

Armitage, J.J., and Allen, P.A., 2010, Cratonic basins and the long-term subsidence history of continental interiors: Journal of the Geological Society of London, v. 167, p. 61-70.

Artemieva, I.M., and Mooney, W.D., 2001, Thermal thickness and evolution of Precambrian lithosphere: A global study: Journal of Geophysical Research, v. 106, p. 16387-16414.

Artyushkov, E.V., 1992, Role of crustal stretching on subsidence of the continental crust: Tectonophysics, v. 215, p. 187-207.

Artyushukov, E.V., 2005, The formation mechanism of the Barents Basin: Russian Geology and Geophysics, v. 47, p. 683-696.

Ashwal, L.D., and Burke, K., 1989, African lithospheric structure, volcanism and topography: Earth and Planetary Science Letters, v. 96, p. 8-14.

Baldwin, B., and Butler, C.O., 1985, Compaction Curves: AAPG Bulletin, v. 69, p. 622-626.

Baumont, D., Paul, A., Zandt, G., Beck, S.L., and Pedersen, H., 2002, Lithospheric structure of the central Andes based on surface wave dispersion: Journal of Geophysical Research, v. 107, p. 18.

Beccaluva, L., Azzouni-Sekkal, A., Benhallou, A., Bianchini, G., Ellam, R.M., Marzola, M., Siena, F., and Stuart, F.M., 2007, Intracratonic asthenosphere upwelling and lithosphere rejuvenation beneath the Hoggar swell (Algeria): Evidence from HIMU metasomatised lherzolite mantle xenoliths: Earth and Planetary Science Letters, v. 260, p. 482 - 494.

Begg, G.C., Griffin, W.L., Natapov, L.M., O'Reilly, S.Y., Grand, S.P., O'Neill, C.J., Hronsky, J.M.A., Djomani, Y.P., Swain, C.J., Deen, T., and Bowden, P., 2009, The lithopsheric

architecture of Africa: Seismic tomography, mantle petrology, and tectonic evolution.: Geosphere, v. 5, p. 23-50.

Bellahsen, N., Daniel, J.-M., Bollinger, L., and Burov, E., 2003, Influence of viscous layers on the growth of normal faults; insights from experimental and numerical models: Journal of Structural Geology, v. 25, p. 1471-1485.

Bellini, E., and Massa, D., 1980, A Stratigraphic contribution to the Paleozoic of the southern basins of Libya, *in* Salem, M.J., and Busrewil, M.T., eds., The Geology of Libya, 2nd Symposium of the Geology of Libya, Volume 1: Amsterdam, Elsevier, p. 3-56.

Best, J.A., Barazangi, M., Al-Saad, D., Sawaf, T., and Gebran, A., 1993, Continental margin evolution of the Northern Arabian platform in Syria: AAPG Bulletin, v. 77, p. 173-193.

Black, R., Latouche, L., Liégeois, J.P., Caby, R., and Bertrand, J.M., 1993, Pan African displaced terranes in the Tuareg Shield (central Sahara): Geology, v. 22, p. 641-644.

Boote, D.R.D., Clark-Lowes, D.D., and Traut, M.W., 1998, Palaeozoic petroleum systems of North Africa, *in* MacGregor, D.S., Moody, R.T.J., and Clark-Lowes, D.D., eds., Petroleum Geology of North Africa: London, The Geological Society of London Special Publications No. 132, p. 7-68.

Braitenberg, C., and Ebbing, J., 2009, New insights into the basement structure of the West Siberian Basin from forward and inverse modelling of GRACE satellite gravity data: Journal of Geophysical Research, v. 114.

Brito Neves, B.B.d., 2002, Main stages of the development of the sedimentary basins of South America and their relationship with the tectonics of supercontinents: Gondwana Research, v. 4, p. 175-196.

Brunet, M.-F., and Cloetingh, S.A.P.L., 2003, Integrated Peri-Tethyan basins studies (Peri-Tethys programme): Sedimentary Geology, v. 156, p. 1-10.

Bumby, A.J., and Guiraud, R., 2005, The geodynamic setting of the Phanerozoic basins of North Africa: Journal of African Earth Sciences, v. 43, p. 1-12.

Caby, R., 2003, Terrane assembly and geodynamic evolution of central-western Hoggar: a synthesis: Journal of African Earth Sciences, v. 37, p. 133-159.

Caby, R., and Monié, P., 2003, Neoproterozoic subductions and differential exhumation of western Hoggar (southwest Algeria): new structural, petrological and geochronological evidence: Journal of African Earth Sciences, v. 37, p. 269-293.

Campbell, I.H., 2007, Testing the plume theory: Chemical Geology, v. 241, p. 153-176.

Campbell, I.H., and Griffiths, R.W., 1990, Implications of mantle plume structure for the evolution of flood basalts: Earth and Planetary Science Letters, v. 99, p. 79-93.

Canil, D., 2008, Canada's craton: A bottoms-up view: GSA Today, v. 18, p. 4-10.

Capitanio, F.A., Faccenna, C., and Funiciello, R., 2009, The opening of the Sirte basin: Result of slab avalanching?: Earth and Planetary Science Letters, v. 285, p. 210-216.

Carbotte, S.M., and Macdonald, K.C., 1994, Comparison of seafloor tectonic fabric at intermediate, fast, and super fast spreading ridges: Influence of spreading rate, plate motions and ridge segmentation on fault patterns: Journal of Geophysical Research, v. 99, p. 13609-13631.

Catuneanu, O., 2004, Retroarc foreland systems - evolution through time: Journal of African Earth Sciences, v. 38, p. 225-242.

Cawood, P.A., and Buchan, C., 2007, Linking accretionary orogenesis with supercontinent assembly: Earth Science Reviews, v. 82, p. 217-257.

Cawood, P.A., Kröner, A., Collins, W.J., Kusky, T.M., Mooney, W.D., and Windley, B.F., 2009, Accretionary orogens through Earth history, *in* Cawood, P.A., and Kröner, A., eds., Earth Accretionary Systems in Space and Time, Volume 318: London, Geological Society Special Publications, p. 1-36.

Christensen, N.I., and Mooney, W.D., 1995, Seismic velocity structure and composition of the continental crust; a global view: Journal of Geophysical Research, v. 100, p. 9761-9788.

Bibliography

Christiansson, P., Faleide, J.I., and Berge, A.M., 2000, Crustal structure in the northern North Sea: An integrated geophysical study, *in* Nottvedt, A., ed., Dynamics of the Norwegian Sea, Volume 167: London, Geological Society Special Publications, p. 15-40.

Cloetingh, S.A.P.L., Lankreijer, A., de Wit, M.J., and Martinez, I., 1992, Subsidence history analyses and forward modelling of the Cape and Karoo Supergroups, *in* de Wit, M.J., and Ransome, I.D., eds., Inversion tectonics of the Cape Fold Belt, Karoo and Cretaceous basins of Southern Africa: Rotterdam, A. A. Balkema, p. 239-248.

Collins, C.D.N., Drummond, B.J., and Nicoll, M.G., 2003, Crustal thickness patterns in the Australian continent, *in* Hills, R.R., and Müller, R.D., eds., Evolution and Dynamics of the Australian Plate, Volume 372: Boulder, Colarado, Geological Society of America Special Paper, p. 121-128.

Collins, W.J., 2002, Hot orogens, tectonic switching, and creation of continental crust: Geology, v. 30, p. 535-538.

Condie, K.C., 1997, Plate tectonics and crustal evolution: Oxford, Butterworth-Heinemann.

Cook, H.E., Zhemchuzhnikov, V.G., Buvtyshkin, V.M., Golub, L.Y., Gatovsky, Y.A., and Zorin, Y.A., 1994, Devonian and Carboniferous passive-margin carbonate platform of southern Kazakhstan: Summary of depositional and stratigraphic models to assist in the exploration and production of coeval giant carbonate platform oil and gas fields in the north Caspian Basin, western Kazakhstan., *in* Embry, A.F., Beauchamp, B., and Glass, G.J., eds., Pangea: Global Environments and Resources, Canadian Society of Petroleum Geologists Memoir 17, p. 363-381.

Corfield, R.I., Watts, A.B., and Searle, M.P., 2005, Subsidence history of the North Indian continental margin, Zanskar-Ladakh Himalaya, NW India: Journal of the Geological Society, London, v. 162, p. 135-146.

Craig, J., Rizzi, C., Said, F., Thusu, B., Lüning, S., Asbali, A.I., Keeley, M.L., Bell, J.F., Durham, M.J., Eales, M.H., Beswetherick, S., and Hamblett, C., 2008, Structural styles and prospectivity in the Precambrian and Paleozoic hydrocarbon systems of North Africa, *in* Salem, M.J., al-Ard, J., and Iil-Naft, M., eds., The Geology of East Libya, Volume 4: Binghazi, Earth Science Society of Libya, p. 51-122.

Crosby, A.G., McKenzie, D., and Sclater, J.G., 2006, The relationship between depth, age and gravity in the oceans: Geophysical Journal International, v. 166, p. 553-573.

Currie, C.A., and Hyndman, R.D., 2006, The thermal structure of subduction zone back arcs: Journal of Geophysical Research, v. 111, p. 1-22.

d'Acremont, E., Leroy, S., and Burov, E.B., 2003, Numerical modelling of a mantle plume: the plume head-lithosphere interaction in the formation of an oceanic large igneous province: Earth and Planetary Science Letters, v. 206, p. 379-396.

De Rito, R.F., Cozzarelli, F.A., and Hodges, D.S., 1983, Mechanisms of subsidence in ancient cratonic rift basins: Tectonophysics, v. 94, p. 141-168.

Debayle, E., and Kennett, B.L.N., 2003, Surface-wave studies of the Australian region, *in* Hillis, R.R., and Müller, R.D., eds., Evolution and Dynamics of the Australian Plate, Volume 372: Boulder, Geological Society of America Special Publications, p. 25-40.

Dewey, J.F., 2007, The secular evolution of plate tectonics and the continental crust: An outline, *in* Hatcher Jr, R.D., Carlson, M.P., McBride, J.H., and Martínez Catalán, J.R., eds., 4-D Framework of Continental Crust: Geological Society of America Memoir 200: Boulder, Colorado, p. 1-7.

Doin, M.-P., and Fleitout, L., 1996, Thermal evolution of the oceanic lithosphere; an alternative view: Earth and Planetary Science Letters, v. 142, p. 121-136.

Echikh, K., 1998, Geology and hydrocarbon occurrences in the Ghadames Basin, Algeria, Tunisia, Libya, *in* MacGregor, D.S., Moody, R.T.J., and Clark-Lowes, D.D., eds., Petroleum geology of North Africa, Volume Special Publication No. 132: London, The Geological Society of London Special Publications, p. 109-129.

Bibliography

Elkins Tanton, L.T., Draper, D.S., Agee, C.B., Jewell, J., Thorpe, A., and Hess, P.C., 2007, The last lavas erupted during the main phase of the Siberian flood volcanic province: results from experimental petrology.: Contributions to Mineralogy and Petrology, v. 153, p. 191-209.

Elkins Tanton, L.T., Grove, T.L., and Donnelly-Nolan, J., 2009, Hot, shallow mantle melting under the Cascades volcanic arc: Geology, v. 29, p. 631-634.

Elkins Tanton, L.T., and Hager, B.H., 2000, Melt intrusion as a trigger for lithospheric foundering and the eruption of the Siberian flood basalts: Geophysical Research Letters, v. 27, p. 3937-3940.

Eyles, C.H., Eyles, N., and Franca, A.B., 1993, Glaciation and tectonics in an active intracratonic basin: the Late Palaeozoic Itararé Group, Paraná Basin, Brazil: Sedimentology, v. 40, p. 1-25.

Farnetani, C.G., and Richards, M.A., 1994, Numerical investigations of the mantle plume initiation model for flood basalt events: Journal of Geophysical Research, v. 99, p. 13813-13833.

Fekirine, B., and Abdallah, H., 1998, Palaeozoic lithofacies correlatives and sequence stratigraphy of the Saharan Platform, Algeria., *in* MacGregor, D.S., Moody, R.T.J., and Clark-Lowes, D.D., eds., Petroleum Geology of North Africa, Volume Special Publications No. 132: London, The Geological Society of London Special Publications, p. 97-108.

Feng, M., van der Lee, S., and Assumpção, M., 2007, Upper mantle structure of South America from joint inversion waveforms and fundamental mode group velocities of Rayleigh waves: Journal of Geophysical Research, v. 112, p. 1-16.

Fishwick, S., Heintz, M., Kennett, B.L.N., Reading, A.M., and Yoshizawa, K., 2008, Steps in lithospheric thickness within eastern Australia, evidence from surface wave tomography: Tectonics, v. 27, p. 1-17.

Frimmel, H.E., and Frank, W., 1998, Neoproterozoic tectno-thermal evolution of the Gariep Belt and its basement, Namibia and South Africa.: Precambrian Research, v. 90, p. 1-28.

Gallagher, K., Demitru, T.A., and Gleadow, A.J.W., 1994, Constraints on the vertical motion of eastern Australia during the Mesozoic: Basin Research, v. 6, p. 77-94.

Gao, S., Luo, T.-C., Zhang, B.-R., Zhang, H.-F., Han, Y.-w., Zhao, Z.-D., and Hu, Y.-K., 1998, Chemical composition of the continental crust as revealed by studies in East China: Geochimica et Cosmochimica Acta, v. 62, p. 1959-1975.

Gao, S., Rudnick, R.L., Xu, W.-L., Yuan, H.-L., Liu, Y.-S., Walker, R.J., Puchtel, I.S., Liu, X., Huang, H., Wang, X.-R., and Yang, J., 2008, Recycling deep cratonic lithosphere and generation of intraplate magmatism in the North China Craton: Earth and Planetary Science Letters, v. 270, p. 41-53.

Garfunkel, Z., 2002, Early Paleozoic sediments of NE Africa and Arabia: Products of continental-scale erosion, sediment transport and deposition: Israeli Journal of Earth Sciences, v. 51, p. 135-156.

Gee, D.G., and Stephenson, R.A., 2006, The European lithosphere: an introduction, *in* Gee, D.G., and Stephenson, R.A., eds., European Lithosphere Dynamics, Volume 32: London, Geological Society Memoirs, p. 1-9.

Ghanoush, H., and Abubaker, H., 2007, Gravity and Magnetic Profile along Seismic Intersect Ku - 89 - 04, Southern Kufra Basin - Libya, International Conference on Geo-resources in the Middle East and North Africa: Cairo University, Cairo.

Glen, R.A., 2005, The Tasmanides of Eastern Australia, *in* Vaughan, A.P.M., Leat, P.T., and Pankhurst, R.J., eds., Terrane Process at the Margins of Gondwana, Volume 246, Geological Society, London, Special Publications, p. 23-96.

Bibliography

Gorbatov, A., Dominguez, J., Suárez, G., Kostoglodov, V., Zhao, D., and Gordeev, E., 1999, Tomographic imaging of the *P*-wave velocity structure beneath the Kamchatka peninsula: Geophysical Journal International, v. 137, p. 269-279.

Gossel, W., Ebraheem, A.M., and Wycisk, P., 2004, A very large scale GIS-based groundwater flow model for the Nubian sandstone aquifer in Eastern Sahara (Egypt, northern Sudan and eastern Libya): Hydrogeology Journal, v. 12, p. 698-713.

Grignani, D., Lanzoni, E., and Elatrash, H., 1991, Paleozoic and Mesozoic subsurface of palynostratigraphy in the Al Kufra Basin, Libya, *in* Salem, M.J., Hammuda, O.S., and Eliagoubi, B.A., eds., The Geology of Libya, 3rd symposium of the Geology of Libya, Volume 4, Elsevier, p. 1159-1228.

Guiraud, R., and Bosworth, W., 1999, Phanerozoic geodynamic evolution of northeastern Africa and the northwestern Arabian platform: Tectonophysics, v. 315, p. 73-108.

Guiraud, R., Bosworth, W., Thierry, J., and Delplanque, A., 2005, Phanerozoic geological evolution of Northern and Central Africa: An overview: Journal of African Earth Sciences, v. 43, p. 83-143.

Halley, R.B., and Schmoker, J.W., 1983, High-porosity Cenzoic carbonate rocks of South Florida; progressive loss of porosity with depth: AAPG Bulletin, v. 67, p. 191-200.

Haq, B.U., Hardenbol, J., and Vail, P.R., 1988, Mesozoic and Cenozoic Chronostratigraphy and cycles of Sea-level Change, *in* Wilgus, C.K., Hastings, B.S., Kendall, C.G.S.C., Posamentier, H.W., Ross, C.A., and Van Wagoner, J.C., eds., Sea-level changes: An Integrated approach, Volume 42: Tulsa Oklahoma, Society of Economic Paleontologists and Mineralogists.

Haq, B.U., and Schutter, S.R., 2008, A chronology of Paleozoic sea-level Changes: Science, v. 322, p. 64-68.

Heine, C., MÜller, R.D., Steinberger, B., and Torsvik, T.H., 2008, Subsidence in intracontinental basins due to dynamic topography: Physics of the Earth And Planetary Interiors, v. 171, p. 252-264.

Heit, B., Yuan, X., Bianchi, M., Sodoudi, F., and Kind, R., 2008, Crustal thickness estimation beneath the southern central Andes at 30 °S and 36 °S from *S* wave receiver function analysis: Geophysical Journal International, v. 174, p. 249-254.

Herzberg, C., Asimow, P.D., Arndt, N., Niu, Y.L., Lesher, C.M., Fitton, J.G., Cheadle, M.J., and Saunders, A.D., 2007, Temperatures in ambient mantle and plumes: Constraints from basalts, picrites, and komatiites: Geochemistry Geophysics Geosystems, v. 8.

Holbrook, W.J., Lizarralde, D., McGeary, S., Bangs, N., and Diebold, J., 1999, Structure and composition of the Aleutian Island Arc and implications for continental crustal growth: Geology, v. 27, p. 31-34.

Holt, P., Allen, M.B., Van Hunen, J., and Bjørnseth, H.M., 2010, Lithospheric cooling as a basin forming mechanism within accretionary crust: Tectonophysics, v. 495, p. 184-194.

Huang, J., and Zhong, S., 2005, Sublithospheric small-scale convection and its implications for the residual topography at old ocean basins and the plate model Pagination: 17: Journal of Geophysical Research, v. 110.

Huang, J., Zhong, S., and van Hunen, J., 2003, Controls on sublithospheric small-scale convection Pagination: 13: Journal of Geophysical Research, v. 108.

Hyndman, R.D., and Currie, C.A., 2011, Why is the North America Cordillera high? Hot backarcs, thermal isostacy, and mountain belts: Geology, v. 39, p. 783-786.

Iwamori, H., McKenzie, D., and Takahashi, E., 1995, Melt generation by isentropic mantle upwelling: Earth and Planetary Science Letters, v. 134, p. 253-266.

Jahn, B.M., 2004, The Central Asian Orogenic Belt and growth of the continental crust in the Phanerozoic, *in* Malpas, J., Fletcher, C.J.N., Ali, J.R., and Aitcheson, J.C., eds., Aspects of the Tectonic Evolution of China, Volume 226: London, Geological Society Special Publications, p. 73-100.

Bibliography

Janssen, M.E., Stephenson, R.A., and Cloetingh, S.A.P.L., 1995, Temporal and spatial correlations between changes in plate motions and the evolution of rifted basins in Africa: Geological Society of America Bulletin, v. 107, p. 1317-1332.

Kaminski, E., and Jaupart, C., 2000, Lithosphere structure beneath the Phanerozoic intracratonic basins of North America: Earth and Planetary Science Letters, v. 178, p. 139-149.

Karner, S.L., Chester, J.S., Chester, F.M., Kronenberg, A.K., and Hajash, A.J., 2005, Laboratory deformation of granular quartz sand; implications for the burial of clastic rocks: AAPG Bulletin, v. 89, p. 603-625.

Kerr, A.C., 1994, Lithospheric thinning during the evolution of continental large igneous provinces: A case study from the North Atlantic Tertiary province.: Geology, v. 22, p. 1027-1030.

Kincaid, C., and Sacks, I.S., 1997, Thermal and dynamical evolution of the upper mantle in subduction zones: Journal of Geophysical Research, v. 102, p. 12295-12315.

King, S.D., and Anderson, D.L., 1998, Edge-driven convection: Earth and Planetary Science Letters, v. 160, p. 289-296.

Klein, G.D., 1995, Intracratonic Basins, *in* Busby, C.J., and Ingersoll, R.V., eds., Tectonics of Sedimentary basins: Oxford, England, Blackwell Science, p. 459-478.

Klein, G.D., and Hsui, A.T., 1987, Origins of intracratonic basins: Geology, v. 17, p. 1094-1098.

Kominz, M., 1995, Thermally subsiding basins and the insulating effect of sediment with application to the Cambro-Ordovician Great Basin sequence, western USA: Basin Research, v. 7, p. 221-233.

Konert, G., Afifi, A.M., Al-Hajri, S.A., Groot, K.d., Naim, A.A.A., and Droste, H.J., 2001, Paleozoic stratigraphy and hydrocarbon habitat of the Arabian Plate, *in* Downey, M.W., Threet, J.C., and Morgan, W.A., eds., Petroleum provinces of the twenty-first century: Tulsa, United States, American Association of Petroleum Geologists, p. 483-515.

Korsch, R.J., Harrington, H.J., Wake-Dyster, K.D., O'Brien, P.E., and Finlayson, D.M., 1988, Sedimentary basins peripheral to the New England Orogen: their contribution to understanding New England tectonics, *in* Kleeman, D., ed., New England Orogen, Tectonics and Metallogenesis: Armidale, Australia, University of New England, p. 134-140.

Kunin, N.Y., and Ioganson, L.I., 1984, Geophysical Characteristics and Structure of the Western Siberian Crust: Moscow, Nauka, 220 (in Russian) p.

Le Heron, D.P., Armstrong, H.A., Wilson, C., and Gindre, L., 2010, Glaciation and deglaciation of the Libyan Desert; the Later Ordovician record: Sedimentary Geology, v. 223, p. 100-125.

Lekic, V., and Romanowicz, B., 2011, Inferring upper-mantle structure by full waveform tomography with the spectral element method: Geophysical Journal International, v. 185, p. 799-831.

Li, H., Morozov, I.B., and Smithson, S.B., 2007, Correlation of *Lg* amplitude ratios from peaceful nuclear explosions to crustal structure in Northern Eurasia: Bulletin of the Seismological Society of America, v. 97, p. 426-439.

Li, X., Kind, R., Yuan, X., Wölbern, I., and Hanka, W., 2004, Rejuvenation of the lithosphere by the Hawaiian plume: Nature, v. 427, p. 827-829.

Liégeois, J.P., Black, R., Navez, J., and Latouche, L., 1994, Early and Later Pan-African orogenies in the Aïr assembly of terranes (Tuareg shield, Niger): Precambrian Research, v. 67, p. 59-88.

Lister, C.R.B., 1982, Geoid anomalies over cooling lithosphere: source for a third kernel of upper mantle parameters and therefore an inversion: Geophysical Journal of the Royal Astronomical Society, v. 68, p. 219-240.

Bibliography

Liu, J., Rudnick, R.L., Walker, R.J., Gao, S., Wu, R.-Y., Piccoli, P.M., Yuan, H.-L., Xu, W.-L., and Xu, Y.G., 2011, Mapping lithospheric boundaries using Os isotopes of mantle xenoliths: An example from the North China Craton: Geochimica et Cosmochimica Acta, v. 75, p. 3881-3902.

Lüning, S., Craig, J., Fitches, B., Mayouf, J., Busrewil, A., El Dieb, M., Gammudi, A., Loydell, D., and McIlroy, D., 1999, Re-evaluation of the petroleum potential of the Kufra Basin (SE Libya, NE Chad): does the source rock barrier fall?: Marine and Petroleum Geology, v. 16, p. 693-718.

Macpherson, C.G., 2008, Lithosphere erosion and crustal growth in subduction zones: insights from initiation of the nascent East Philippine Arc: Geology, v. 36, p. 311-314.

Makhous, M., and Galushkin, Y.I., 2003, Burial history and thermal evolution of the northern and eastern Saharan basins: AAPG Bulletin, v. 87, p. 1623-1651.

Maruyama, S., 1997, Pacific-type orogeny revisited: Miyashiro-type orogeny proposed: Island Arc, v. 6, p. 91-120.

McGillivray, J.G., and Husseini, M.I., 1992, The Palaeozoic petroleum geology of Central Arabia: AAPG Bulletin, v. 76, p. 1473-1490.

McKenzie, D., 1978, Some remarks on the development of sedimentary basins: Earth and Planetary Science Letters, v. 40, p. 25-32.

McKenzie, D., Jackson, J., and Priestley, K., 2005, Thermal structure of oceanic and continental lithosphere: Earth and Planetary Science Letters, v. 233, p. 337-349.

Metcalfe, I., 2006, Palaeozoic and Mesozoic tectonic evolution and palaeogeography of East Asian crustal fragments: The Korean Peninsula in context: Gondwana Research, v. 9, p. 24-46.

Milani, E.J., and De Wit, M.J., 2008, Correlations between the classic Paraná and Cape - Karoo sequences of South America and southern Africa and their basin infills flanking the Gondwanides: du Toit revisited, *in* Pankhurst, R.J., Trouw, R.A.J., Brito Neves, B.B., and De Wit, M.J., eds., Pre-Cenozoic correlations across the South Atlantic region, Volume 294: Special Publications: London, Geological Society, p. 319-342.

Moore, W.B., Schubert, G., and Tackley, P.J., 1999, The role of rheology in lithospheric thinning by mantle plumes: Geophysical Research Letters, v. 26, p. 1073-1076.

Moores, E.M., and Twiss, R.J., 1995, Tectonics: New York, W H Freeman.

Morozova, E.A., Morozov, I.B., Smithson, S.B., and Solodilov, L.N., 1999, Heterogeneity of the uppermost mantle beneath Russian Eurasia from the ultra-long-range profile QUARTZ: Journal of Geophysical Research, v. B9, p. 20329-20348.

Murphy, J.B., and Nance, R.D., 1991, Supercontinent model for the contrasting character of late Proterozoic orogenic belts: Geology, v. 19, p. 469-472.

Natal'in, B.A., and Şengör, A.M.C., 2005, Late Palaeozoic to Triassic evolution of the Turan and Scythian platforms; the pre-history of the palaeo-Tethyan closure: Tectonophysics, v. 404, p. 175-202.

Neumann, E.R., Olsen, K.H., Balbridge, W.S., and Sundvoll, B., 1992, The Oslo rift: a review: Tectonophysics, v. 208, p. 1-18.

Nikishin, A.M., Ziegler, P.A., Panov, D.I., Nazarevich, B.P., Brunet, M.-F., Stephenson, R.A., Bolotov, S.N., Korotaev, M.V., and Tikhomirov, P.L., 2001, Mesozoic and Cainozoic evolution of the Scythian Platform - Black Sea - Caucasus domain, *in* Ziegler, P.A., Cavazza, W., Robertson, A.H.F., and Crasqui-Soleau, S., eds., Peri-Tethyan rift/wrench basins and passive margins, Volume 6: Peri-Tethys Memoir: Paris, Mémoires du Muséum national d'Histoire Naturelle, p. 295-346.

Nyblade, A.A., and Sleep, N.H., 2003, Long lasting epeirogenic uplift from mantle plumes and the origin of the Southern African Plateau: Geochemistry Geophysics Geosystems, v. 4, p. 1-29.

Bibliography

Oliveira, D.C.d., and Mohriak, W.U., 2003, Jaibaras trough: an important element in the early tectonic evolution of the Parnaíba interior sag basin, Northern Brazil: Marine and Petroleum Geology, v. 20, p. 351-383.

Paquette, J.L., Caby, R., Djouadi, M.T., and Bouchez, J.L., 1998, U-Pb dating of the end Pan-African orogeny in the Tuareg shield: the post-collisional syn-shear Tioueine pluton (Western Hoggar, Algeria): Lithos, v. 45, p. 245-253.

Parsons, B., and Sclater, J.G., 1977, An analysis of the variation of the ocean floor bathymetry and heat flow with age.: Journal of Geophysical Research, v. 108, p. 803-827.

Pasyanos, M.E., 2010, Lithospheric thickness modeled from long-period surface wave dispersion: Tectonophysics, v. 481, p. 38-50.

Pasyanos, M.E., and Nyblade, A.A., 2007, A top to bottom lithospheric study of Africa and Arabia: Tectonophysics, v. 444, p. 27-44.

Peterson, J.A., and Clark, J.W., 1991, Geology and hydrocarbon habitat of the West Siberian Basin: Tulsa, Oklahoma, AAPG.

Priestley, K., and McKenzie, D., 2006, The thermal structure of the lithosphere from shear wave velocities: Earth and Planetary Science Letters, v. 244, p. 285-301.

Priestley, K., and Tilmann, F., 2009, Relationship between the upper mantle high velocity seismic lid and the continental lithosphere: Lithos, v. 109, p. 112-124.

Reichow, M.K., Pringle, M.S., Al'Mukhamedov, A.I., Allen, M.B., Andreichev, V.L., Buslov, M.M., Davies, C.E., Fedoseev, G.S., Fitton, J.G., Inger, S., Medvedev, A.Y., Mitchell, C., Puchkov, V.N., Safonova, I.Y., Scott, R.A., and Saunders, A.D., 2009, The timing and extent of the eruption of the Siberian Traps large igneous province: Implications for the the end-Permian environmental crisis: Earth and Planetary Science Letters, v. 277, p. 9-20.

Reichow, M.K., Saunders, A.D., White, R.V., Al'Mukhamedov, A.I., and Medvedev, A.Y., 2005, Geochemistry and petrogenesis of the basalts from the West Siberian Basin: an extension of the Permo-Triassic Siberian Traps, Russia: Lithos, v. 79, p. 425-452.

Revil, A., Grauls, D., and Brévart, O., 2002, Mechanical compaction of sand/clay mixtures: Journal of Geophysical Research, v. 107, p. 1-11.

Ribe, N.M., and Christensen, U.R., 1999, The dynamical origin of Hawaiian volcanism: Earth and Planetary Science Letters, v. 171, p. 517-531.

Richards, M.A., Duncan, R.A., and Courtillot, V.E., 1989, Flood basalts and hot-spot tracks: Plume heads and tails: Science, v. 246, p. 103-107.

Richter, F.M., and Parsons, B., 1975, On the interaction of two scales of convection in the mantle: Journal of Geophysical Research, v. 80, p. 2529-2541.

Ritzmann, O., and Faleide, J.I., 2009, The crust and mantle lithosphere in the Barents Sea/Kara Sea region: Tectonophysics, v. 470, p. 89-104.

Rudnick, R.L., 1995, Making continental crust: Nature, v. 378, p. 571-578.

Rudnick, R.L., McDonough, W.F., and O'Connell, R.J., 1998, Thermal structure, thickness and composition of continental lithosphere: Chemical Geology, v. 145, p. 395-411.

Sahagian, D., 1993, Structural evolution of African basins: stratigraphic synthesis: Basin Research, v. 5, p. 41-54.

Saunders, A.D., England, R.W., Reichow, M.K., and White, R.V., 2005, A mantle plume origin for the Siberian traps: uplift and extension in the West Siberian Basin, Russia: Lithos, v. 79, p. 407-424.

Saunders, A.D., Jones, S.M., Morgan, L.A., Pierce, K.L., Widdowson, M., and Xu, Y.G., 2007, Regional uplift associated with continental large igneous provinces: The roles of mantle plumes and the lithosphere: Chemical Geology, v. 241, p. 282-318.

Schmitz, M., Heinsohn, W.-D., and Schilling, F.R., 1997, Seismic, gravity and petrological evidence for partial melt beneath the thickened Central Andean crust (21-23°S): Tectonophysics, v. 270, p. 313-326.

Bibliography

Schurr, B., Rietbrock, A., Asch, G., Kind, R., and Oncken, O., 2006, Evidence for lithospheric detachment in the central Andes from local earthquake tomography: Tectonophysics, v. 415, p. 203-223.

Sclater, J.G., and Christie, P.A.F., 1980, Continental stretching; an explanation of the post-Mid-Cretaceous subsidence of the central North Sea basin: Journal of Geophysical Research, v. 85, p. 3711-3739.

Seber, D., Sandvol, E., Sandvol, C., Brindisi, C., and Barazangi, M., 2001, Crustal model for the Middle East and North Africa region: implications for the isostatic compensation mechanism: Geophysical Journal International, v. 147, p. 630-638.

Selley, R.C., 1997, The basins of Northwest Africa; structural evolution, *in* Selley, R.C., ed., African basins: Sedimentary basins of the world: Amsterdam, Elsevier, p. 17-26.

Şengör, A.M.C., and Natal'in, B.A., 1996, Paleotectonics of Asia: fragments of a synthesis, *in* Yin, A., and Harrison, T.M., eds., The Tectonic Evolution of Asia: World and regional Geology series: Cambridge, Cambridge University Press, p. 486-640.

Şengör, A.M.C., Natal'in, B.A., and Burtman, V.S., 1993, Evolution of the Altaid tectonic collage and Palaeozoic crustal growth in Eurasia: Nature, v. 364, p. 299-307.

Şengör, A.M.C., and Okurogullari, A.H., 1991, The role of accretionary wedges in the growth of continents: Asiatic examples from Argand to Plate Tectonics: Eclogae Geologicae Helveticae, v. 84, p. 535-597.

Shaw, D.M., Cramer, J.J., Higgins, M.D., and Truscott, M.G., 1986, Composition of the Canadian Precambrian shield and the continental crust of the earth, *in* Dawson, J.B., Carson, D.A., Hall, J., and Wedepohl, K.H., eds., The Nature of the Lower Continental Crust, Volume 24: London, Geological Society of London Special Publications, p. 275-282.

Stampfli, G.M., and Borel, G.D., 2002, A plate tectonic model for the Paleozoic and Mesozoic constrained by dynamic plate boundaries and restored synthetic oceanic isochrons: Earth and Planetary Science Letters, v. 196, p. 17-33.

Stein, C.A., and Stein, S., 1992, A model for the global variation in oceanic depth and heat flow with lithospheric age: Nature, v. 359, p. 123-129.

Stel, H., Cloetingh, S.A.P.L., Heeremans, M., and Van der Beek, P., 1993, Anorogenic granites, magmatic underplating and the origin of intracratonic basins in a non-extensional setting: Tectonophysics, v. 226, p. 285-299.

Stern, R.J., 1994, Arc assembly and continental collision in the Neoproterozoic East African orogen: Implications for the consolidation of Gondwanaland: Annual Review of Earth and Planetary Science, v. 22, p. 319-351.

—, 2002, Subduction zones: Reviews of Geophysics, v. 40.

Sultan, M., Chamberlain, K.R., Bowring, S.A., Arvidson, R.E., Abuzied, H., and Kaliouby, B.E., 1990, Geochronologic and isotopic evidence for involvement of pre-Pan-African crust in the Nubian Shield, Egypt: Geology, v. 18, p. 761-764.

Takahashi, N., Kodaira, S., Klemperer, S.L., Tatsumi, Y., Kaneda, Y., and Suyehiro, K., 2007, Crustal structure and evolution of the Mariana intra-oceanic island arc: Geology, v. 35, p. 203-206.

Takanami, T., Sacks, I.S., and Hasegawa, A., 2000, Attenuation structure beneath the volcanic front in northeastern Japan from broad-band seismograms: Physics of the Earth And Planetary Interiors, v. 121, p. 339-357.

Tankard, A., Welsink, H., Aukes, P., Newton, R., and Stettler, E., 2009, Tectonic evolution of the Cape and Karoo basins of South Africa: Marine and Petroleum Geology, v. 26, p. 1379-1412.

Thomas, J.C., Cobbold, P.R., Shein, V.S., and Le Douaran, S., 1999, Sedimentary record of late Paleozoic to Recent tectonism in central Asia - analysis of subsurface data from the Turan and south Kazak domains: Tectonophysics, v. 313, p. 243-263.

Turcotte, D.L., and Schubert, G., 2002, Geodynamics: Cambridge, Cambridge University Press.

Bibliography

Turner, B.R., 1978, Paleozoic sedimentology of the south eastern part of the Al Kufrah Basin, Libya: A model for oil exploration, *in* Salem, M.J., and Busrewil, M.T., eds., The Geology of Libya, 2nd symposium of the Geology of Libya, Volume 2, p. 351-375.

Turner, B.R., Armstrong, H.A., and Holt, P., 2011, Visions of ice sheets in the early Ordovician greenhouse world: Evidence from the Peninsula Formation, Cape Peninsula, South Africa: Sedimentary Geology, v. 236, p. 226-238.

Van Hinsbergen, D.J.J., Buiter, S.J.H., Torsvik, T.H., Gaina, C., and Webb, S.J., 2011, The formation and evolution of Africa from the Archaean to Present: introduction, *in* Van Hinsbergen, D.J.J., Buiter, S.J.H., Torsvik, T.H., Gaina, C., and Webb, S.J., eds., 2011, Volume 357: London, Geological Society Special Publications, p. 1-8.

van Hunen, J., Zhong, S., Shapiro, N.M., and Ritzwoller, M.H., 2005, New evidence for dislocation creep from 3-D geodynamic modeling of the Pacific upper mantle structure: Earth and Planetary Science Letters, v. 238, p. 146-155.

van Keken, P.E., 2003, The structure and dynamics of the mantle wedge: Earth and Planetary Science Letters Frontiers, v. 215, p. 323-338.

van Staal, C.R., Dewey, J.F., Mac Niocall, C., and McKerrow, W.S., 1998, The Cambrian-Silurian tectonic evolution of the Northern Appalachian and British Caledonides: history of a complex west and southwest Pacific-type segment of Iapetus, *in* Bundell, D.J., and Scott, A.C., eds., Lyell: The Past is the Key to the Present, Volume 143: London, Geological Society Special Publications, p. 199-242.

Van Wees, J.-D., van Bergen, F., David, P., Nepveu, M., Beekman, F., Cloetingh, S.A.P.L., and Bonté, D., 2009, Probabilistic tectonic heat flow modeling for basin maturation: Assessment method and applications: Marine and Petroleum Geology, v. 26, p. 536-551.

Veevers, J.J., 2004, Gondwanaland from 650-500 Ma assembly through 320 Ma merger in Pangea to 185-100 Ma breakup: supercontinental tectonics via stratigraphy and radiometric dating: Earth Science Reviews, v. 68, p. 1-132.

Vyssotski, A.V., Vyssotski, V.N., and Nezhdanov, A.A., 2006, Evolution of the West Siberian Basin: Marine and Petroleum Geology, v. 23, p. 93-126.

Watson, S., and McKenzie, D., 1991, Melt generation by plumes: A study of Hawaiian volcanism: Journal of Petrology, v. 32, p. 501-537.

Watts, A.B., and Ryan, W.B.F., 1976, Flexure of the lithosphere and continental margin basins: Tectonophysics, v. 36, p. 25-44.

Wedepohl, K.H., 1995, The composition of the continental crust: Geochimica et Cosmochimica Acta, v. 59, p. 1217-1232.

Westphal, M., Gurevitch, E.L., Samsonov, B.V., Feinberg, H., and Pozzi, J.P., 1998, Magnetostratigraphy of the lower Triassic volcanics from deep drill SG6 in western Siberia: evidence for the long-lasting Permo-Triassic volcanic activity: Geophysical Journal International, v. 134, p. 254-266.

Wignall, P.B., 2001, Large igneous provinces and mass extinctions: Earth Science Reviews, v. 53, p. 1-33.

Williams, H., Hoffman, P.F., Lewry, J.F., Monger, J.W.H., and Rivers, T., 1991, Anatomy of North America: thematic geologic portrayals of the continent: Tectonophysics, v. 187, p. 117-134.

Windley, B.F., and Garde, A.A., 2009, Arc-generated blocks with crustal sections in the North Atlantic craton of West Greenland: Crustal growth in the Archean with modern analogues: Earth Science Reviews, v. 93, p. 1-30.

Xie, X., and Heller, P.L., 2009, Plate tectonics and basin subsidence history: Geological Society of America Bulletin, v. 121, p. 55-64.

Zalán, P.V., Wolff, S., Astolfi, M.A.M., Vieira, I.S., Concelção, J.C.J., Appi, V.T., Neto, E.V.S., Cerqueira, J.R., and Marques, A., 1990, The Paraná Basin, Brazil, *in* Leighton, M.W.,

Kolata, D.R., Oltz, D.F., and Eidel, J.J., eds., Interior Cratonic Basins: AAPG memoir 51: Tulsa Oklahoma, p. 681-708.

Zhao, D., Hasegawa, A., and Kanamori, H., 1994, Deep structure of Japan subduction zone as derived from local, regional, and teleseismic events: Journal of Geophysical Research, v. 99, p. 22313-22329.

Zhao, D., Xu, Y., Wiens, D.A., Dorman, L., Hildebrand, J., and Webb, S., 1997, Depth extent of the Lau back-arc spreading centre and its relation to subduction processes: Science, v. 278, p. 254-257.

Zhong, S., 2005, Dynamics of thermal plumes in three-dimensional isoviscous thermal convection: Geophysical Journal International, v. 162, p. 289-300.

Zor, E., Sandvol, E., Gürbüz, C., Türkelli, N., Seber, D., and Barazangi, M., 2003, The Crustal structure of the East Anatolian plateau (Turkey) from receiver functions: Geophysical Research Letters, v. 30, p. 8044-8048.